Imidazolium-Based Organic Structure Directing
Agents for the Synthesis of Microporous
Materials

Thesis by

Joel Edward Schmidt

In Partial Fulfillment of the Requirements for the degree

of

Doctor of Philosophy

CALIFORNIA INSTITUTE OF TECHNOLOGY

Pasadena, California

2016

(Defended August 6, 2015)

ACKNOWLEDGEMENTS

Receiving a PhD from Caltech certainly could not have been accomplished without the support and encouragement of numerous people throughout my life. First and foremost I would like to thank my family and especially my parents, Ed and Karen, for everything they did to support me throughout my life to even get me to a position to begin a PhD at Caltech and for all of the encouragement they provided along the way.

At the University of Dayton I would like to thank all of the faculty for their help in getting me to Caltech, especially Professor Myers and Professor Elsass. While at Dayton, I was able to spend three years working as a Research Engineer intern with the Air Force Research Labs at Wright Patterson Air Force base, where I worked in the Thermal Sciences and Materials Branch (AFRL/RXBT). I would especially like to thank Dr. Doug Dudis, who served as my mentor and research advisor while I was there. Doug more than anyone else pushed me to excel in the lab and was the person who suggested I look at Caltech in the first place. I would also like to thank Dr. Joseph Shumaker for countless hours spent in the lab with me and all of the practical chemistry knowledge he gave me (along with a tremendous amount of glassware cleaning experience).

At Caltech I would first and foremost like to thank my research advisor Professor Mark Davis for finding the funding and providing the environment for all the work I did and especially for the research ideas and all of his knowledge and insights. I would also like to thank my other committee members Professor Flagan and Professor Rossmann. Professor Rossmann also provided me with a great amount of assistance in evaluating some of the materials I synthesized. For all of their insight into crystallography and in collecting and solving structures for me, I would like to thank Professor Michael Takase and Larry Henling in the Beckmann Institute. In my lab I would like to thank many people for countless hours spent debating, bouncing ideas off of each other, maintaining and fixing a constant stream of broken equipment, and trying new ideas, as well as

ABSTRACT

The central theme of this thesis is the use of imidazolium-based organic structure directing agents (OSDAs) in microporous materials synthesis. Imidazoliums are advantageous OSDAs as they are relatively inexpensive and simple to prepare, show robust stability under microporous material synthesis conditions, have led to a wide range of products, and have many permutations in structure that can be explored. The work I present involves the use of mono-, di-, and triquaternary imidazolium-based OSDAs in a wide variety of microporous material syntheses. Much of this work was motivated by successful computational predictions (Chapter 2) that led me to continue to explore these types of OSDAs. Some of the important discoveries with these OSDAs include the following: 1) Experimental evaluation and confirmation of a computational method that predicted a new OSDA for pure-silica STW, a desired framework containing helical pores that was previously very difficult to synthesize. 2) Discovery of a number of new imidazolium OSDAs to synthesize zeolite RTH, a zeolite desired for both the methanol-to-olefins reaction as well as NO_X reduction in exhaust gases. This discovery enables the use of RTH for many additional investigations as the previous OSDA used to make this framework was difficult to synthesize, such that no large scale preparations would be practical. 3) The synthesis of pure-silica RTH by topotactic condensation from a layered precursor (denoted CIT-10), that can also be pillared to make a new framework material with an expanded pore system, denoted CIT-11, that can be calcined to form a new microporous material, denoted CIT-12. CIT-10 is also interesting since it is the first layered material to contain 8 membered rings through the layers, making it potentially useful in separations if delamination methods can be developed. 4) The synthesis of a new microporous material, denoted CIT-7 (framework code CSV) that contains a 2-dimensional system of 8 and 10 membered rings with a large cage at channel intersections. This material is especially important since it can be synthesized as a pure-silica framework under low-water, fluoride-mediated synthesis conditions, and as an aluminosilicate material under hydroxide mediated conditions. 5) The synthesis of high-

silica heulandite (HEU) by topotactic condensation as well as direct synthesis, demonstrating

new, more hydrothermally stable compositions of a previously known framework. 6) The synthesis

of germanosilicate and aluminophosphate LTA using a triquaternary OSDA. All of these materials

show the diverse range of products that can be formed from OSDAs that can be prepared by

straightforward syntheses and have made many of these materials accessible for the first time under

facile zeolite synthesis conditions.

TABLE OF CONTENTS

LIST OF FIGURES

LIST OF TABLES

Chapter 1. Introduction to Microporous Material Synthesis and Motivations

for the Use of Imidazolium Organic Structure Directing Agents

1.1 Introduction to microporous material synthesis

Microporous materials are crystalline solids with pores less than 2 nm (mesoporous materials

have pores from 2 to 50 nm) that are formed from three-dimensional networks of oxide

tetrahedra. Three-dimensional crystalline materials are formed when the oxide tetrahedra bond,

first assembling into what are referred to as secondary building units that then assemble into large

units to form regular, crystalline materials. A view of these various levels of order is shown in

Figure 1-1.
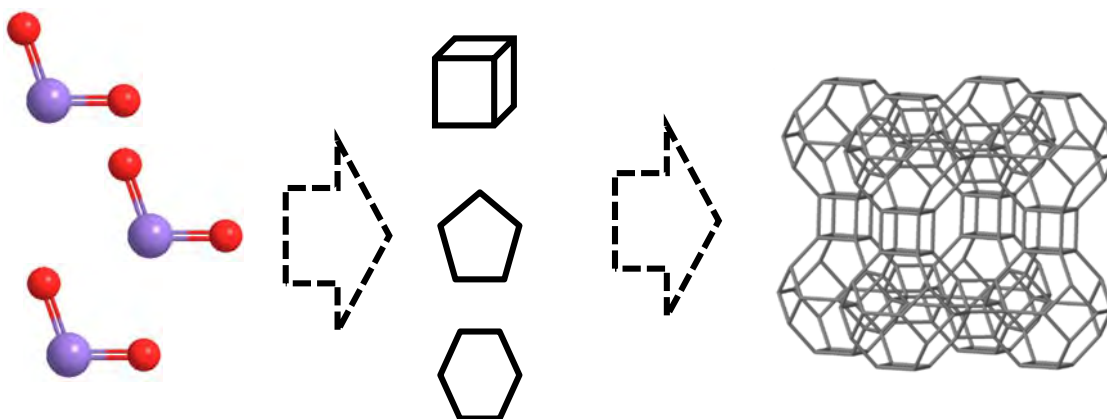
Figure 1-1. Microporous material levels of organization starting with oxides, which then assemble

into secondary building units and finally three-dimensional crystalline materials (LTA framework

from the IZA website).

There are currently recognized to be over 200 distinct microporous material frameworks, a

figure that has tripled in the past thirty years, out of an estimated hundreds of thousands (or

more) hypothetical frameworks.[1] In a neutral framework material the charge of the oxygen (-2) that bridges two metal atoms is balanced by the charge of the metal atoms. For example, in a pure-silica material, the Si^{4+} completely balances the oxygen charge, resulting in no net charge. Zeolites are aluminosilicate microporous materials where replacing the framework Si^{4+} with Al^{3+} results in a negative charge that is normally balanced by an alkali metal, alkaline earth metal, proton, ammonium cation or some other charged species. This charge imbalance can lead to catalytic activity or sites for adsorption. For example, if H^+ balances the charge, then acidic activity is observed. However, zeolites are only one type of molecular sieve. Aluminophosphates ($AlPO_4$) are another type of molecular sieve, in which Al^{3+} is balanced by P^{5+} to form a neutral structure. Again in these materials, catalytic activity can be obtained by replacing framework atoms to form charge mismatches. Examples of this are the replacement P^{5+} with Si^{4+} or Al^{3+} with Me^{2+} (where Me is any metal in a +2 oxidation state).[2,3]

The well-defined pore structure of molecular sieves allows them to serve in a wide variety of applications such as catalysis, ion exchange, and separations, where their shape selectivity and stability can lead to superior performance over other technologies.[4] The framework structures of a microporous material are normally described by their pore diameters and dimensionalities as well as internal cage sizes. The pores of a microporous material are determined by the number of oxide tetrahedral that circumscribe them. The smallest pore sizes that are considered to be accessible are circumscribed by 8 tetrahedral atoms, and are called 8-membered rings (MRs). Pore sizes generally range from 8 to 12 MRs (a few 14MR materials are known) and structures can have pores in 1, 2, or 3 directions and can have pores of more than one size in a single direction. Additionally, many frameworks contain internal cages and channel intersections that are larger than the pores that lead to them. This allows large reactive intermediates to form that cannot

escape the framework.

The motivation to develop new materials is strong as there normally is only a single structure and composition for satisfactory performance in a given application.[1] As microporous materials often exhibit robust hydrothermal stability they are used in a wide variety of demand processes such as fluidized catalytic cracking, reduction of NO_X in exhaust streams, and the methanol-to-olefins (MTO) reaction as a few examples. It is estimated that over 90% of chemical processes use a catalyst, with 80% being a heterogeneous catalyst, amounting to a global demand of $15 to $20 billion per year, motivating the economics behind the demand to innovate in these materials.[2]

Microporous materials occur as both nature minerals as well as synthetic materials. The synthetic materials are normally prepared under hydrothermal reaction conditions. They are prepared by combining inorganic elements (silica, alumina, germanium, boron, etc.), water, a mineralizing agent (inorganic or organic bases or fluoride), and possibly an organic structure directing agent (generally an amine or quaternary amine). These elements are then reacted under hydrothermal conditions (100 to 200°C) until a crystalline material forms.

The crystallization process is very complex, with many variables, and many excellent reviews are available that discuss current understanding in detail.[1,3–13] In general, the crystallization of high-silica materials is generally thought to proceed through the following steps, as studied experimentally for MFI using a variety of spectroscopic techniques.[13] First, a hydrophobic hydration sphere of silicate species forms around the OSDA. These hydration spheres then begin to order and aggregate, forming structures on the order of 1-10 nm. Crystal nucleation then occurs within these aggregates. Subsequently, additional hydration spheres join with the crystallized product, forming crystals and crystallites on the order of 10s of nanometers to microns. There are many additional factors which will influence the formation of a microporous material. Generally

the framework formed is thought to be determined by a combination of kinetic and thermodynamic factors. It has been determined experimentally that all molecular sieves are metastable relative to quartz, but only by a small range of 6.8-14.4 kJ/mol for a set of pure-silica frameworks investigated.[14] When combined with an experimental study of the interaction energies of OSDAs with frameworks, it was determined that neither the enthalpy nor entropy dominates the Gibbs free energy, and that the relatively small differences observed between frameworks suggests that kinetic factors are of major importance in determining the formation of microporous materials.[15]

The kinetics of microporous material formation are influenced by a wide range of variables such as water content, amount and type of mineralizing agent (hydroxide or fluoride), heteroatom identity and amount, inorganic cations, and OSDAs used. However, if all inorganic parameters are held relatively constant with only small pertubations, then the use of OSDAs can be seen to be one of the most important factors governing the synthesis of microporous materials; their use is considered to be the top reason for the explosive growth of discovery of new frameworks and compositions in recent years. OSDAs are normally alkylammonium cations, though phosphorous based compounds are known as well. The first OSDAs used in molecular sieve synthesis were simple quaternary ammonium compounds such as tetramethyl, tetraethyl, tetrapropyl, and tetrabutyl ammonium salts, which are normally employed in hydroxide form, but in some cases are used in the form of a halide salt. Since this time, a wide variety of amines have been investigated starting with the simple quaternization of commercially available amines and progressing to multi-step syntheses to produce ever more complex and tailored organics.[5]

The use of organics in molecular sieve synthesis has been described by Wagner and Davis[16] to fall into three broad categories: pore filling, structure directing, and templating. Pore filling occurs

when there is a weak interaction between the organic molecule and inorganic framework, with little match between the framework and organic being used. Pore filling is often observed with frameworks for which many different organics can be used, such as ZSM-48, which can be produced by at least 13 different organics, or with *BEA. Structure direction describes the situation where there are strong van der Waals interactions between the organic and framework, but is distinct from templating due to the absence of symmetry between the organic and framework. In the case of structure direction, the molecules often retain some degrees of freedom, but the strong interaction between organic and framework can be observed by ^{1}H-^{29}Si CPMAS NMR (in the case of a silica material). Templating occurs when both the organic and inorganic exhibit similar symmetry. The most commonly cited example of templating is ZSM-18, synthesized with a triquaternary ammonium cation (triquat), but it is still unknown if this is true templating.[9-11]

Many factors influence the utility of an organic in molecular sieve synthesis such as size, geometry, rigidity, and hydrophobicity. Some general trends compiled by Zones et al., which are observed between the type of organic used and the molecular sieve produced, are summarized in Table 1-1.[5] Besides geometric and rigidity considerations, the hydrophobicity of the organic is of paramount importance in determining whether it will be useful in making a molecular sieve. The hydrophobicity is generally characterized by measuring the partitioning between water and chloroform. For high silica materials, it has been found that organics of intermediate hydrophobicity are the most useful; these generally have C/N$^+$ ratios of 11 to 15.[5,8,13] This phenomenon has been explained by reasoning that if an organic is too hydrophilic, it will preferentially interact with the aqueous medium, and if it is too hydrophobic, it will phase separate.

Table 1-1. General trends between organic and molecular sieve formed[5].

Organic Type	Molecular Sieve Type
None	Dense phases
Small globular molecules	Clathrasils
Excess alkali metal cations	Layered structures, mordenite
Linear molecules	One-dimensional medium-pore zeolites
Branched molecules	Three-dimensional medium-pore zeolites
Large polycyclic molecules	Three-dimensional large-pore zeolites
Large globular molecules	One-dimensional large-pore zeolites
Large globular molecules + Al	Three-dimensional large-pore zeolites
Large globular molecules + B	Three-dimensional large-pore zeolites
Large globular molecules + Zn	VPI-8 a one-dimensional large-pore zeolite

While OSDAs have led to many new materials, their cost contributes a significant portion of the material cost that often cannot be recovered as they are generally removed using combustion.[7,8,17] In some systems, it is possible to partially replace high cost OSDAs with cheaper organics, such as with SSZ-13, where it has been shown that over 80% of the expensive trimethyl-N-1-adamantammonium hydroxide OSDA can be replaced with the much cheaper benzyltrimethylammonium hydroxide.[8] Alternatively, methods to synthesize the materials in the absence of OSDAs are being explored. However, this route can often lead to limited product compositions, and does not eliminate processing steps such as ion exchange and calcination.[18] Therefore, an attractive route to lower OSDA costs is to find simpler OSDAs to synthesize desired materials.

1.2 Previous Uses of Imidazolium OSDAs
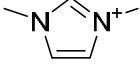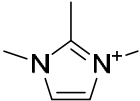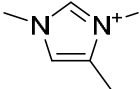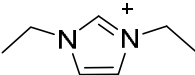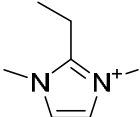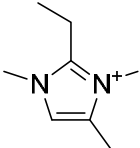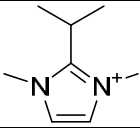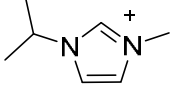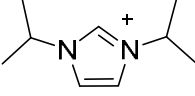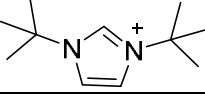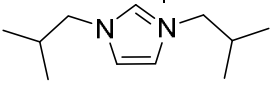
One class of potentially inexpensive OSDAs are based on imidazoliums, which are formed from

imidazoles. Industrially, imidazoles are produced using the Radziszewski reaction or by

dehydrogenation of imidazolines and are available in high purity; quaternary imidazoliums can

then be prepared by standard alkylation methods.[19] The facile synthesis of these molecules and

their industrial availability makes them attractive targets to explore as OSDAs in microporous

materials synthesis. Indeed, significant investigation has already been reported with these

molecules, and Table 1-2 shows some imidazoles along with the reported frameworks they form.

In addition to the limited set of simple, monoquaternary imidazoliums shown in Table 1-2,

diquaternary imidazoliums have been investigated and a variety of products have been found such

as MFI, TON, MTW, and NU-86.[19,20] A more novel type of microporous material synthesis

conditions has also been investigated with imidazoliums, where they are present as ionic liquids,

serving as both the OSDA and reaction medium. In this type of chemistry, a variety of new

materials have been observed.[20,21]

While the above listings are by no means comprehensive, they do demonstrate that

imidazoliums have already been investigated in molecular sieve synthesis. However, there are a

multitude of new combination of OSDAs as well as microporous material synthesis conditions to

explore. As imidazoles are simple, potentially inexpensive OSDAs, there is additional motivation

for their use in molecular sieve synthesis. Previously in our lab fairly comprehensive studies of

imidazolium OSDAs were performed by Raymond Archer[22,23] In addition to these diquaternary

imidazoliums have also been investigated and a variety of products have been found such as MFI,

TON, MTW, and NU-86.[24,25] While the above listings are by no means comprehensive, they do

demonstrate that imidazoliums have already been investigated in molecular sieve synthesis.

However, there are always a multitude of new combination of OSDAs as well as microporous

material synthesis conditions to explore. As imidazoles are simple, potentially inexpensive OSDAs

there is additional motivation for their use in molecular sieve synthesis.

Table 1-2. Some imidazolium based OSDAs and reported microporous material frameworks.

Imidazolium	Reported Products
	Pure-silica TON and ITW[22,26] Borosilicate TON[22] Borosilicate MTW[27] ZSM-22[28]
	Pure-silica ITW[26] ZSM-12 aluminosilicate[28,29]
	Pure-silica TON and ITW[26]
	Pure-silica TON[22] Borosilicate MFI[22]
	Aluminosilicate ZSM-5[28]
	Pure silica STW, ITW[30–32]
	Borosilicate MTW[27]
	ZSM-23[28] ZSM-48[28]
	ZSM-23[28] Pure-silica MTT[22] Borosilicate SSZ-70, MTW, MTT[22] Aluminosilicate MTT[22]
	Pure-silica *BEA[22]
	Pure-silica SSZ-70, MTW[22] Borosilicate SSZ-70[22] Aluminosilicate *BEA, MTW, SSZ-70[22]

1.3 Computational Prediction of OSDAs

Despite decades of experimental work with OSDAs, there is currently little ability to target specific frameworks through the prediction of OSDAs, and much discovery continues to be based on trial and error.[33] *A priori* prediction of OSDAs to target the synthesis of desired frameworks is a long-standing challenge in microporous materials synthesis.[34–37] Many predictive examples have relied on scoring the framework interaction energies with the OSDA or leveraging methods developed for the pharmaceutical industry to design organic molecules that bind to proteins.[1,35,37,38] While these procedures do allow for the *de novo* prediction of OSDAs, they suffer from many shortcomings; paramount among these is that many of the molecules can be difficult or impossible to synthesize.[35]

A new method to predict chemically synthesizable OSDAs for crystalline molecular sieves has recently been reported.[1] The key advantage of this method is that is makes molecules through known chemical reactions. Therefore, it is able to provide synthesis routes for all the molecules that it predicts. This method is one of the first that provides such comprehensive prediction of OSDAs.

1.4 Thesis Overview

The general themes of this thesis are the use of imidazolium OSDAs as well as the computational prediction of OSDAs. Chapter 2 discusses my work in providing the first experimental validation of the computational method to predict OSDAs for desired frameworks using known chemical reactions. This work led me to screen a number of imidazolium OSDAs

through various microporous material synthesis reactions. The first success of this work was

demonstrating that the computational technique can correctly predict chemically synthesizable

OSDAs for desired frameworks. The use of imidazoliums in this context is what motivated much of

the subsequent work exploring imidazolium OSDAs. Chapters 3 and 4 detail the synthesis of

aluminosilicate RTH using a variety of imidazolium OSDAs. The discovery of this structure direction

to RTH was an experimental finding during the course of screening reactions. It makes this

framework accessible across a wide compositional range using very simple OSDAs. Additionally,

reactivity for the MTO reaction is reported along with hydrothermal stability testing. Chapter 5

discusses synthesis of pure-silica RTH by topotactic condensation from a layered precursor

(denoted CIT-10), that can also be pillared to make a new framework material with an expanded

pore system, denoted CIT-11, that can be calcined to form a new microporous material, denoted

CIT-12. CIT-10 is also interesting since it is the first layered material to contain 8 membered rings

through the layers, making it potentially useful in separations if delamination methods can be

developed. Chapter 6 discusses the discovery of a new microporous material framework, denoted

CIT-7 (framework code CSV), which is made using a diquaternary OSDA based on

tetramethylimidazole. The framework contains a 2-dimensional system of 8 and 10MRs and can

be prepared across a wide range of compositions including pure-silica, aluminosilicate, and

titanosilicate materials. The structure of this material was solved by Dan Xie (Chevron Energy

Technology Company) using a combination of synchrotron powder x-ray diffraction and rotation

electron diffraction. Chapter 7 describes the synthesis of high-silica heulandite by direct synthesis

and topotactic condensation, using OSDAs similar to those used for CIT-7. Heulandite has long

been known as a natural mineral, but this work reports the framework at a much higher Si/Al

ratio, which should lead to a more robust framework. Chapter 8 details the first work

(chronologically) that I did with an imidazolium based OSDA. In this work a large, triquaternary OSDA was used to prepare the LTA framework across a range of compositions including $AlPO_4$, SAPO and germanosilicate materials. Finally, chapter 9 gives a short summary of this work and recommendations for future microporous material synthesis using imidazolium-based OSDAs. The appendix to this work contains references to other publications that I had during my time at Caltech that did not fit the theme of this thesis.

1.5 References

(1)   Pophale, R.; Daeyaert, F.; Deem, M. W. Computational Prediction of Chemically Synthesizable Organic Structure Directing Agents for Zeolites. *J. Mater. Chem. A* **2013**, *1* (23), 6750–6760.

(2)   Bravo-suárez, J. J.; Chaudhari, R. V; Subramaniam, B. Design of Heterogeneous Catalysts for Fuels and Chemicals Processing: An Overview. In *Novel Materials for Catalysis and Fuels Processing*; Bravo-Suárez, J. J., Kidder, M. K., Schwartz, V., Eds.; ACS Symposium Series; American Chemical Society: Washington, DC, 2013; Vol. 1132, pp 3–68.

(3)   Davis, M. E. The Quest For Extra-Large Pore, Crystalline Molecular Sieves. *Chem. - A Eur. J.* **1997**, *3* (11), 1745–1750.

(4)   Jiang, J.; Yu, J.; Corma, A. Extra-Large-Pore Zeolites: Bridging the Gap between Micro and Mesoporous Structures. *Angew. Chem. Int. Ed. Engl.* **2010**, *49* (18), 3120–3145.

(5)   Weitkamp, J. Zeolites and Catalysis. *Solid State Ionics* **2000**.

(6)   Moliner, M.; Martínez, C.; Corma, A. Multipore Zeolites: Synthesis and Catalytic Applications. *Angew. Chemie Int. Ed.* **2015**, *54* (12), 3560–3579.

(7)   Zones, S. I.; Lee, H.; Davis, M. E.; Casci, J.; Burton, A. W. Strategies in Developing Routes to Commercialization of Novel High Silica Zeolites. *Stud. Surf. Sci. Catal.* **2005**, *158*, 1–10.

(8)   Zones, S. I. Translating New Materials Discoveries in Zeolite Research to Commercial Manufacture. *Microporous Mesoporous Mater.* **2011**, *144* (1-3), 1–8.

(9)   Martínez, C.; Corma, A. Inorganic Molecular Sieves: Preparation, Modification and Industrial Application in Catalytic Processes. *Coord. Chem. Rev.* **2011**, *255* (13-14), 1558–1580.

(10)   Cundy, C. S.; Cox, P. A. The Hydrothermal Synthesis of Zeolites: History and Development from the Earliest Days to the Present Time. *Chem. Rev.* **2003**, *103* (3), 663–702.

(11)   Cundy, C. S.; Cox, P. A. The Hydrothermal Synthesis of Zeolites: Precursors, Intermediates and Reaction Mechanism. *Microporous Mesoporous Mater.* **2005**, *82* (1-2), 1–78.

(12)   Corma, A.; Davis, M. E. Issues in the Synthesis of Crystalline Molecular Sieves: Towards the Crystallization of Low Framework-Density Structures. *ChemPhysChem* **2004**, *5* (3), 304–313.

(13)   De Moor, P.-P. E. A.; Beelen, T. P. M.; Komanschek, B. U.; Beck, L. W.; Wagner, P.; Davis, M. E.; van Santen, R. A. Imaging the Assembly Process of the Organic-Mediated Synthesis of a Zeolite. *Chem. - A Eur. J.* **1999**, *5* (7), 2083–2088.

(14)   Piccione, P. M.; Laberty, C.; Yang, S.; Camblor, M. a.; Navrotsky, A.; Davis, M. E. Thermochemistry of Pure-Silica Zeolites. *J. Phys. Chem. B* **2000**, *104* (43), 10001–10011.

(15)   Piccione, P. M.; Yang, S.; Navrotsky, A.; Davis, M. E. Thermodynamics of Pure-Silica Molecular Sieve Synthesis. *J. Phys. Chem. B* **2002**, *106* (14), 3629–3638.

(16)   Wagner, P.; Davis, M. E. Towards the Rational Design of Zeolite Frameworks. In *Supramolecular Organization and Materials Design*; Jones, W., Rao, C. N. R., Eds.; Cambridge University Press: Cambridge, 2002; pp 83–102.

(17)   Zones, S. I.; Hwang, S.-J. Synthesis of High Silica Zeolites Using a Mixed Quaternary Ammonium Cation, Amine Approach: Discovery of Zeolite SSZ-47. *Chem. Mater.* **2002**, *14* (1), 313–320.

(18) Iyoki, K.; Itabashi, K.; Okubo, T. Progress in Seed-Assisted Synthesis of Zeolites without Using Organic Structure-Directing Agents. *Microporous Mesoporous Mater.* **2013**, *8* (7), 1419–1427.

(19) Ebel, K.; Koehler, H.; Gamer, A.; Jackh, R. Imidazole and Derivatives. In *Ullmann's Encyclopedia of Industrial Chemistry*; Wiley-VCH Verlag GmbH & Co. KGaA: Weinheim, Germany, 2000; pp 637–645.

(20) Parnham, E. R.; Morris, R. E. Ionothermal Synthesis of Zeolites, Metal-Organic Frameworks, and Inorganic-Organic Hybrids. *Acc. Chem. Res.* **2007**, *40* (10), 1005–1013.

(21) Parnham, E. R.; Morris, R. E. Ionothermal Synthesis Using a Hydrophobic Ionic Liquid as Solvent in the Preparation of a Novel Aluminophosphate Chain Structure. *J. Mater. Chem.* **2006**, *16* (37), 3682.

(22) Archer, R. H.; Zones, S. I.; Davis, M. E. Imidazolium Structure Directing Agents in Zeolite Synthesis: Exploring Guest/host Relationships in the Synthesis of SSZ-70. *Microporous Mesoporous Mater.* **2010**, *130* (1-3), 255–265.

(23) Archer, R. H. Molecular Sieve Synthesis Using Imidazolium Structure Directing Agents, Caltech, 2009.

(24) Rojas, A.; Gómez-Hortigüela, L.; Camblor, M. a. Zeolite Structure Direction by Simple Bis(methylimidazolium) Cations: The Effect of the Spacer Length on Structure Direction and of the Imidazolium Ring Orientation on the 19F NMR Resonances. *J. Am. Chem. Soc.* **2012**, *134* (8), 3845–3856.

(25) Zones, S. I.; Hwang, S.-J.; Elomari, S.; Ogino, I.; Davis, M. E.; Burton, A. W. The Fluoride-Based Route to All-Silica Molecular Sieves; a Strategy for Synthesis of New Materials Based upon Close-Packing of Guest–host Products. *Comptes Rendus Chim.* **2005**, *8* (3-4), 267–282.

(26) Rojas, A.; Martínez-Morales, E.; Zicovich-Wilson, C. M.; Camblor, M. A. Zeolite Synthesis in Fluoride Media: Structure Direction toward ITW by Small Methylimidazolium Cations. *J. Am. Chem. Soc.* **2012**, *134* (4), 2255–2263.

(27) S.I. Zones, L.T. Yuen, S.D. Toto, U.S. Patent 5,187,132, 1993. US 5,187,132.

(28) Zones, S. I. Synthesis of Pentasil Zeolites from Sodium Silicate Solutions in the Presence of Quaternary Imidazole Compounds. *Zeolites* **1989**, *9* (6), 458–467.

(29) Zones, S. I. S.I. Zones. U.S. Patent 4,483,835, 1984. US4483835 A, 1984.

(30) Rojas, A.; Camblor, M. A. A Pure Silica Chiral Polymorph with Helical Pores. *Angew. Chem. Int. Ed. Engl.* **2012**, *51* (16), 3854–3856.

(31) Rojas, A.; Arteaga, O.; Kahr, B.; Camblor, M. a. Synthesis, Structure, and Optical Activity of HPM-1, a Pure Silica Chiral Zeolite. *J. Am. Chem. Soc.* **2013**, *135* (32), 11975–11984.

(32) Rojas, A.; Camblor, M. A. Structure-Direction in the Crystallization of ITW Zeolite Using 2–ethyl– 1,3,4–trimethylimidazolium. *Dalt. Trans.* **2014**.

(33) Zones, S. I.; Nakagawa, Y.; Lee, G. S.; Chen, C. Y.; Yuen, L. T. Searching for New High Silica Zeolites through a Synergy of Organic Templates and Novel Inorganic Conditions. *Microporous Mesoporous Mater.* **1998**, *21* (4-6), 199–211.

(34) Moliner, M.; Rey, F.; Corma, A. Towards the Rational Design of Efficient Organic Structure-Directing Agents for Zeolite Synthesis. *Angew. Chem. Int. Ed. Engl.* **2013**, *52* (52), 13880–13889.

(35) Lewis, D. W.; Willock, D. J.; Catlow, C. R. A.; Thomas, J. M.; Hutchings, G. J. De Novo Design of Structure-Directing Agents for the Synthesis of Microporous Solids. *Nature* **1996**, *382* (6592), 604–606.

(36) Lewis, D. W.; Sankar, G.; Wyles, J. K.; Thomas, J. M.; Catlow, C. R. A.; Willock, D. J. Synthesis of

a Small-Pore Microporous Material Using a Computationally Designed Template. *Angew. Chem. Int. Ed. Engl.* **1997**, *36* (23), 2675–2677.

(37) Lewis, D. W.; Freeman, C. M.; Catlow, C. R. A. Predicting the Templating Ability of Organic Additives for the Synthesis of Microporous Materials. *J. Phys. Chem.* **1995**, *99* (28), 11194–11202.

(38) Schmitt, K. D.; Kennedy, G. J. Toward the Rational Design of Zeolite Synthesis: The Synthesis of Zeolite ZSM-18. *Zeolites* **1994**, *14* (8), 635–642.

Chapter 2. Synthesis of a Specified, Silica Molecular Sieve Using

Computationally Predicted Organic Structure Directing Agents

2.1 Abstract:

Crystalline molecular sieves are used in numerous applications, where the properties

exploited for each technology are the direct consequence of structural features. New materials are

typically discovered by trial and error, and in many instances, organic structure-directing agents

(OSDAs) are used to direct their formation. Here, we report the first successful synthesis of a

specified molecular sieve through the use of an OSDA that is predicted from a recently developed

computational method that constructs chemically synthesizable OSDAs. Pentamethylimidazolium

is computationally predicted to have the largest stabilization energy in the STW framework, and is

experimentally shown to strongly direct the synthesis of pure-silica STW. Other OSDAs with lower

stabilization energies did not form STW. The general methodology demonstrated here to create

STW may lead to new, simpler OSDAs for existing frameworks and provide a way to predict OSDAs

for desired, theoretical frameworks.

2.2 Introduction

Molecular sieves are crystalline, microporous materials (pores less than 2 nm) that consist of

three-dimensional networks of oxide tetrahedra. These materials are used in a wide variety of

applications, and at present, over 200 different frameworks have been identified.[1,2] In many

applications, only a single structure will give optimal performance. This specificity in the structure-

property relationships is one of the major driving forces behind much of the research directed at

creating new structures.[3] It is estimated from theory that there are well over a million possible

frameworks,[4] but of the 200 that have been synthesized, fewer than 10% are in commercial use.[5,6]

As an example of the utility within these possible frameworks, recent studies on carbon capture

have identified numerous predicted frameworks with calculated performance superior to known

materials.[7] Thus, the motivation to create these structures remains high.

The crystallization of a microporous material is a complicated process that is still not well

understood.[2,8–10] Through the use of organic structure directing agents (OSDAs), most that are

charged alkylammonium cations, there is some level of "design", e.g., there is a correlation

between the shape and size of the OSDA used and the resulting framework.[2,11–13] Despite

extensive work in this area, there is currently little ability to target specific frameworks through

the prediction of OSDAs, and much discovery continues to be based on trial and error,[14] which has

only provided a small fraction of the many possible predicted frameworks

A priori prediction of OSDAs to target the synthesis of desired frameworks is a long-standing

challenge in microporous materials synthesis.[2,15–17] Many previous predictive examples have relied

on scoring the framework interaction energies with the OSDA or leveraging methods developed

for the pharmaceutical industry to design organic molecules that bind to proteins.[3,15,17,18] While

these procedures do allow for the *de novo* prediction of OSDAs, they suffer from many

shortcomings; paramount among these is that many of the molecules can be difficult or

impossible to synthesize.[15] A new method to predict chemically synthesizable OSDAs for crystalline

molecular sieves has recently been reported.[3] Here, we provide the first experimental validation

for this new method using fluoride-mediated, pure-silica chemistry to create pure-silica

frameworks. This system is selected to avoid the use of inorganic cations, heteroatoms such as

aluminum, and other variables commonly encountered in microporous materials synthesis, in

order to more clearly test the structure-property relationships between the framework and the

OSDA that is predicted by the new method.[8,19] To illustrate the methodology, we synthesized

pure-silica STW (HPM-1).[20,21] HPM-1 was selected as the target framework as prior to our work

only a single OSDA (**2**) has been reported to produce HPM-1 under a very narrow range of

synthesis conditions.

2.3 Results and Discussions

The previously published computational method was used to screen an evolving population of

potential OSDAs.[3] The population was created by the application of known organic chemistry

reactions to a library of available reagents using a standard reagent library and a custom library of

imidazole based organics. Each member of the evolving population of potential OSDAs was

evaluated by calculating its stabilization energy in STW, which is the average difference in energy

between the OSDA/STW composite and the isolated OSDA and the empty STW.   A subset of

particularly interesting compounds were subjected to a further eight evaluations of the

stabilization energy to confirm results from a single run, and the compounds selected for

experimental evaluation are shown in Figure 2-1, entries 1-6 (2 is reported to form HPM-1).

Synthesis reactions were conducted with OSDAs 1-6 at temperatures and H_2O/SiO_2 ratios

typical for pure-silica, fluoride-mediated syntheses. In general, reactions were allowed to proceed

until a crystalline product was observed or all the reaction material had been consumed by taking

aliquots for analysis. A summary of the experimental results is provided in Table 2-1, and a

complete listing of experimental results is in the Supplementary Information (SI) for this chapter

along with the experimental and characterization details. Representative powder X-ray diffraction

(XRD) patterns for each of the as-made materials are shown in Fig. S1.
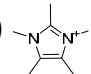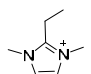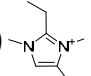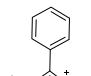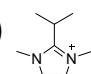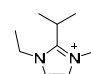
Molecule	Energy	Molecule	Energy
1)	-16.5	4)	-15.6
2)	-16.5	5)	-14.8
3)	-15.7	6)	-14.2

Figure 2-1. OSDAs used to prepare pure-silica molecular sieves and their calculated stabilization energy in the STW frramework (stabilzation energy in kJ/(mol Si)).

Table 2-1. Summary of experimental results (a complete listing is in the SI).

OSDA	H_2O/SiO_2	Temperature (°C)	Time (days)	Results
1	4, 7	140, 160, 175	5-23	STW
	14	140, 175	35, 16	U, Dense
	14	160	7	STW
2	4	140, 160, 175	40, 16, 16	STW
	7	140, 160	70, 41	STW
	7	175	20	HPM-2[22]
	14	140, 160	70, 47	HPM-2[22]
	14	175	20	Dense
3	4, 7, 14	140, 160, 175	9-80	MTW, STF, A
4	4	160	16	STW+ITW
	7, 14	160	22-44	ITW, MTW
	4, 7, 14	140, 175	10-49	ITW, MTW, STF, A
5	4, 7, 14	140, 160, 175	13-60	MFI, A
6	4, 7, 14	140, 160, 175	5-56	STF, A

A=Amorphous, U=Unidentified

The computational screening identified **1** as the only molecule with a stabilization energy comparable to the published OSDA, **2**. When **1** was used in the synthesis reactions, it was shown to be more strongly directing towards STW, as it produced this framework across a greater range of synthesis conditions and in shorter times. In order to conclusively demonstrate that **1** was responsible for producing HPM-1 and not a decomposition fragment, ^{13}C CP-MAS NMR was used to determine that **1** was occluded intact (Fig. S2). This result provides the first experimental evidence that validates the new computational methodology for predicting chemically synthesizable OSDAs.

As **1** and **2** have similar stabilization energies in HPM-1, additional factors must account for the reasons that **1** forms HPM-1 across a greater range of synthesis conditions. In contrast to **2**, **1** does not possess any rotational degrees of freedom. OSDAs with many conformational degrees of freedom tend to be less effective at structure direction than OSDAs with fewer conformational degrees of freedom.[9,23] The rotational degrees of freedom in **2** likely allow many different conformations in solution, and therefore lead to a decrease in the probability that a molecule has the correct conformation to structure direct HPM-1. Due to this reason, and since the stabilization energies of compounds **1** and **2** are roughly the same, we expect the stabilization free energy of compound **1** will be more favorable than that of compound **2**.

A critical parameter of the computational algorithm used in this work is the occupancy of OSDAs per unit cell, as this is treated as a fixed value when determining the stabilization energies. With **1**, we iterated across OSDA occupancies and found stabilization energy values of -11.3, -14.2, and -16.5 kJ/(mol Si), for 4, 5, and 6 OSDAs per unit cell, respectively. It was not possible to fit 7 OSDAs per unit cell. Thermogravimetric analysis (TGA) showed that the HPM-1 made using **1** was 20.7 wt% organic and fluoride (Fig. S3). The theoretical mass loss assuming 6 molecules per unit

cell and one fluoride anion per OSDA molecule is 20.0 wt%, which agrees well with the

experimental value. If either 5 or 7 molecules of **1** per unit cell were occluded in HPM-1, the mass

losses would be 17.2 wt% and 22.6 wt%, respectively. The fact that the occupancy determined by

the algorithm matches the experimental value provides another point of validation for the

computational screening method. A view of the conformation of the organic in the STW

framework calculated from the molecular simulations is shown in Figure 2-2.
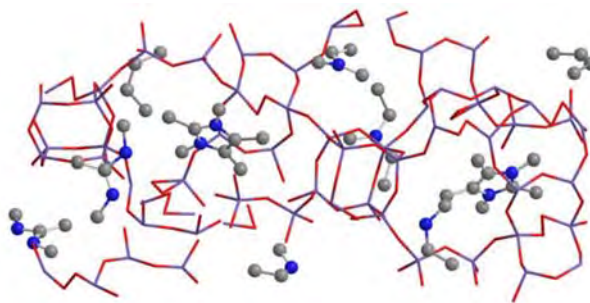
Figure 2-2. Unit cell of STW with the conformation of the occluded pentamethylimidazolium

determined from molecular simulations.

All of the other OSDAs selected for experimental validation had stabilization energies at least

0.8 kJ/(mol Si) less favorable than **2**. They were evaluated to elucidate the range in stabilization

energies between OSDA and the target structure required for structure direction of the predicted

phase. Based on our accumulated experience with calculated energies, differences of 2 kJ/(mol Si)

are considered significant. With the four remaining OSDAs, HPM-1 was never observed as a pure

product, though it was encountered as a phase mixture with OSDA **4** (see complete results in the

SI). Our molecular sieve synthesis results agree with those from other studies involving OSDAs that

demonstrate small structural differences can completely change product selectivity.[24–27]

In addition to STW, several other products were observed, including ITW, MFI, MTW, STF, and

others that could not be identified or consisted of phase mixtures or organosilicate layered materials. The synthesis of ITW, MFI, and MTW is not surprising, as these are commonly observed in microporous materials syntheses and have been previously reported with similar OSDAs.[25,28,29] Pure-silica STF would not be expected as a product using the OSDAs in this study, but as our work highlights, stabilization can occur under conditions that may not be apparent from simple visual comparisons of OSDAs.[12,30,31]

In conclusion, we have demonstrated experimental validation of a computational method that is not only able to screen a large number of OSDAs, but is also able to construct OSDAs in an automated manner using known chemical reactions so that they will be synthetically accessible. The results of our study have provided experimental evidence that this method is able to (i) successfully predict OSDAs for a specified framework using known chemical reactions, and (ii) yield predicted occupancies that are measured in the products. The ability to provide theoretical guidance to the creation of a crystalline molecular sieve is valuable, as it reduces the scope of an impossibly large synthetic problem in the quest to synthesize a desired framework. As this method has been applied to prepare a framework that is difficult to access, it is likely that the method can be extended to other, desired frameworks.

2.4 Experimental Section

All computations were conducted using the method of reference 3. The Dreiding forcefield was used in the GULP molecular modeling program to calculate the stabilization energies. Six OSDAs were first placed in sterically optimal locations in the zeolite unit cell and energy minimized. Molecular dynamics was performed at 343 K for 30 ps, and averages were collected over the last 5 ps of the run. A custom library that contained the four alkylating reagents

methyliodide, ethyliodide, 1-propyliodide, and 2-propyliodide, as well as 47 imidazole

derivatives available from Sigma-Aldrich, 17 additional commercially available imidazoles, and 25

imidazolium based OSDAs that could be synthesized from commercially available materials in one

or two steps was used.

Detailed synthesis and characterization details for each of the experimentally tested OSDAs

can be found in the SI. In general, organics were quaternized with iodomethane or iodoethane,

purified using recrystallization, exchanged to hydroxide form using hydroxide exchange gel, and

titrated.

Pure silica syntheses were performed using standard methods, and details can be found in the

SI. The final molar ratios of the gel were: $1SiO_2:0.5ROH:0.5HF:xH_2O$ (x=4, 7, 14). Each composition

was run at 140, 160, and 175°C and aliquots were periodically taken by first quenching the reactor

in water and then removing enough material for powder X-ray diffraction (PXRD).

2.5 Acknowledgements

2.6 References

(1)   Davis, M. E. Ordered Porous Materials for Emerging Applications. *Nature* **2002**, *417* (6891),

      813–821.

(2)   Moliner, M.; Rey, F.; Corma, A. Towards the Rational Design of Efficient Organic Structure-

Directing Agents for Zeolite Synthesis. *Angew. Chem. Int. Ed. Engl.* **2013**, *52* (52), 13880–13889.

(3) Pophale, R.; Daeyaert, F.; Deem, M. W. Computational Prediction of Chemically Synthesizable Organic Structure Directing Agents for Zeolites. *J. Mater. Chem. A* **2013**, *1* (23), 6750–6760.

(4) Pophale, R.; Cheeseman, P.; Deem, M. W. A Database of New Zeolite-like Materials. *Phys. Chem. Chem. Phys.* **2011**, *13* (27), 12407–12412.

(5) Vermeiren, W.; Gilson, J.-P. Impact of Zeolites on the Petroleum and Petrochemical Industry. *Top. Catal.* **2009**, *52* (9), 1131–1161.

(6) Zones, S. I. Translating New Materials Discoveries in Zeolite Research to Commercial Manufacture. *Microporous Mesoporous Mater.* **2011**, *144* (1-3), 1–8.

(7) Lin, L.-C.; Berger, A. H.; Martin, R. L.; Kim, J.; Swisher, J. a; Jariwala, K.; Rycroft, C. H.; Bhown, A. S.; Deem, M. W.; Haranczyk, M.; Smit, B. In Silico Screening of Carbon-Capture Materials. *Nat. Mater.* **2012**, *11* (7), 633–641.

(8) Cundy, C. S.; Cox, P. A. The Hydrothermal Synthesis of Zeolites: Precursors, Intermediates and Reaction Mechanism. *Microporous Mesoporous Mater.* **2005**, *82* (1-2), 1–78.

(9) Corma, A.; Davis, M. E. Issues in the Synthesis of Crystalline Molecular Sieves: Towards the Crystallization of Low Framework-Density Structures. *ChemPhysChem* **2004**, *5* (3), 304–313.

(10) De Moor, P.-P. E. A.; Beelen, T. P. M.; Komanschek, B. U.; Beck, L. W.; Wagner, P.; Davis, M. E.; van Santen, R. A. Imaging the Assembly Process of the Organic-Mediated Synthesis of a Zeolite. Chem. - A Eur. J. 1999, 5 (7), 2083–2088.

(11) Nakagawa, Y.; Lee, G. S.; Harris, T. V; Yuen, L. T.; Zones, S. I. Guest/host Relationships in Zeolite Synthesis: Ring-Substituted Piperidines and the Remarkable Adamantane Mimicry by 1-Azonio Spiro [5.5] Undecanes. *Microporous Mesoporous Mater.* **1998**, *22* (1-3), 69–85.

(12) Wagner, P.; Nakagawa, Y.; Lee, G. S.; Davis, M. E.; Elomari, S.; Medrud, R. C.; Zones, S. I. Guest/Host Relationships in the Synthesis of the Novel Cage-Based Zeolites SSZ-35, SSZ-36, and SSZ-39. *J. Am. Chem. Soc.* **2000**, *122* (2), 263–273.

(13) Burton, A.; Zones, S. Organic Molecules in Zeolite Synthesis: Their Preparation and Structure-Directing Effects. *Stud. Surf. Sci. Catal.* **2007**, *168*, 137–179.

(14) Zones, S. I.; Nakagawa, Y.; Lee, G. S.; Chen, C. Y.; Yuen, L. T. Searching for New High Silica Zeolites through a Synergy of Organic Templates and Novel Inorganic Conditions. *Microporous Mesoporous Mater.* **1998**, *21* (4-6), 199–211.

(15) Lewis, D. W.; Willock, D. J.; Catlow, C. R. A.; Thomas, J. M.; Hutchings, G. J. De Novo Design of Structure-Directing Agents for the Synthesis of Microporous Solids. *Nature* **1996**, *382* (6592), 604–606.

(16) Lewis, D. W.; Sankar, G.; Wyles, J. K.; Thomas, J. M.; Catlow, C. R. A.; Willock, D. J. Synthesis of a Small-Pore Microporous Material Using a Computationally Designed Template. *Angew. Chem. Int. Ed. Engl.* **1997**, *36* (23), 2675–2677.

(17) Lewis, D. W.; Freeman, C. M.; Catlow, C. R. A. Predicting the Templating Ability of Organic Additives for the Synthesis of Microporous Materials. *J. Phys. Chem.* **1995**, *99* (28), 11194–11202.

(18) Schmitt, K. D.; Kennedy, G. J. Toward the Rational Design of Zeolite Synthesis: The Synthesis of Zeolite ZSM-18. *Zeolites* **1994**, *14* (8), 635–642.

(19) Zones, S. I.; Nakagawa, Y.; Yuen, L. T.; Harris, T. V. Guest/Host Interactions in High Silica Zeolite Synthesis: [5.2.1.0 2.6]Tricyclodecanes as Template Molecule. *J. Am. Chem. Soc.* **1996**, *118* (32), 7558–7567.

(20) Rojas, A.; Arteaga, O.; Kahr, B.; Camblor, M. a. Synthesis, Structure, and Optical Activity of

HPM-1, a Pure Silica Chiral Zeolite. *J. Am. Chem. Soc.* **2013**, *135* (32), 11975–11984.

(21) Rojas, A.; Camblor, M. A. A Pure Silica Chiral Polymorph with Helical Pores. *Angew. Chem. Int. Ed. Engl.* **2012**, *51* (16), 3854–3856.

(22) Rojas, A.; Camblor, M. a. HPM-2, the Layered Precursor to Zeolite MTF. *Chem. Mater.* **2014**, *26* (2), 1161–1169.

(23) Shantz, D. F.; Lobo, R. F. Guest-Host Interactions in Zeolites as Studied by NMR Spectroscopy: Implications in Synthesis, Catalysis and Separations. *Top. Catal.* **1999**, *9*, 1–11.

(24) Zones, S. I.; Burton, A. W.; Lee, G. S.; Olmstead, M. M. A Study of Piperidinium Structure-Directing Agents in the Synthesis of Silica Molecular Sieves under Fluoride-Based Conditions. *J. Am. Chem. Soc.* **2007**, *129* (29), 9066–9079.

(25) Rojas, A.; Martínez-Morales, E.; Zicovich-Wilson, C. M.; Camblor, M. A. Zeolite Synthesis in Fluoride Media: Structure Direction toward ITW by Small Methylimidazolium Cations. *J. Am. Chem. Soc.* **2012**, *134* (4), 2255–2263.

(26) Wang, Z.; Yu, J.; Xu, R. Needs and Trends in Rational Synthesis of Zeolitic Materials. *Chem. Soc. Rev.* **2012**, *41* (5), 1729–1741.

(27) Jackowski, A.; Zones, S. I.; Hwang, S.-J.; Burton, A. W. Diquaternary Ammonium Compounds in Zeolite Synthesis: Cyclic and Polycyclic N-Heterocycles Connected by Methylene Chains. *J. Am. Chem. Soc.* **2009**, *131* (3), 1092–1100.

(28) S.I. Zones, L.T. Yuen, S.D. Toto, U.S. Patent 5,187,132, 1993. US 5,187,132.

(29) Zones, S. I. S.I. Zones. U.S. Patent 4,483,835, 1984. US4483835 A, 1984.

(30) Villaescusa, L. A.; Barrett, P. A.; Camblor, M. A. Synthesis and Structure of ITQ-9: A New Microporous SiO2 Polymorph. *Chem. Commun.* **1998**, No. 21, 2329–2330.

(31) Camblor, M.; Villaescusa, L.; Diaz-Cabanas, M. Synthesis of All-Silica and High-Silica Molecular

Sieves in Fluoride Media. *Top. Catal.* **1999**, *9*, 59–76.

2.7 Supporting Information for Chapter 2

Experimental Details

Unless otherwise noted all reagents were purchased from Sigma-Aldrich and were used as received. Hydroxide ion exchanges were performed using Supelco Dowex Monosphere 550A UPW hydroxide exchange resin with an exchange capacity of 1.1 meq/mL. Titrations were performed using a Mettler-Toledo DL22 autotitrator using 0.01 M HCl as the titrant. All liquid NMR spectra were recorded with a 500 MHz Spectrometer.

The ^{13}C CP-MAS NMR was recorded using a Bruker Avance 200 MHz spectrometer with a 7 mm rotor at a spinning rate of 4 kHz and were conducted in a 4.7 T magnetic field corresponding to Larmor frequencies of 200 MHz and 50.29 MHz for ^1H and ^{13}C respectively. The ^{13}C spectra are referenced to adamantane as a secondary external standard relative to tetramethylsilane.

All TGA/DSC measurements were performed on Netzsch STA 449C Jupiter. Unless otherwise noted samples were heated in air to 900°C at a rate of 1 K/min.

All argon isotherms were performed at 87.45 K using a Quantachrome Autosorb iQ and were conducted using a quasi-equilibrium, volumetric technique.

All powder X-ray diffraction characterization was conducted on a Rigaku MiniFlex II with Cu K_α radiation.

Microporous Materials Synthesis

A general synthesis procedure was as follows. Tetraethylorthosilicate (TEOS) was added to the organic in its hydroxide form. The container was closed and stirred for at least 12 hours to allow for complete hydrolysis. The lid was then removed and the ethanol and an appropriate amount of water were allowed to evaporate under a stream of air. Composition was monitored

gravimetrically. It was assumed that all the ethanol evaporated along with the water. Additional water was added as necessary and then aqueous HF was added and the mixture was stirred by hand until a homogenous gel was obtained. (Caution: Use appropriate PPE, ventilation, and other safety measures when working with HF.) In situations where $H_2O/SiO_2=4$, an additional evaporation step was used after the addition of HF. The final molar ratios of the gel were:

$1SiO_2:0.5ROH:0.5HF:xH_2O$ (x=4, 7, 14).

The autoclave was sealed and placed in a rotating oven, and each composition was run at 140, 160, and 175°C. Aliquots of the material were taken periodically by first quenching the reactor in water and then removing enough material for powder X-ray diffraction (PXRD).

OSDA Synthesis

1 was synthesized by dissolving 1,2,4,5-tetramethylimidazole (TCI Chemicals) in methanol and then cooling in a dry ice bath. A three-fold molar excess of iodomethane was then slowly added (Caution: Highly exothermic reaction!) and the mixture was then slowly warmed to room temperature and stirred for one day. The solvent and excess iodomethane were then removed using rotary evaporation (Caution: Highly toxic vapors present, use appropriate precautions) and the product was recrystallized from acetone. The structure was verified using ^1H and ^{13}C NMR (D_2O) and the product was converted from the iodide to the hydroxide form using hydroxide exchange resin in water. ^1H-NMR (500 MHz, D_2O): δ 3.60 (s, 6H), 2.54 (s, 3H), 2.20 (s, 6H). ^{13}C-NMR (125 MHz, D_2O): δ 7.99, 9.76, 31.58, 125.42, 142.21.

2 was synthesized by the method reported by Camblor and co-workers.

3 was synthesized by exhaustive methylation of 2-isopropylimidazole (TCI Chemicals) in acetonitrile at reflux in the presence of potassium bicarbonate. The solvent was removed using rotary evaporation and the product was separated using chloroform. The product was

recrystallized from acetone. ^{1}H-NMR (500 MHz, D$_2$O): δ 1.44 (d, 6H), 3.60 (7, 1H), 3.84 (s, 6H), 7.23 (s, 2H). ^{13}C-NMR (125 MHz, D$_2$O): δ 17.55, 24.79, 35.68, 122.65, 149.69.

4 was synthesized exhaustive methylation of 2-ethylimidazole (TCI Chemicals) in acetonitrile at reflux in the presence of potassium bicarbonate. The solvent was removed using rotary evaporation and the product was separated using chloroform. The product was recrystallized from acetone. ^{1}H-NMR (500 MHz, D$_2$O): δ 1.28 (t, 3H), 3.03 (q, 2H), 3.83 (s, 6H), 7.32 (s, 2H). ^{13}C-NMR (125 MHz, D$_2$O): δ 9.92, 16.59, 34.71, 122.07, 148.16.

5 was synthesized from 2-phenylimidazole (TCI Chemicals) and an excess of ethyl iodide in chloroform at reflux in the presence of potassium bicarbonate. The solvent was removed using rotary evaporation and the product was separated using chloroform. The product was recrystallized from acetone. ^{1}H-NMR (500 MHz, D$_2$O): δ 1.35 (t, 6H), 4.03 (q, 4H), 7.63 (s, 2H), 7.64-7.77 (phenyl aromatic protons). ^{13}C-NMR (125 MHz, D$_2$O): δ 14.73, 43.94, 121.39, 129.73, 130.35, 132.62, 144.05.

6 was synthesized in two steps. First a stoichiometric amount of methyl iodide was added to 2-isopropylimidazole in acetonitrile along with 2 molar equivalents of KOH and then stirred for 4 hours at room temperature. The solvent was removed using rotary evaporation and the product was extracted with chloroform 3 times, and then washed with water and dried with magnesium sulfate. An excess of ethyl iodide was added and refluxed overnight. The solvent was removed using rotary evaporation, and the product was recrystallized from acetone. ^{1}H-NMR (500 MHz, D$_2$O): δ 1.43-1.46 (m, 9H), 3.62 (M, 1H), 3.86 (s, 3H), 4.22 (q, 2H), 7.26 (d, 1H), 7.32 (d, 1H). ^{13}C-NMR (125 MHz, D$_2$O): δ 20.28, 23.11, 29.85, 40.97, 125.75, 128.49, 154.47.

XRD

Products were prepared by washing with water and acetone consecutively and collecting the

products via centrifugation and then drying at 105°C. Products were ground to a fine powder

before XRD characterization. All PXRD characterization was conducted on a Rigaku MiniFlex II with

Cu K$_\alpha$ radiation. Diffraction patterns were then compared to known spectra to determine

products.
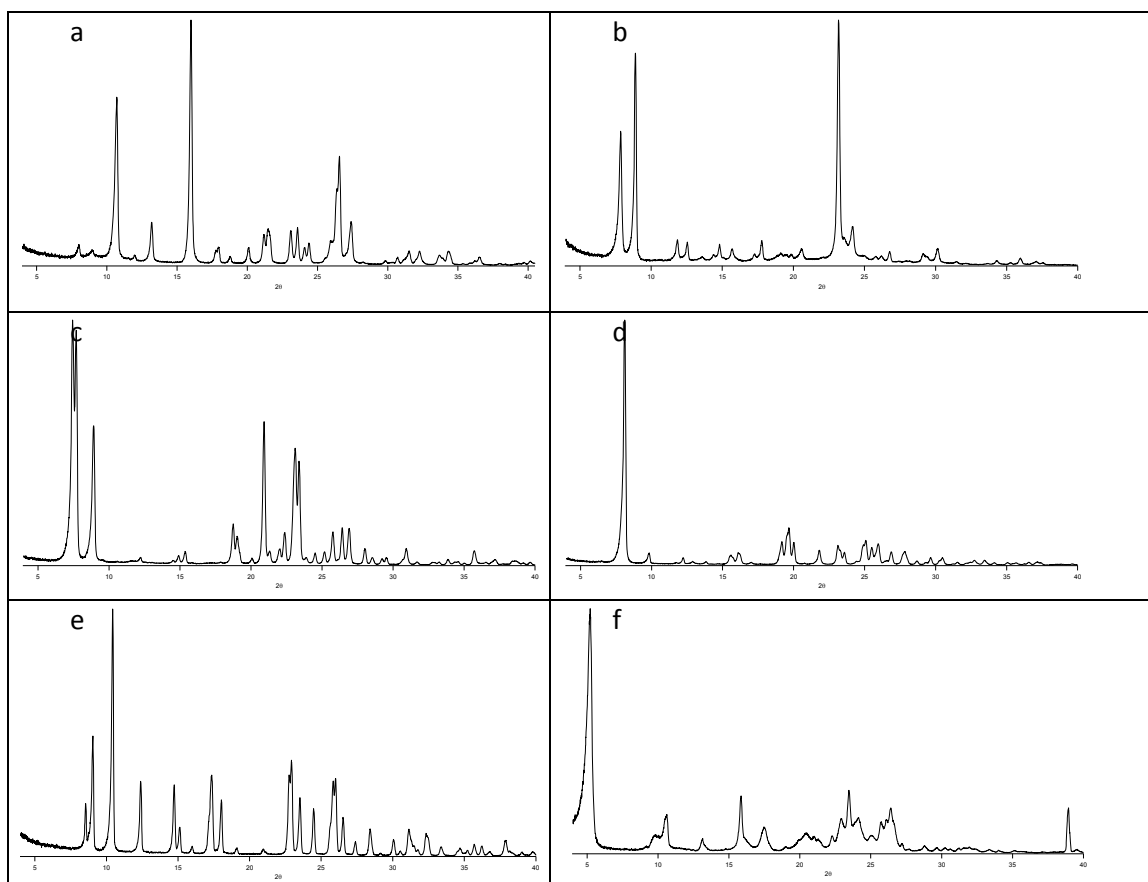
Figure S1. Representative powder X-ray diffraction patterns of as-made materials. **a**, ITW. **b**, MFI.

c, MTW. **d**. STF. **e**. STW. **f**. HPM-2.

Characterization of STW:
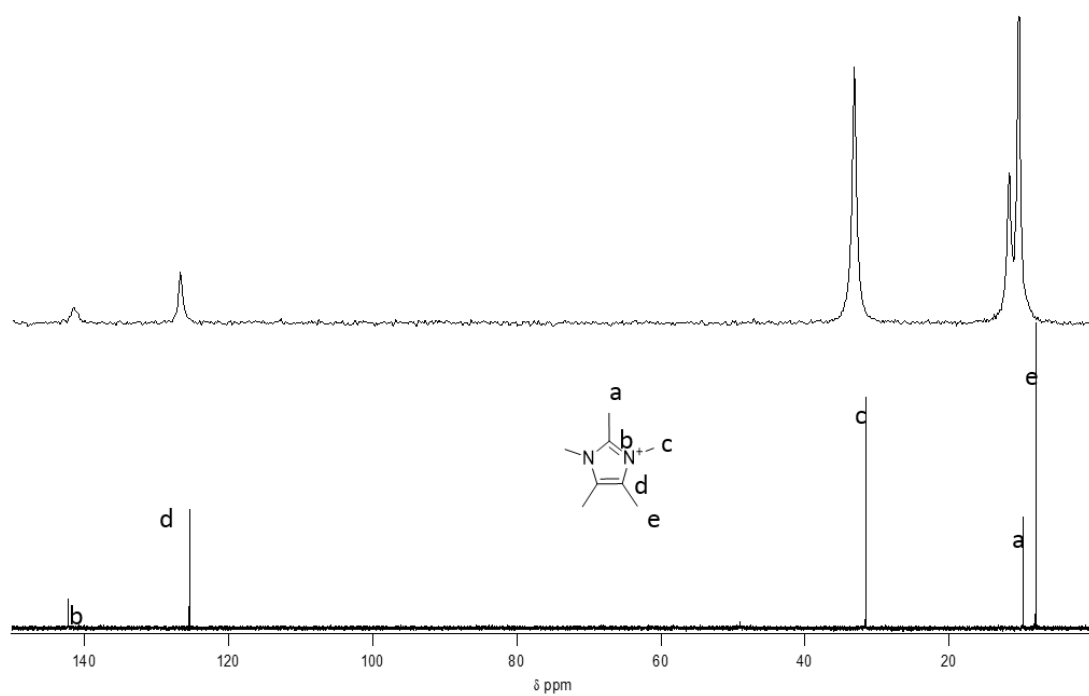
Figure S2. ^{13}C CP-MAS NMR of **1** in (top) compared to the ^{13}C liquid NMR (D$_2$O) of **1** (bottom).
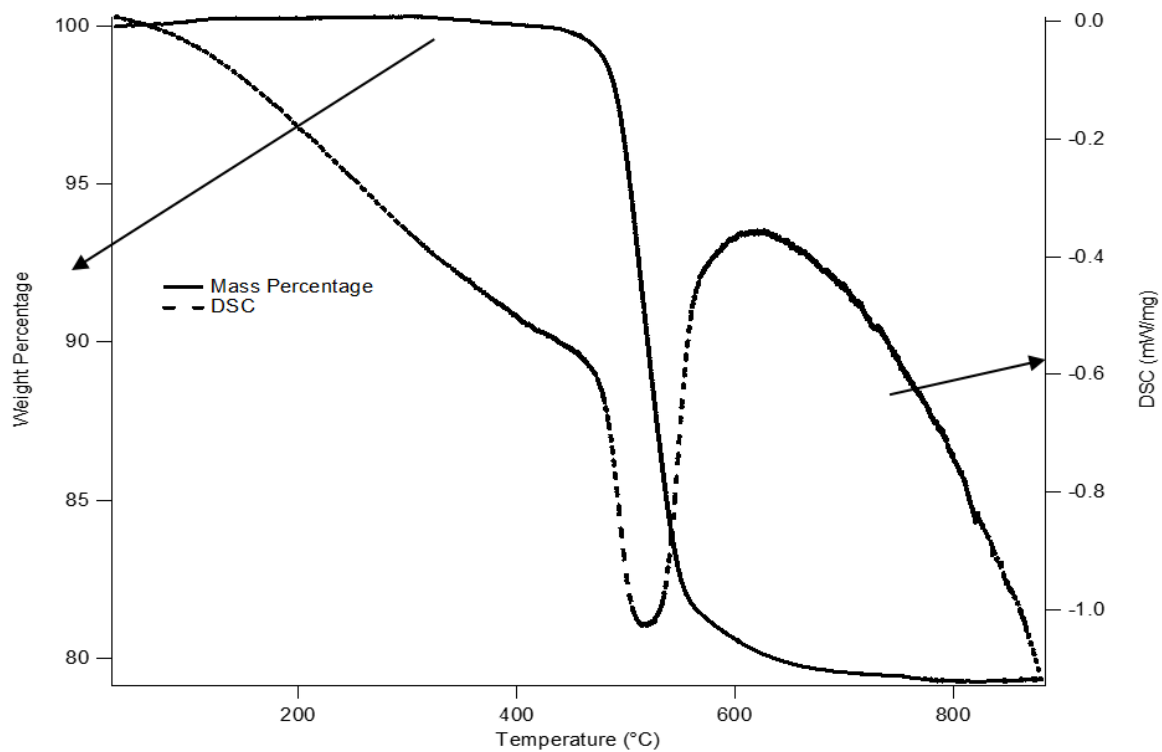
Figure S3. TGA of **1** occluded in STW.
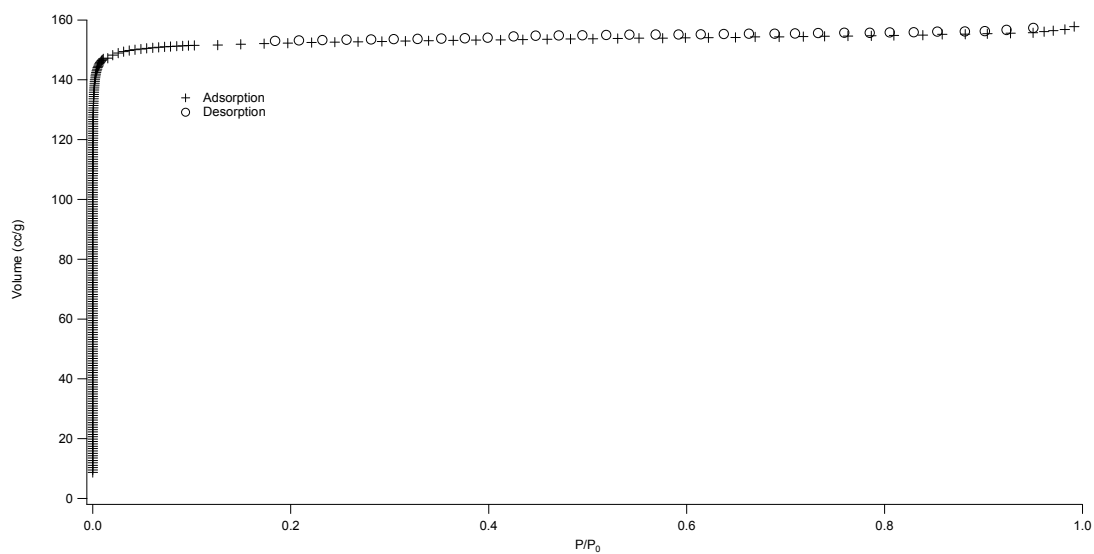
Figure S4. Argon adsorption isotherm at 87.45 K of the calcined material.

Full Reaction results

?=Unidentified Product

Amph=Amorphous

OSDA	H_2O/SiO_2	Temperature (°C)	Time	Result
1	4	140	12	STW
1	7	140	23	STW
1	14	140	35	?
1	4	160	8	STW
1	7	160	7	STW
1	14	160	7	STW
1	4	175	5	STW
1	7	175	7	STW
1	14	175	16	Dense

OSDA	H_2O/SiO_2	Temperature (°C)	Time	Result
2	4	140	40	STW
2	7	140	70	STW
2	14	140	70	HPM-2
2	4	160	16	STW
2	7	160	41	STW
2	14	160	47	HPM-2
2	4	175	16	STW
2	7	175	20	HPM-2
2	14	175	20	Dense

OSDA	H_2O/SiO_2	Temperature (°C)	Time	Result
3	4	140	80	?
3	7	140	74	STF
3	14	140	40	MTW
3	4	160	28	STF
3	7	160	21	MTW+STF
3	14	160	41	MTW
3	4	175	9	STF
3	7	175	21	?
3	14	175	32	MTW

OSDA	H$_2$O/SiO$_2$	Temperature (°C)	Time	Result
4	4	140	49	STF
4	7	140	49	Amph
4	14	140	49	Amph
4	4	160	16	STW+ITW
4	7	160	22	ITW+MTW
4	14	160	44	ITW
4	4	175	10	?
4	7	175	29	ITW
4	14	175	21	MTW

OSDA	H$_2$O/SiO$_2$	Temperature (°C)	Time	Result
5	4	140	19	MFI+layered phase+impurity
5	7	140	46	Layered
5	14	140	55	Amph
5	4	160	49	MFI
5	7	160	49	MFI
5	14	160	58	Amph
5	4	175	13	MFI
5	7	175	60	Amph
5	14	175	60	Amph

OSDA	H$_2$O/SiO$_2$	Temperature (°C)	Time	Result
6	4	140	8	STF
6	7	140	18	STF
6	14	140	56	Amph
6	4	160	6	STF
6	7	160	11	STF
6	14	160	46	STF
6	4	175	5	STF
6	7	175	8	STF
6	14	175	19	dense

Chapter 3. The Facile Preparation of Aluminosilicate RTH Across a Wide Composition Range Using a New Organic Structure Directing Agent

Chapter 3 previously appeared as: Schmidt, J. E.; Deimund, M. A.; Davis, M. E. Facile Preparation of Aluminosilicate RTH across a Wide Composition Range Using a New Organic Structure-Directing Agent. *Chem. Mater.* **2014**, *26*, 7099–7105. doi: 10.1021/cm503625u

3.1 Abstract

RTH-type zeolite (aluminosilicate) is a potentially useful catalytic material that is limited by the inability to easily prepare the material over a wide composition range. Here, we report the use of pentamethylimidazolium to prepare aluminosilicate RTH across a wide range of compositions in both fluoride and hydroxide inorganic systems. RTH-type zeolites are crystallized with a calcined product Si/Al of 7-27 from fluoride media and 6-59 from hydroxide media. The use of this new, simple organic structure directing agent that can be prepared in one step, allows for dramatic improvement in the compositional space where aluminosilicate RTH can be formed. RTH is tested as a catalyst for the methanol-to-olefins reaction, and at complete conversion shows a high propylene to ethylene ratio of 3.9 at a propylene selectivity of 43%.

3.2 Introduction

Molecular sieves have diverse applications including catalysis, ion exchange, and adsorption, where their utility depends on the properties of each material, such as pore size, composition and hydrothermal stability.[1–3] In many applications, there is only a single structure and composition to achieve optimal performance, motivating much of the research directed at creating new

materials.[4] Currently, most discovery of new materials is based on trial and error, although there are a growing number of guiding principles and advances in methodologies that attempt to computationally predict materials.[5,6] One of the most important methods of discovery has been the use of organic structure directing agents (OSDAs), that are normally alkylammonium cations. The use of OSDAs began with the work of Barrer and Denny to incorporate alkylammonium cations in reactions,[7] and since that time, numerous mono-, di-, and polyquaternary OSDAs have been examined.[8–18] OSDAs have been instrumental in the discovery of new frameworks, and they have also expanded the composition range for many materials, that has allowed for enhanced material properties, e.g., catalytic activity and stability.

Recently, microporous materials with 8-membered rings (MRs, number of tetrahedral atoms in the ring) have received considerable interest as catalysts for the methanol-to-olefins reaction (MTO) and NO_x reduction. MTO is of high economic demand due to the increasing price of petroleum feedstocks.[19] Many different frameworks have been considered for this application, but microporous materials with 8MRs have been found to give good yields of olefins,[20] and selecting materials with the right number and location of acid sites can limit the formation of coke.[20] SAPO-34 (CHA framework topology) has been commercialized for MTO, and shows good performance with high selectivity to light olefins and a suppressed rate of coke formation.[19,20] SSZ-13 (aluminosilicate CHA) is also promising for MTO, as its high silica to alumina ratio helps prevent the severe coking found on CHA with a lower silica to alumina ratio.[20] One limitation of CHA type materials is the high cost of the OSDA used to prepare them.[21]

A second, high-demand application of 8MR materials is for NO_x reduction, as these small-pore materials exhibit long-term hydrothermal stability under demanding conditions.[22] The CHA framework exchanged with either Cu^{2+} or Fe^{2+} is promising,[23] and both Cu-SSZ-13 and Cu-SAPO-34

function well as catalysts for this reaction.[24,25] In order to accommodate the charge of the copper, these materials generally have lower silica to alumina ratios (one Cu^{2+} requires two closely spaced aluminum atoms to balance the charge). As with the MTO reaction, limitations of using CHA type materials for NO_x reduction include the high cost of the OSDA required to make these materials as well as catalyst lifetime. Another promising material for NO_x reduction is SSZ-39 (AEI framework), that has a three-dimensional, 8MR system and shows superior activity and hydrothermal stability to Cu-CHA, but is limited in that it can only be produced at very narrow Si/Al ratios.[26] The results from SSZ-39 demonstrate that improvement is possible for NO_x reduction applications with new, 8MR materials with specific Si/Al ratios.

A promising zeolite type for the aforementioned catalytic applications is the RTH framework, a graphical representation of the structure can be found on the IZA website.[27–31] RTH has 8MRs with openings of 4.1 x 3.8 Å and 5.6 x 2.5 Å along the *a* and *c* axes, respectively, and a free volume of 408 $Å^3$ (smaller than that of CHA, 415 $Å^3$).[29] The geometry of the cages is different, as the largest sphere that can be occluded in the CHA framework is 7.37 Å in diameter while in RTH it is 8.18 Å in diameter. As RTH has a unique framework structure, it may exhibit catalytic properties indicative of an 8MR system but with specific new attributes. RTH was first disclosed as a borosilicate (RUB-13) in 1995 using 1,2,2,6,6-pentamethylpiperidine as the OSDA.[23,32] The aluminosilicate version of this material (SSZ-50) was first reported in 2002 (date of first publication, first patent application filed in 1999), and is made using the N-ethyl-N-methyl-5,7,7-trimethylazoniumbicyclo[4.1.1]octane cation.[28,33] This OSDA was found to be strongly directing to SSZ-50, as it directed its formation across a wide synthesis gel composition range. Small changes to the organic were found to alter the product selectivity, thus demonstrating the specificity of this organic for SSZ-50. It was reported that pure-phase SSZ-50 could be prepared in gel compositions ranging from Si/Al=15 all

the way to the pure-silica material, but product compositions were not reported.[15,28,34] Unfortunately, this organic is not commercially available and must be prepared through an elaborate, multi-step synthesis, limiting the potential applications of SSZ-50 unless other preparation methods can be found.

Recently, methods to prepare RTH without an OSDA have been reported, and draw upon methods employed to find OSDA-free methods for other frameworks such as *BEA.[29,30,35,36] It was reported that RTH could be synthesized without any organics by using RUB-13 as seeds and carefully controlling the amount of sodium hydroxide and water in the synthesis.[29] Using this method, the product Si/Al ratio was limited to the range of 37 to 57.[29,35] It was also found that a wide variety of amines could be used in the synthesis of aluminoborosilicate RTH to give products with Si/Al=48-259 and Si/B=18-66.[35] The catalytic activity of aluminosilicate RTH prepared without OSDAs (TTZ-1) was evaluated for the MTO reaction, and it showed a higher selectivity to propylene than SAPO-34 or ZSM-5, as well as a longer catalyst lifetime.[29] While these OSDA-free methods do show promise for the production of aluminosilicate RTH, they suffer from a limited composition range. The relatively high Si/Al values reported for OSDA-free RTH are unusual for organic free syntheses and are higher than those generally used for MTO and NO_x reduction.

In order to fully evaluate the catalytic potential of RTH, a method to easily produce this material across a wide composition range with an OSDA that is easy to prepare (if an OSDA is necessary) is needed. Recently, we have been exploring substituted imidazoles in fluoride-mediated, low-water systems (pioneered by Corma and Camblor).[14,15,17] While several substituted imidazoles have been previously evaluated, there are many permutations of carbon atoms around the imidazole ring that remain to be explored, as well as their combinations with different inorganic conditions. In particular, we have been investigating fluoride-mediated syntheses of

aluminosilicates in order to produce materials with catalytic activity. In some known synthetic

systems, it is possible to add aluminum to obtain catalytically active materials, though a change in

zeolite product selectivity can sometimes be observed.[37–39] We recently reported using a

computational method to predict chemically synthesizable OSDAs for desired microporous

material frameworks, and used pure-silica STW (HPM-1) as the test case for this method.[40]

Pentamethylimidazolium was predicted to be the most strongly directing OSDA for STW, and this

was confirmed experimentally. In attempting to prepare aluminosilicate STW in fluoride media, we

found that the RTH framework formed instead. Here, we use this ODSA for the preparation and

characterization of aluminosilicate RTH (in both fluoride and hydroxide mediated syntheses) that

has a wide composition range. Included in the product characterizations are results from MTO

reaction testing.

3.3 Experimental Section

3.3.1 Synthesis

OSDA Synthesis

Pentamethylimidazolium was synthesized by dissolving 1,2,4,5-tetramethylimidazole (TCI

Chemicals) in methanol and then cooling in a dry ice bath. A three-fold molar excess of

iodomethane (Aldrich) was then slowly added (Caution: Highly exothermic reaction!), and the

mixture was then slowly warmed to room temperature and stirred for one day. The solvent and

excess iodomethane were then removed using rotary evaporation (Caution: Highly toxic vapors

present, use appropriate precautions), and the product was recrystallized from acetone and

washed with ether. The structure was verified using ^{1}H and ^{13}C NMR (D$_2$O, methanol added as

internal standard) and the product was converted from the iodide to the hydroxide form using

hydroxide exchange resin (Dowex Marathon A, hydroxide form) in water, and the product was titrated using a Mettler-Toledo DL22 autotitror using 0.01 M HCl as the titrant. ^{1}H-NMR (500 MHz, D_2O): δ 3.60 (s, 6H), 2.54 (s, 3H), 2.20 (s, 6H). ^{13}C-NMR (125 MHz, D_2O): δ 7.99, 9.76, 31.58, 125.42, 142.21.

Microporous Materials Synthesis

<u>Fluoride mediated reactions</u>

A general synthesis procedure was as follows. Tetraethylorthosilicate (Aldrich) and aluminum isopropoxide (Aldrich) were added to the organic in its hydroxide form in a Teflon Parr reactor liner. The container was closed and stirred for at least 12 hours to allow for complete hydrolysis. The lid was then removed, and the alcohol and appropriate amount of water were allowed to evaporate under a stream of air. Composition was monitored gravimetrically. Additional water was added as necessary, and then aqueous HF (Aldrich) was added and the mixture was stirred by hand until a homogenous gel was obtained. (Caution: Use appropriate personal protective equipment, ventilation, and other safety measures when working with HF.) The final molar ratios of the gel were:

$$(1\text{-}x)SiO_2 : x Al : 0.5 ROH : 0.5 HF : y H_2O$$

The parameters *x* and *y* were varied depending on the synthesis and the desired composition. For low water syntheses, a final evaporation step was used after the addition of HF to reach the desired water ratio. The Teflon-lined Parr reactor was sealed and placed in a rotating oven at 160°C. Aliquots of the material were taken periodically by first quenching the reactor in water and then removing enough material for powder X-ray diffraction (PXRD).

<u>Hydroxide Mediated Syntheses</u>

For the hydroxide syntheses, several variations on gel Si/Al as well as the sources of silica and alumina were used. Specific synthesis preparations are below. For all hydroxide reactions, seeds were added after 1 day at reaction temperature, once a decrease in pH was observed. Normally seeds were added as a homogeneous aliquot of the contents of a previous, completed reaction (less than 0.3 mL) as these were found to be more active than seeds that had been washed. The use of seeds was found to speed the formation of RTH and to help avoid the formation of dense phases, but this influence was not extensively investigated. Aliquots were taken periodically, and crystallization was monitored by both PXRD and pH, as an increase in pH was generally observed when the product crystallized. After the product crystallized, the material was washed with DI water and then collected via centrifugation. This process was repeated at least three times, and a final wash was performed using acetone. The product was dried at 100°C in air.

Sodium aluminate (or Reheiss F-2000) and Ludox AS-40 (or Cabosil)

The OSDA in its hydroxide form, sodium hydroxide (if necessary), any necessary water and sodium aluminate (Pfaltz & Bauer) were combined in a Teflon Parr reactor liner and stirred until the sodium aluminate completely dissolved. Ludox AS-40 (Aldrich) was then added and stirred until a homogenous gel was obtained. In sodium-free syntheses, Reheiss F-2000 (55wt% Al_2O_3) was used as the source of aluminum instead of sodium aluminate, and Cabosil M-5 was used instead of Ludox AS-40. The gel pH was measured, and then the Teflon-lined Parr reactor was placed in a rotating oven at 160°C.

Si/Al=15 (NH4-Y and Sodium Silicate)

Following the method of Wagner et al.[41] 2 mmol of OSDA was mixed with 0.20 g of 1 M NaOH,

and water was added to give a total mass of 6 g. Then 2.5 grams of sodium silicate (PQ

Corporation, 28.6wt% SiO_2 and 8.9wt% Na_2O) was added to the mixture and finally 0.25 g of NH_4-Y

(Zeolyst CBV 500, Si/Al=2.55) was added. The solution was heated at 140°C in a rotating oven.

Si/Al=15 (CBV 720)

3 mmol of OSDA was mixed with 1 g of 1 M NaOH and water was added to bring the total

mass to 7 g. Then 1 g of CBV 720 (Zeolyst, Si/Al=15) was added. The solution was heated at 175°C

in a rotating oven.

Si/Al=30 (CBV 760)

3 mmol of OSDA was mixed with 1 g of 1 M NaOH and water was added to bring the total

mass to 7 g. Then 1 g of CBV 760 (Zeolyst. Si/Al=30) was added. The solution was heated at 175°C

in a rotating oven.

SSZ-13 Synthesis

SSZ-13 was synthesized using a standard method.[42] In a typical preparation, 3.33 g of 1 M

NaOH was mixed with 2.81 g of N,N,N-trimethyl-1-adamantammonium hydroxide (Sachem, 1.18

mmol OH/g) and 6.62 g of water. Then 0.077 g of Reheiss F-2000 (55wt% Al_2O_3) was added and

stirred until the solution cleared. Finally, 1.00 g of Cabosil M-5 was added and stirred until a

homogeneous solution was obtained. The solution was heated at 160°C in a rotating oven for

approximately 6 days.

SAPO-34 Synthesis

SAPO-34 was prepared from the following gel composition:

$0.5(TEA)_2O:1.5Pr_2NH:0.6SiO_2:1Al_2O_3:1P_2O_5:70H_2O$. In a typical preparation, 11.5 g of 85 wt%

phosphoric acid were dissolved in 4.35 g of water and stirred for 5 minutes. Then 6.875 g of

Catapal B alumina were added to 20 g of water and stirred for 10 minutes. The mixtures were then

slowly combined and stirred for 1 hour at room temperature. Next 4.48 g of Ludox HS-40 was

added and stirred by hand until a homogenous gel was obtained. Then 20.8 g of 35 wt% TEAOH

and 7.61 g of dipropylamine were added and the gel was homogenized by manual stirring. Then

the gel was stirred at room temperature for 2 hours. Finally, the gel was added to a Teflon-lined

Parr reactor and heated at 200°C without stirring for 24 hours.

Calcination

All products were calcined in breathing grade air. The material was heated to 150°C at

1°C/min, held for three hours, then heated to 580°C at 1°C/min and held for six hours to assure

complete combustion of the organic.

3.3.2 Characterization

The ^{13}C CP-MAS NMR spectra were recorded using a Bruker Avance 200 MHz spectrometer

with a 7 mm rotor at a spinning rate of 4 kHz and were conducted in a 4.7 T magnetic field,

corresponding to Larmor frequencies of 200 MHz and 50.29 MHz for ^{1}H and ^{13}C respectively. The

^{13}C spectra are referenced to adamantane as a secondary external standard relative to

tetramethylsilane. The ^{27}Al MAS NMR were recorded using a Bruker AM 300 MHz spectrometer

with a 4 mm rotor at a spinning rate of 8 kHz, and were conducted in a 7.0 T magnetic field

corresponding to a Larmor frequency of 78.172 MHz. The ^{27}Al spectra are referenced to 1.1 M

$Al(NO_3)_3$ as an external standard. All argon adsorption isotherms were performed at 87.45 K using

a Quantachrome Autosorb iQ and were conducted using a quasi-equilibrium, volumetric

technique.[43] All powder X-ray diffraction (PXRD) characterization was conducted on a Rigaku

MiniFlex II with Cu K$_\alpha$ radiation. SEM images were acquired on a ZEISS 1550 VP FESEM, equipped

with in-lens SE. EDS spectra were acquired with an Oxford X-Max SDD X-ray Energy Dispersive

Spectrometer system.

3.3.3 Reaction Testing

Prior to reaction testing, all materials were calcined as described in section 2.1. After

calcination they were exchanged to ammonium form using 1 M NH_4NO_3 (100 mL of solution per

gram of catalyst) at 95°C with stirring for three hours; this was done a total of three times per

sample. After ammonium exchange the materials were washed with water and dried and then

calcined using the method above. The calcined materials were then pelletized, crushed, and

sieved. Particles between 0.6 mm and 0.18 mm were supported between glass wool beds in an

Autoclave Engineers BTRS, Jr. SS-316 tubular, continuous flow reactor.

All catalysts were dried at 150°C in situ in a 30 cm^3/min flow of 5% Ar/95% He for 4 h prior to

the reaction. The reactions were conducted at 400°C in a 10% methanol/inert flow. Methanol was

introduced via a liquid syringe pump at 5.4 μL/min into a gas stream of the inert blend at

30 cm^3/min. The reactant flow had a weight hourly space velocity of 1.3 h^{-1}. In a typical run, 200

mg of dry catalyst was loaded. Effluent gases were evaluated using an on-stream GC/ MS (Agilent

GC 6890/MSD5793N) with a Plot-Q capillary column installed. Conversions and selectivities were

computed on a carbon mole basis. Catalyst regeneration between reaction tests was done in-situ

by exposing the catalyst to breathing grade air at reaction temperature, ramping to 580°C at

1°C/min, holding at 580°C for 6 hours, and then cooling to reaction temperature.

3.4 Results and Discussions

3.4.1 Fluoride-Mediated Reactions

We recently reported a computational method to construct chemically synthesizable OSDAs

for desired frameworks that successfully identified pentamethylimidazolium as an OSDA for producing pure-silica STW.[40] After the successful synthesis of pure-silica STW using this OSDA, fluoride-mediated aluminosilicate reactions were then conducted with pentamethylimidazolium. These reactions produced aluminosilicate RTH (SSZ-50). This is the first report of aluminosilicate RTH produced in fluoride media (Zones and co-workers reported pure-silica RTH in fluoride media[15]). This result highlights the influence that small amounts of aluminum can have on low-water, fluoride-mediated syntheses.[39]

A representative PXRD of the calcined material produced in fluoride media (sample F3) is shown in the upper diffraction pattern in Figure 3-1, and a summary of all synthetic results is presented in Table 3-1. The fluoride method was able to produce RTH across a wide range of compositions, but at the highest Si/Al ratios tested STW appeared as a competitive phase (sample F9). This phase competition is an expected result based on work using pentamethylimidazolium to make pure-silica STW.[40] A representative SEM of the material produced in the fluoride method is shown in Figure 3-2a (sample F4). The crystal size and morphology are consistent with pure-silica RTH produced in fluoride media,[15] and the large crystal size is what is generally observed for low-water, fluoride-mediated syntheses. It was determined that pentamethylimidazolium, and not a decomposition product, led to the formation of aluminosilicate RTH using ^{13}C CP-MAS NMR, and the spectrum compared to the ^{13}C liquid NMR of pentamethylimidazolium is shown in Figure 3-3. In order to determine the coordination of the aluminum in the material, ^{27}Al MAS NMR was performed on the calcined sample containing the highest amount of aluminum (sample F2), and the spectrum is shown in Figure 3-4. The single resonance in this sample at 54 ppm is consistent with tetrahedrally coordinated aluminum, and there is no evidence of octahedrally coordinated aluminum, normally found around 0 ppm.
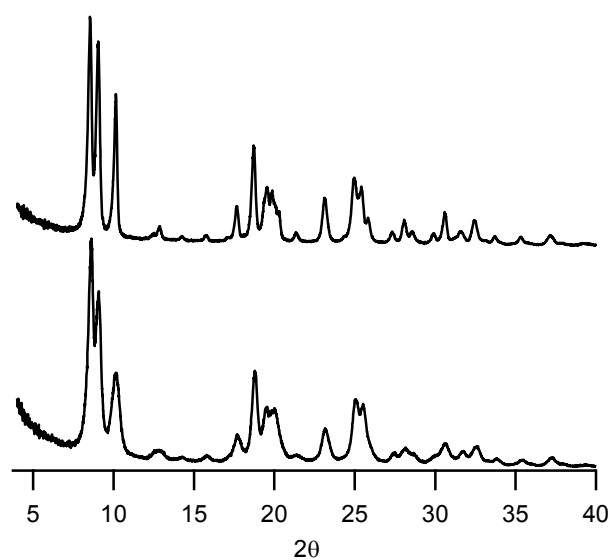
Figure 3-1. Calcined aluminosilicate RTH prepared in fluoride (upper, sample F3) and hydroxide media (lower, sample H4).

Table 3-1. Synthesis of RTH in fluoride media.

Gel Si/Al	Product Si/Al[a]	Gel H_2O/SiO_2	Time (days)	Sample
5	--	7	No product	F1
10	7	7	29	F2
15	10	14	46	F3
20	16	14	22	F4
20	18	4	10	F5
33	22	14	20	F6
40	26	14	17	F7
50	27	14	20	F8
150	STW impurity	7	7	F9
[a]Reported Si/Al is of calcined material				
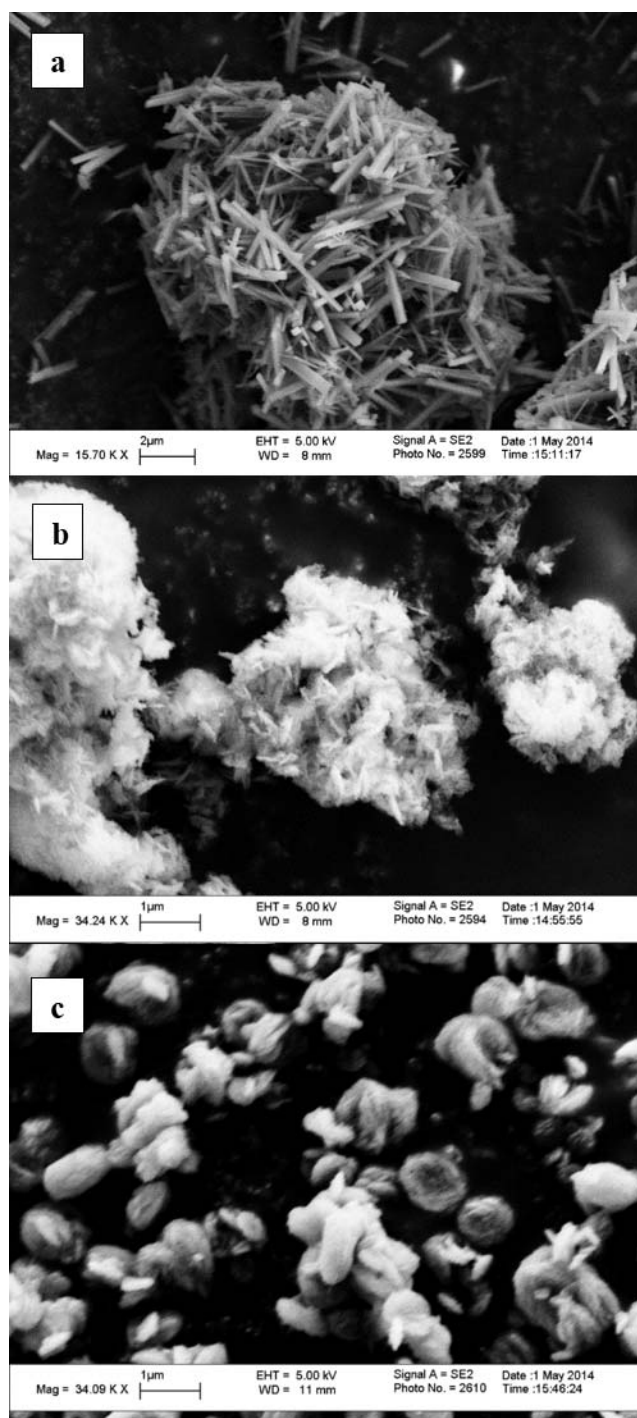
Figure 3-2. SEM images: (a) Calcined RTH prepared in fluoride media (sample F4), (b) calcined RTH synthesized in hydroxide media with sodium (sample H4), (c) calcined RTH synthesized in hydroxide media without sodium (sample H5).
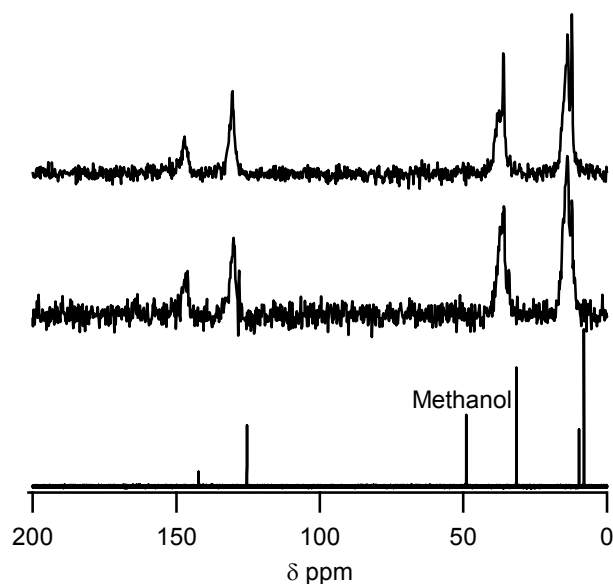
Figure 3-3. ^{13}C NMR of pentamethylimidazolium in D_2O with methanol standard (lower), ^{13}C CP-MAS NMR of as-made RTH prepared in hydroxide media (middle, sample H4), and ^{13}C CP-MAS NMR of as-made RTH prepared in fluoride media (upper, sample F4).
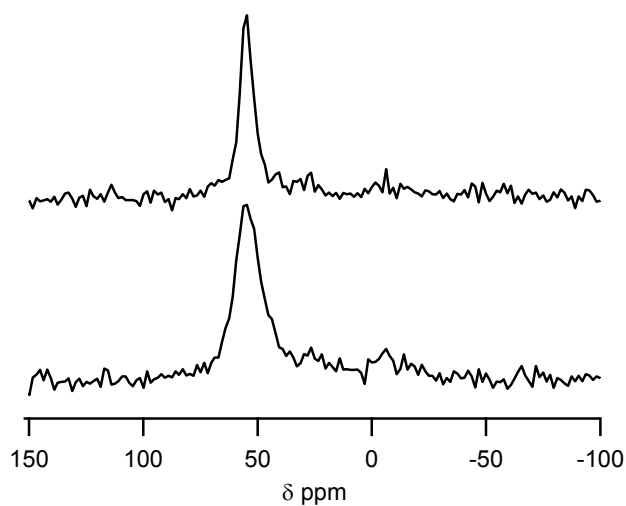
Figure 3-4. 27Al MAS NMR of low silica RTH synthesized in hydroxide media (lower, sample H1) and prepared in fluoride media (upper, sample F2). The single resonance is at 54 ppm.

3.4.2 Hydroxide-Mediated Reactions

The success of using pentamethylimidazolium in fluoride-mediated reactions to produce aluminosilicate RTH led us to work in hydroxide-mediated reactions as well, with seeds of RTH added to promote its formation. The results of the syntheses are shown in Figure 3-2.

In general, these syntheses were found to be sensitive to reaction time and temperature, and required careful monitoring to avoid the formation of dense phases. Seeds of RTH were added to all reactions to promote the formation of RTH, but the exact influence of the seeds was not extensively investigated. A representative PXRD of the calcined material produced in hydroxide media is shown in the lower diffraction pattern in Figure 3-1. The crystal sizes of the products were generally much smaller in hydroxide syntheses than in the fluoride syntheses, as is shown in Figure 3-2. The smaller crystal sizes observed under these conditions are consistent with what is generally reported in hydroxide syntheses. It is interesting to note that the aggregation appeared to be different in reactions where no sodium was present compared to those with sodium present (Figure 3-2). ^{13}C CP-MAS NMR showed that pentamethylimidazolium was also occluded intact in the material prepared in hydroxide media (Figure 3-3). ^{27}Al MAS NMR was used to characterize the sample containing the largest amount of aluminum (sample H1), as was done in the fluoride-mediated case, and is shown in Figure 3-4. There is a single resonance at 54 ppm corresponding to tetrahedrally coordinated aluminum and no evidence of any significant amount of octahedral aluminum. An argon adsorption isotherm for sample H4 is shown in Figure 3-5, and the micropore volume was calculated to be 0.16 cm^3/g (t-plot method). The EDS analyses of the materials synthesized in hydroxide media are given in Table 3-2, and the results show that RTH can be crystallized across a wide range of compositions from Si/Al of 6 to 59 in the calcined product (a large expansion over previously reported results). Of significant interest are the low-silica syntheses (the lowest product found was Si/Al=6, sample H1), which are much lower than any

other reported compositions.

Table 3-2. Synthesis results in hydroxide media

Gel Si/Al	Product Si/Al[a]	Gel Na/Si	Gel ROH/Si	Gel H_2O/Si	Time (days)	Sample
5[b]	6	0.16	0.16	30	10	H1
10[b]	9	0.16	0.16	30	10	H2
15[c]	9				9	H3
15[b]	14	0.16	0.16	30	10	H4
15[d]	15		0.32	30	15	H5
15[e]	17				10	H6
20[b]	20	0.16	0.16	30	12	H7
30[f]	29				13	H8
50[b]	45	0.10	0.20	30	9	H9
75[b]	59	0.10	0.20	30	9	H10
[a]Reported Si/Al is of calcined material. [b]Made with Ludox AS-40 and sodium aluminate [c]Made with NH_4-Y and sodium silicate [d]Made using Cabosil M-5 and Reheiss F-2000 [e]Made using CBV 720 as only source of Si and Al [f]Made using CBV 760 as only source of Si and Al						
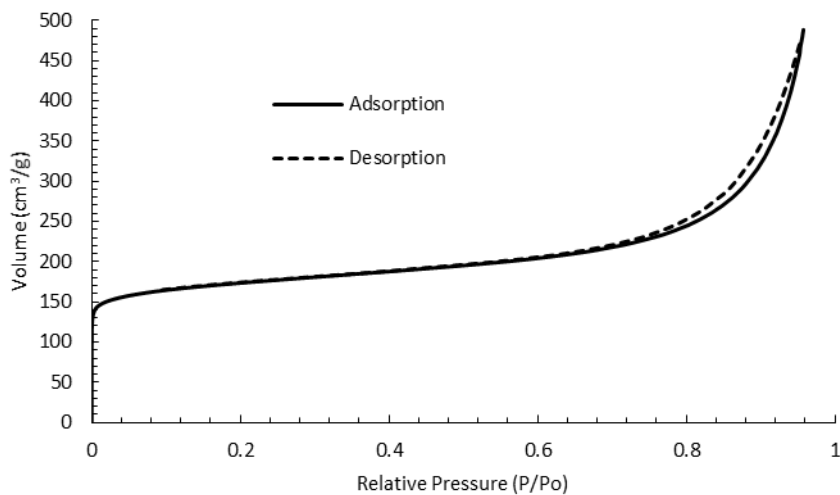
Figure 3-5. Argon isotherm for aluminosilicate RTH prepared in hydroxide media with product

Si/Al=14 (sample H4).

3.4.3 Comparisons Between Materials Prepared from Fluoride and Hydroxide Media

Pentamethylimidazolium was successful in preparing aluminosilicate RTH in both fluoride and hydroxide mediated syntheses. The size and morphology of the RTH crystals are very different between the two synthetic methods, and this could lead to differences in catalyst activity and lifetime. The product composition ranges produced using pentamethylimidazolium are much wider than the previously reported results. The ability to vary the composition of the material will likely be important for specific applications. NO_x reduction generally requires lower Si/Al ratios than MTO reactions, so the ability of pentamethylimidazolium to produce RTH across such a wide composition space is important. Using the OSDA-free methods, the lowest Si/Al ratio reported is 37, and in the results reported by Zones and co-workers, the synthesis using the largest amount of aluminum resulted in ANA as a phase impurity, so the current method is a significant improvement over the known methods.

3.4.4 Reaction Testing

The catalytic activity of RTH for the MTO reaction was evaluated using three different samples of RTH prepared in hydroxide media at different Si/Al ratios, and the results were compared to samples of SSZ-13 and SAPO-34. The samples of RTH tested were prepared using the CBV 720, CBV 760, and the sodium aluminate and Ludox synthesis routes, with product Si/Al values of 17, 29, and 59, respectively (samples H6, H8, H10). The sample of SSZ-13 had a product Si/Al of 19. The MTO reaction data for the RTH materials is given in Figure 3-6, the data for SSZ-13 and SAPO-34 are given in Figures S1 and S2, respectively.

The propylene to ethylene ratio is much higher for RTH than SSZ-13 or SAPO-34. In sample H6 with Si/Al=17, the maximum propylene to ethylene selectivity ratio observed was 3.6 at 96 minutes on stream. For sample H8 with Si/Al=29, the maximum propylene to ethylene selectivity ratio observed was 3.9 at 96 minutes on stream. For sample H10 with Si/Al=59, the maximum

propylene to ethylene selectivity ratio observed was 3.6 between 25 and 41 minutes on stream.

These selectivity ratios are much higher than those observed with SSZ-13 or SAPO-34, where the

maximum propylene to ethylene ratios are 1.7 at 96 minutes on stream and 1.3 across several

time points, respectively (Figure S1 and Figure S2). This result shows that RTH would be a superior

catalyst in applications where a higher propylene to ethylene ratio is desired.

The selectivity towards butene is also higher for RTH than for SSZ-13 or SAPO-34. The

maximum selectivities to butene for the RTH samples were 0.22, 0.27, and 0.25 for the samples

with Si/Al=17, 29, and 59, respectively (H6, H8, H10). The highest selectivity observed for SSZ-13

was 0.15 and for SAPO-34 was 0.17 (Figure S1 and S2).

With the RTH samples, one of the main differences between the samples was the selectivity to

C_1-C_4 saturates (mainly propane). The maximum selectivity for each sample occurred at the first

time point, and the values were 0.39, 0.28, and 0.19 for the samples with Si/Al=17, 29, and 59,

respectively (samples H6, H8, H10). It was also observed that time on stream with complete

methanol conversion decreased with increasing Si/Al ratios. We are currently investigating the

origins of these phenomena.

When comparing RTH to SSZ-13 or SAPO-34, one of the main differences observed is the time

on stream until the catalyst deactivates. In all the RTH samples, this was significantly less than it

was for either SSZ-13 (Figure S1) or SAPO-34 (Figure S2). However, an industrial scale MTO

reaction will likely be run in a fluidized-bed reactor, which allows continuous regeneration of the

catalyst.[44] This will allow a system to be operated at any time point along a fixed bed reactor

profile, assuming the catalyst can be regenerated. To this end, the ability of RTH to be regenerated

was tested by running the Si/Al=17 material (sample H6) for three consecutive MTO reaction runs

with regeneration between each run, and the results are given in the supporting information,

Figures S3 through S5. There are some small differences between the fresh catalyst (Figure S3)

and first regeneration of the catalyst (Figure S4), but the MTO reaction behavior is similar between

the first regeneration (Figure S4) and second regeneration (Figure S5) of the material. The

regeneration experiment demonstrates that RTH would be suitable for use in fluidized bed

systems, as it can maintain its activity across multiple regeneration cycles.
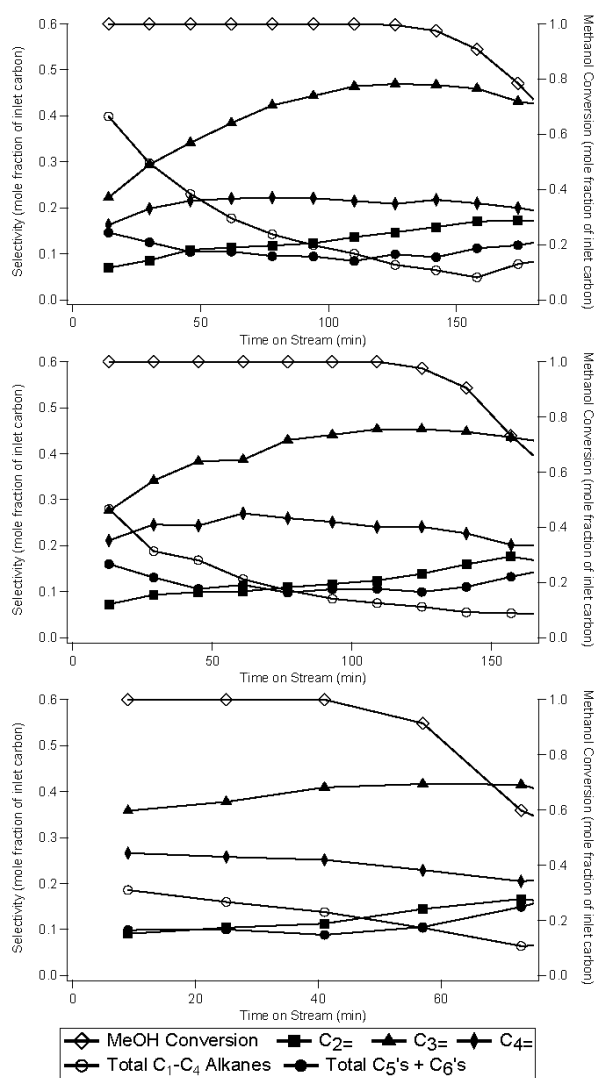
Figure 3-6. MTO reactivity data for (from top to bottom): RTH with Si/Al=17 (sample H6), RTH with

Si/Al=29 (sample H8), RTH with Si/Al=59 (sample H10).

3.5 Conclusions

Pentamethylimidazolium can be easily synthesized from commercially available 1,2,4,5-tetramethylimidazole, and is used to form aluminosilicate RTH in both fluoride and hydroxide-containing syntheses across a wide range of compositions. The flexibility of product composition and relative ease of preparing the OSDA may open new opportunities for evaluating the potential of RTH in applications such as MTO, NO_x reduction, and other catalytic uses. When tested for the MTO reaction, RTH shows a higher propylene to ethylene ratio, as well as a higher selectivity towards butene compared to SSZ-13.

3.6 Funding Sources

3.7 Supporting Information Available

Plots of the MTO reaction data for the SSZ-13, SAPO-34, and regeneration of the RTH catalyst are available in the supporting information.

3.8 Acknowledgment

3.9 References

(1)   Davis, M. E. Ordered Porous Materials for Emerging Applications. *Nature* **2002**, *417* (6891),

813–821.

(2)   Vermeiren, W.; Gilson, J.-P. Impact of Zeolites on the Petroleum and Petrochemical Industry. *Top. Catal.* **2009**, *52* (9), 1131–1161.

(3)   Cundy, C. S.; Cox, P. A. The Hydrothermal Synthesis of Zeolites: History and Development from the Earliest Days to the Present Time. *Chem. Rev.* **2003**, *103* (3), 663–702.

(4)   Pophale, R.; Daeyaert, F.; Deem, M. W. Computational Prediction of Chemically Synthesizable Organic Structure Directing Agents for Zeolites. *J. Mater. Chem. A* **2013**, *1* (23), 6750–6760.

(5)   Verheyen, E.; Joos, L.; Van Havenbergh, K.; Breynaert, E.; Kasian, N.; Gobechiya, E.; Houthoofd, K.; Martineau, C.; Hinterstein, M.; Taulelle, F.; Van Speybroeck, V.; Waroquier, M.; Bals, S.; Van Tendeloo, G.; Kirschhock, C. E. A.; Martens, J. A. Design of Zeolite by Inverse Sigma Transformation. *Nat. Mater.* **2012**, *11* (12), 1059–1064.

(6)   Moliner, M.; Rey, F.; Corma, A. Towards the Rational Design of Efficient Organic Structure-Directing Agents for Zeolite Synthesis. *Angew. Chem. Int. Ed. Engl.* **2013**, *52* (52), 13880–13889.

(7)   Barrer, R. M.; Denny, P. J. 201. Hydrothermal Chemistry of the Silicates. Part IX. Nitrogenous Aluminosilicates. *J. Chem. Soc.* **1961**, 971–9825.

(8)   Burton, A.; Zones, S. Organic Molecules in Zeolite Synthesis: Their Preparation and Structure-Directing Effects. *Stud. Surf. Sci. Catal.* **2007**, *168*, 137–179.

(9)   Zones, S. I.; Burton, A. W.; Lee, G. S.; Olmstead, M. M. A Study of Piperidinium Structure-Directing Agents in the Synthesis of Silica Molecular Sieves under Fluoride-Based Conditions. *J. Am. Chem. Soc.* **2007**, *129* (29), 9066–9079.

(10)   Jones, W.; Rao, C. Towards the Rational Design of Zeolite Frameworks. In *Supramolecular organization and materials design*; Cambridge University Press: Cambridge, UK, 2002; pp 83–

102.

(11) Zones, S. I.; Hwang, S. A Novel Approach to Borosilicate Zeolite Synthesis in the Presence of Fluoride. *Microporous Mesoporous Mater.* **2011**, *146* (1-3), 48–56.

(12) Moini, A.; Schmitt, K.; Valyocsik, E.; Polomski, R. The Role of Diquaternary Cations as Directing Agents in Zeolite Synthesis. *Zeolites* **1994**, *14* (7), 504–511.

(13) Ren, L.; Wu, Q.; Yang, C.; Zhu, L.; Li, C.; Zhang, P.; Zhang, H.; Meng, X.; Xiao, F.-S. Solvent-Free Synthesis of Zeolites from Solid Raw Materials. *J. Am. Chem. Soc.* **2012**, *134* (37), 15173–15176.

(14) Camblor, M.; Villaescusa, L.; Diaz-Cabanas, M. Synthesis of All-Silica and High-Silica Molecular Sieves in Fluoride Media. *Top. Catal.* **1999**, *9*, 59–76.

(15) Zones, S. I.; Hwang, S.-J.; Elomari, S.; Ogino, I.; Davis, M. E.; Burton, A. W. The Fluoride-Based Route to All-Silica Molecular Sieves; a Strategy for Synthesis of New Materials Based upon Close-Packing of Guest–host Products. *Comptes Rendus Chim.* **2005**, *8* (3-4), 267–282.

(16) Camblor, M. A.; Barrett, P. A.; Díaz-Cabañas, M.-J.; Villaescusa, L. A.; Puche, M.; Boix, T.; Pérez, E.; Koller, H. High Silica Zeolites with Three-Dimensional Systems of Large Pore Channels. *Microporous Mesoporous Mater.* **2001**, *48* (1-3), 11–22.

(17) Jiang, J.; Yu, J.; Corma, A. Extra-Large-Pore Zeolites: Bridging the Gap between Micro and Mesoporous Structures. *Angew. Chem. Int. Ed. Engl.* **2010**, *49* (18), 3120–3145.

(18) Takewaki, T.; Beck, L. W.; Davis, M. E. Zeolite Synthesis Using 1,4-diazabicyclo[2,2,2]octane (DABCO) Derivatives as Structure-Directing Agents. *Microporous Mesoporous Mater.* **1999**, *33* (1-3), 197–207.

(19) Olsbye, U.; Svelle, S.; Bjørgen, M.; Beato, P.; Janssens, T. V. W.; Joensen, F.; Bordiga, S.; Lillerud, K. P. Conversion of Methanol to Hydrocarbons: How Zeolite Cavity and Pore Size

Controls Product Selectivity. *Angew. Chem. Int. Ed. Engl.* **2012**, *51* (24), 5810–5831.

(20) Zhu, Q.; Kondo, J. N.; Ohnuma, R.; Kubota, Y.; Yamaguchi, M.; Tatsumi, T. The Study of Methanol-to-Olefin over Proton Type Aluminosilicate CHA Zeolites. *Microporous Mesoporous Mater.* **2008**, *112* (1-3), 153–161.

(21) Zones, S. I. Translating New Materials Discoveries in Zeolite Research to Commercial Manufacture. *Microporous Mesoporous Mater.* **2011**, *144* (1-3), 1–8.

(22) Martínez, C.; Corma, A. Inorganic Molecular Sieves: Preparation, Modification and Industrial Application in Catalytic Processes. *Coord. Chem. Rev.* **2011**, *255* (13-14), 1558–1580.

(23) Fickel, D. W.; Lobo, R. F. Copper Coordination in Cu-SSZ-13 and Cu-SSZ-16 Investigated by Variable-Temperature XRD. *J. Phys. Chem. C* **2010**, *114* (3), 1633–1640.

(24) Kwak, J. H.; Tonkyn, R. G.; Kim, D. H.; Szanyi, J.; Peden, C. H. F. Excellent Activity and Selectivity of Cu-SSZ-13 in the Selective Catalytic Reduction of NOx with NH3. *J. Catal.* **2010**, *275* (2), 187–190.

(25) Martínez-Franco, R.; Moliner, M.; Franch, C.; Kustov, A.; Corma, A. Rational Direct Synthesis Methodology of Very Active and Hydrothermally Stable Cu-SAPO-34 Molecular Sieves for the SCR of NOx. *Appl. Catal. B Environ.* **2012**, *127* (x), 273–280.

(26) Moliner, M.; Franch, C.; Palomares, E.; Grill, M.; Corma, A. Cu-SSZ-39, an Active and Hydrothermally Stable Catalyst for the Selective Catalytic Reduction of NOx. *Chem. Commun. (Camb).* **2012**, *48* (66), 8264–8266.

(27) Vortmann, S.; Marler, B.; Gies, H.; Daniels, P. Synthesis and Crystal Structure of the New Borosilicate Zeolite RUB-13. *Microporous Mater.* **1995**, *4* (2-3), 111–121.

(28) Lee, G. S.; Zones, S. I. Polymethylated [4.1.1] Octanes Leading to Zeolite SSZ-50. *J. Solid State Chem.* **2002**, *167* (2), 289–298.

(29) Yokoi, T.; Yoshioka, M.; Imai, H.; Tatsumi, T. Diversification of RTH-Type Zeolite and Its Catalytic Application. *Angew. Chem. Int. Ed. Engl.* **2009**, *48* (52), 9884–9887.

(30) Liu, M.; Yokoi, T.; Yoshioka, M.; Imai, H.; Kondo, J. N.; Tatsumi, T. Differences in Al Distribution and Acidic Properties between RTH-Type Zeolites Synthesized with OSDAs and without OSDAs. *Phys. Chem. Chem. Phys.* **2014**, *16* (9), 4155–4164.

(31) Baerlocher, C.; Mccusker, L. B. Database of Zeolite Structures, <http://www.iza-structure.org/databases/>. Accessed December 8, 2014.

(32) Gies, H.; Vortmann, S.; Marler, B.; Muller, U.; Dingerdissen, U. Crystalline Solids Having the RUB-13 Structure. US 5,614,166, March 25, 1997.

(33) Lee, Greg S., Zones, Stacey I. Zeolite SSZ-50. US 6,605,267 B1, August 12, 2003.

(34) Kim, C.; Hwang, S.-J.; Burton, A. W.; Zones, S. I. A Case Study of Divergent Structure Directing Effects of Geometric Isomers: The Discovery of a New Structure Directing Agent for an All-Silica RTH Zeolite Prepared in Fluoride Media. *Microporous Mesoporous Mater.* **2008**, *116* (1-3), 227–232.

(35) Yoshioka, M.; Yokoi, T.; Liu, M.; Imai, H.; Inagaki, S.; Tatsumi, T. Preparation of RTH-Type Zeolites with the Amount And/or Kind of Organic Structure-Directing Agents (OSDA): Are OSDAs Indispensable for the Crystallization? *Microporous Mesoporous Mater.* **2012**, *153*, 70–78.

(36) Meng, X.; Xiao, F.-S. Green Routes for Synthesis of Zeolites. *Chem. Rev.* **2014**, *114* (2), 1521–1543.

(37) Corma, A.; Rey, F.; Rius, J.; Sabater, M. J.; Valencia, S. Supramolecular Self-Assembled Molecules as Organic Directing Agent for Synthesis of Zeolites. *Nature* **2004**, *431* (7006), 287–290.

(38) Camblor, M. a.; Corma, A.; Valencia, S. Synthesis in Fluoride Media and Characterisation of Aluminosilicate Zeolite Beta. *J. Mater. Chem.* **1998**, *8* (9), 2137–2145.

(39) Díaz-Cabañas, M. J.; Camblor, M. A.; Liu, Z.; Ohsuna, T.; Terasaki, O. Zeolite Syntheses Using Linear Diquats of Varying Length in Fluoride Media. The Synthesis of ITQ-8, ITQ-10, ITQ-14 and High Silica Nu-87. *J. Mater. Chem.* **2002**, *12* (2), 249–257.

(40) Schmidt, J. E.; Deem, M. W.; Davis, M. E. Synthesis of a Specified, Silica Molecular Sieve by Using Computationally Predicted Organic Structure-Directing Agents. *Angew. Chem. Int. Ed. Engl.* **2014**, *53* (32), 8372–8374.

(41) Wagner, P.; Nakagawa, Y.; Lee, G. S.; Davis, M. E.; Elomari, S.; Medrud, R. C.; Zones, S. I. Guest/Host Relationships in the Synthesis of the Novel Cage-Based Zeolites SSZ-35, SSZ-36, and SSZ-39. *J. Am. Chem. Soc.* **2000**, *122* (2), 263–273.

(42) Robson, H. Verified Synthesis of Zeolitic Materials; 2001.

(43) Hathaway, P. E.; Davis, M. E. High Resolution, Quasi-Equilibrium Sorption Studies of Molecular Sieves. *Catal. Letters* **1990**, *5* (4-6), 333–347.

(44) Moliner, M.; Martínez, C.; Corma, A. Synthesis Strategies for Preparing Useful Small Pore Zeolites and Zeotypes for Gas Separations and Catalysis. *Chem. Mater.* **2014**, *26* (1), 246–258.

3.10 Supporting Information for Chapter 3

Methanol to Olefins Reactivity Data
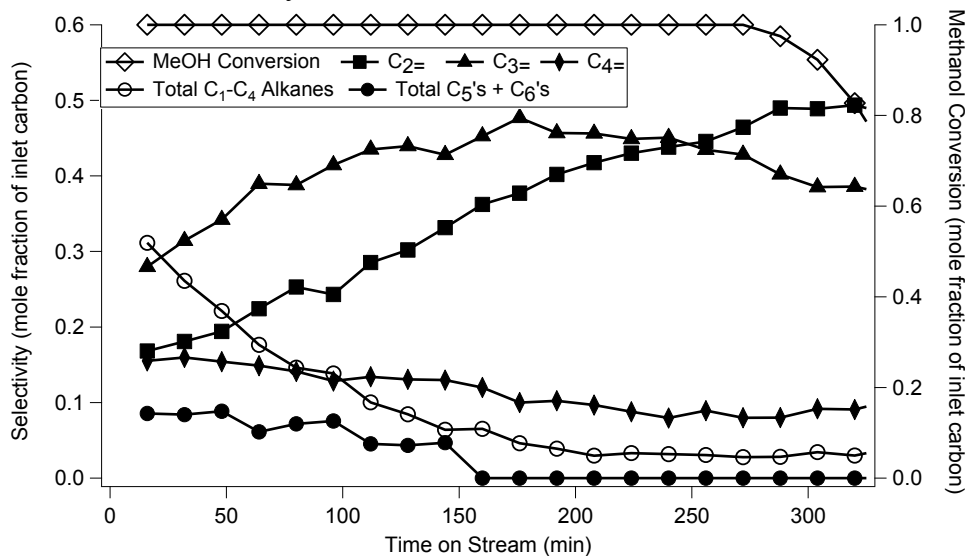
Figure S1. SSZ-13 with Si/Al=19
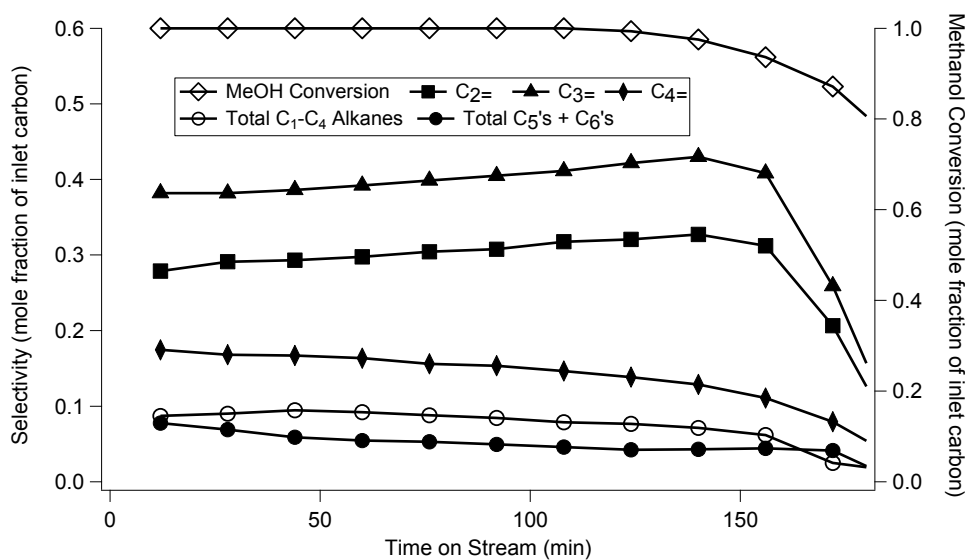
Figure S2. SAPO-34
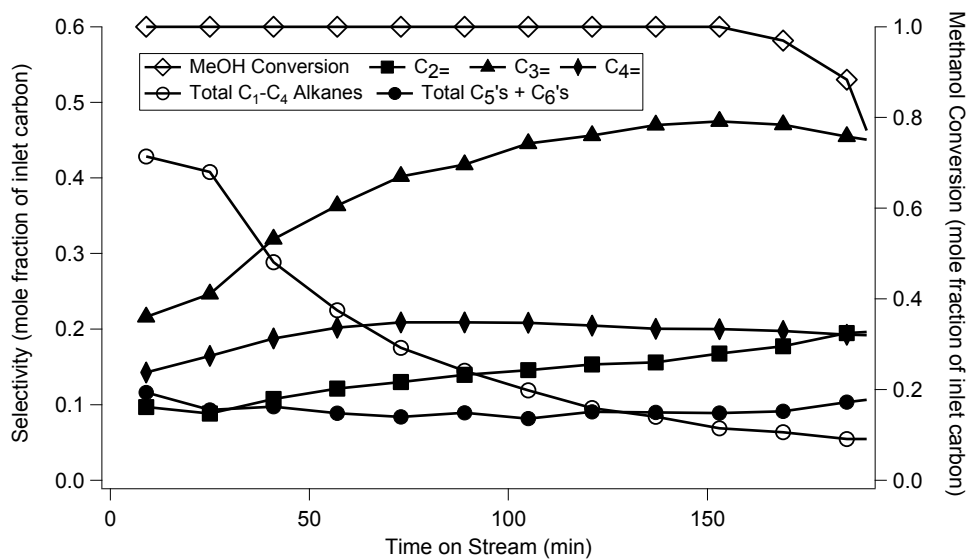
Figure S4. Fresh Si/Al=17 RTH (sample H6)
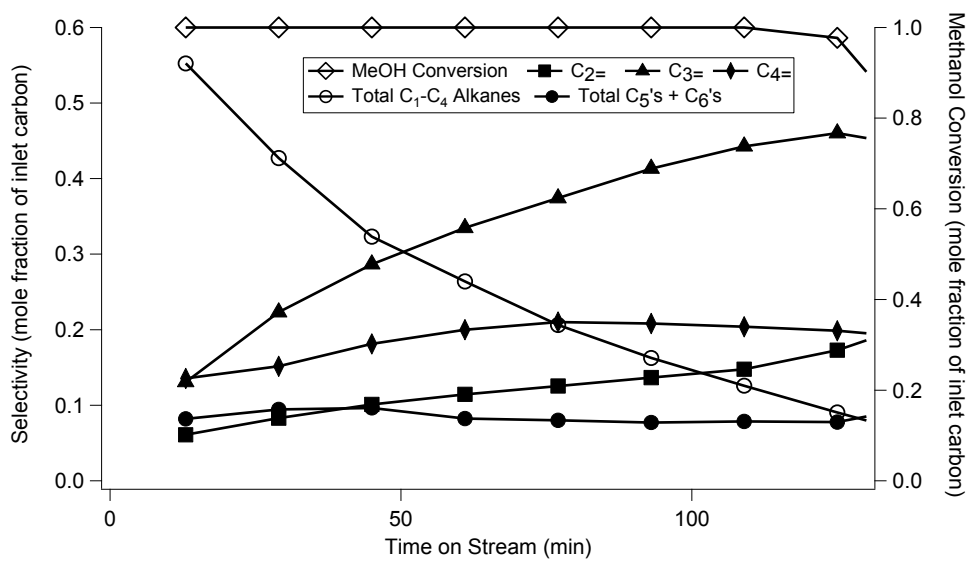
Figure S4. Si/Al=17 RTH regenerated one time (sample H6)
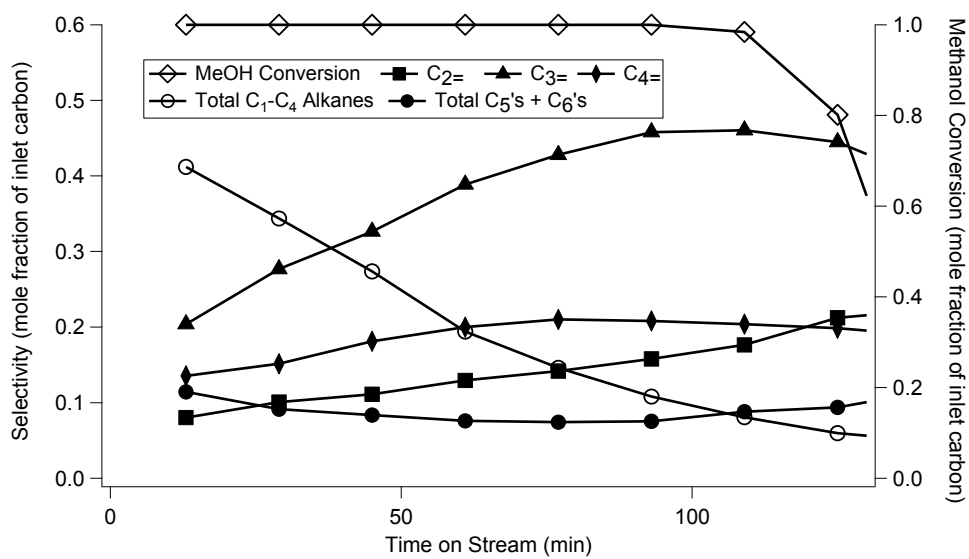
Figure S5. Si/Al=17 RTH regenerated two times (sample H6)

Chapter 4. Synthesis of RTH-type Zeolites Using a Diverse Library of Imidazolium Cations

4.1 Abstract

RTH-type zeolites are promising catalytic materials for applications that include the important methanol-to-olefins (MTO) and NO_X reduction reactions. Here, **RTH**-type zeolites are prepared using a wide-range of imidazolium-based, cationic organic structure directing agents (OSDAs), that greatly expand the methodologies and compositions that can be used to synthesize these materials. The abilities of the OSDAs to produce **RTH**-type zeolites agree well with results from molecular modeling studies of predicted stabilization energies of the OSDAs in the **RTH** framework. The **RTH**-type zeolites are stable to steaming up to 900°C, and are shown to be active MTO catalysts.

4.2 Introduction

It is estimated that over 90% of chemical processes use a catalyst, with 80% being a heterogeneous catalyst, amounting to a global demand of $15 to $20 billion per year.[1] Microporous materials (pores less than 2 nm) are an important type of heterogeneous catalyst, as they offer shape and size selective environments for catalysis to occur. Additionally, they often exhibit robust hydrothermal stability that allows them to be used under demanding process conditions, such as fluidized catalytic cracking or NO_X reduction in exhaust streams. Synthetic

zeolites are produced on a scale 1.7-2 million metric tons per year, and their use as catalysts

makes up 27% of the world market for zeolites.[2] As the cost of the catalyst is estimated to be only

0.1% of the cost of the final product, the demand to innovate in this area remains high.[1]

There currently exist over 200 known microporous material frameworks, but of these, less

than 20 have been commercialized, and the market is dominated by only five major frameworks.[2,3]

The motivation to develop new materials is strong as there normally is only a single structure and

composition for satisfactory performance in a given application.[4] Much of the discovery of new

frameworks and compositions in recent years has resulted from the use of organic structure

directing agents (OSDAs) that are normally alkylammonium cations. While OSDAs have led to

many new materials, their cost contributes a significant portion of the material cost, that often

cannot be recovered as they are generally removed using combustion.[3,5,6] In some systems, it is

possible to partially replace high cost OSDAs with cheaper organics, such as with SSZ-13, where it

has been shown that over 80% of the expensive trimethyl-N-1-Adamantammonium hydroxide

OSDA can be replaced with the much cheaper benzyltrimethylammonium hydroxide.[3]

Alternatively, methods to synthesize the materials in the absence of OSDAs are being explored.

However, this route can often lead to limited product compositions, and does not eliminate

processing steps such as ion exchange and calcination.[7] Therefore, an attractive route to lower

OSDA costs is to find simpler OSDAs to synthesize desired materials.

We have recently reported on a method to synthesize aluminosilicate **RTH** (SSZ-50) across a

wide compositional range using a simple OSDA, pentamethylimidazolium.[8] Prior to this discovery,

SSZ-50 was prepared using a difficult to produce OSDA (Figure 4-1) requiring an elaborate, multi-

step synthesis or by OSDA free methods that only reported the material over a very limited

compositional range.[9–12] **RTH** has a 2-dimensional system of 8-membered ring (8MR) pores,

leading to larger cages. It shows good activity for the methanol-to-olefins reaction (MTO) and

has also been proposed as a material for catalytic NO_X reduction.[8]
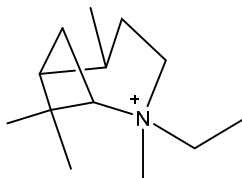
Figure 4-1. Original OSDA reported to synthesize aluminosilicate **RTH** (SSZ-50)**.**

Here, we show that **RTH**-type zeolites can be produced by a wide range of substituted

imidazolium OSDAs. The general structure directing ability of these OSDAs agrees well with the

molecular modelling predictions. This study was prompted by our recent work in which we

screened a number of imidazoliums to make pure-silica **STW**.[13] We found with many of these

OSDAs that the addition of aluminum to fluoride-mediated systems caused **RTH** to form instead of

STW. These results are not trivial, as in the original work to produce SSZ-50, modifying the OSDA

by a single carbon atom led to a change in product.[9] Additionally, the hydrothermal stability of the

RTH materials is evaluated and the zeolites are found to be stable under severe hydrothermal

conditions and maintain good catalytic activity (MTO).

4.3 Experimental Section

4.3.1 OSDA Synthesis

Two different types of reactions were used to produce the imidazolium OSDAs in this work.

Specific details including reaction types and product characterizations for each OSDA can be found

in Table 4-1.

Reaction type 1: The parent imidazole was dissolved in methanol and then cooled in a dry

ice/acetone bath. Then a three-fold molar excess of methyl iodide was slowly added. (Caution:

These reactions can be highly exothermic, use appropriate precautions.) The mixture was then allowed to slowly warm to room temperature and finally refluxed overnight. After cooling, the solvent and excess methyl iodide were removed using rotary evaporation (Caution: Highly toxic vapors present, use appropriate precautions), and the product was recrystallized from acetone and washed with ether.

Reaction type 2: The parent imidazole was dissolved in chloroform and then a two-fold molar excess of potassium carbonate was added. The mixture was cooled in a dry ice/acetone bath and then a two-fold molar excess of methyl iodide was slowly added. (Caution: These reactions can be highly exothermic, use appropriate precautions.) The mixture was then allowed to slowly warm to room temperature and finally refluxed overnight. After cooling to room temperature the potassium carbonate was filtered, and the solids were rinsed with extra chloroform to recover all the product. Then the solvent and excess methyl iodide were removed using rotary evaporation (Caution: Highly toxic vapors present, use appropriate precautions), and the product was recrystallized from acetone and washed with ether.

In both types of reactions the structure was verified using ^{13}C NMR in D_2O with methanol added as an internal standard. The products were then converted from iodide to hydroxide form using hydroxide exchange resin (Dowex Marathon A, hydroxide form) in water, and the product was titrated using a Mettler-Toledo DL22 autotitrator using 0.01 M HCl as the titrant.

Table 4-1. Characterization of imidazolium cations.

Organic	Parent Imidazole	Supplier	Reaction Type	^{13}C NMR δ (ppm)
1	N-methylimidazole	Aldrich	1	36.32, 123.76, 136.86
2	1,2-Dimethylimidazole	Aldrich	1	8.52, 34.48, 121.64, 144.63
3	4-methylimidazole	Aldrich	2	8.52, 33.37, 35.87, 120.37, 132.33, 135.86
4	2-ethylimidazole	Aldrich	2	9.92, 16.59, 34.71, 122.07, 148.16
5	2,4-dimethylimidazole	Synquest	2	8.62, 9.38, 31.46, 34.36, 118.64, 130.14, 143.89
6	2-ethyl-4-methylimidazole	Aldrich	2	8.80, 10.17, 16.93, 31.52, 34.36, 118.83, 120.23, 130.23, 147.32
7	2-isopropylimidazole	TCI	2	17.55, 24.79, 35.68, 122.65, 149.69
8	1,2,4,5-tetramethylimidazole	TCI	1	7.99, 9.76, 31.58, 125.42, 142.21

4.3.2 Microporous Materials Synthesis

Characterization

A general synthesis procedure for the microporous materials can be found below. In all situations the samples were spun at 43 rpm in a rotating oven. The ^{27}Al MAS NMR were recorded using a Bruker AM 300 MHz spectrometer with a 4 mm rotor at a spinning rate of 8 kHz, and were conducted in a 7.0 T magnetic field corresponding to a Larmor frequency of 78.172 MHz. The ^{27}Al spectra are referenced to 1.1 M Al(NO$_3$)$_3$ as an external standard. Prior to ^{27}Al NMR analysis, the samples were hydrated by placing them in a desiccator containing a saturated aqueous salt solution. All powder X-ray diffraction (PXRD) characterization was conducted on a Rigaku MiniFlex II with Cu Kα radiation. Nitrogen adsorption isotherms were performed on a Quantachrome Autosorb iQ at 77 K. Micropore volume was determined using the t-plot method. Scanning electron microscope (SEM) images were acquired on a ZEISS 1550 VP FESEM, equipped with in-lens SE. EDS spectra were acquired with an Oxford X-Max SDD X-ray Energy Dispersive

Spectrometer system.

For all microporous material syntheses, aliquots of the material were taken periodically (generally every 3-4 days) by first quenching the reactor in water and then removing enough material for PXRD. Syntheses were considered to be finished when a crystalline product was observed via PXRD and the broad peak indicative of amorphous material, between 20 and 30° 2θ, had disappeared. If incomplete crystallization or no crystalline product was observed in PXRD, the syntheses were replaced in the oven. For all syntheses that produced **RTH**, representative synthesis times are included in Table 4-2. As some variation in synthesis times is generally observed in zeolite synthesis, all samples were evaluated using PXRD to determine completion.

Fluoride-mediated reactions

Tetraethylorthosilicate (TEOS) and aluminum isopropoxide (if necessary) were added to the OSDA in its hydroxide form in a Teflon Parr Reactor. The container was closed and stirred overnight to allow for complete hydrolysis. The lid was then removed, and the ethanol and appropriate amount of water were allowed to evaporate under a stream of air. Once the appropriate mass was reached, aqueous HF was added and the mixture was stirred by hand until a homogenous gel was obtained. In the cases of $H_2O/SiO_2=4$ a second evaporation step was normally used. The final gel molar ratios were:
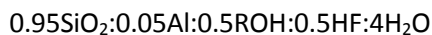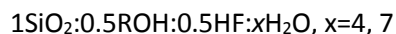
$$1SiO_2:0.5ROH:0.5HF:xH_2O, x=4, 7$$

$$0.95SiO_2:0.05Al:0.5ROH:0.5HF:4H_2O$$

The autoclave was sealed and placed in a rotating oven at 175°C. Aliquots of the material were taken periodically by first quenching the reactor in water and then removing enough material for XRD.

Si/Al=15 (NH₄-Y and Sodium Silicate)

Following the method of Wagner et al.[14] 2 mmol of OSDA was mixed with 0.20 g of 1 M NaOH, and water was added to give a total mass of 6 g. Then 2.5 grams of sodium silicate (PQ Corporation, 28.6wt% SiO_2 and 8.9wt% Na_2O) was added to the mixture and finally 0.25 g of NH_4-Y (Zeolyst CBV 500, Si/Al=2.55) was added. The solution was heated at 140°C in a rotating oven.

Si/Al=15 (CBV 720)

3 mmol of OSDA was mixed with 1 g of 1 M NaOH and water was added to bring the total mass to 7 g. Then 1 g of CBV 720 (Zeolyst, Si/Al=15) was added. The solution was heated at 160°C in a rotating oven.

Si/Al=30 (CBV 760)

3 mmol of OSDA was mixed with 1 g of 1 M NaOH and water was added to bring the total mass to 7 g. Then 1 g of CBV 760 (Zeolyst, Si/Al=30) was added. The solution was heated at 175°C in a rotating oven.

Si/Al=50 (Ludox AS-40 and sodium aluminate)

4 mmol of OSDA was mixed with 1.56 g of 1 M NaOH and the total mass was brought to 9.66 g with the addition of water. Then 0.038 g of sodium aluminate (Pfaltz & Bauer) was added and stirred until dissolved. Finally 3 g of Ludox AS-40 was added and stirred until a homogeneous gel was obtained. Seeds were added and then the gel was heated at 160°C in a rotating oven.

4.3.3 Calcination and Ammonium Exchange

All products were calcined in breathing grade air. The material was heated to 150°C at 1°C/min, held for three hours, then heated to 580°C at 1°C/min and held for six hours to assure complete combustion of the organic. After calcination they were exchanged to ammonium form using 1 M NH_4NO_3 (100 mL of solution per gram of catalyst) at 95°C with stirring for three hours, this was done a total of three times per sample. After ammonium exchange the materials were

washed with water and dried and then calcined to proton form using the standard method.

4.3.4 Material Steaming

Steaming was performed at atmospheric pressure in an MTI OTF-1200X horizontal tube furnace fitted with a 3 in. ID mullite tube. Proton form **RTH** samples (approximately 0.5 g in a typical experiment) were loaded into ceramic calcination boats and placed in the center of the tube furnace. The furnace was then ramped at 1°C/min to the desired steaming temperature (700°C-1000°C) and held at this temperature for 8 h before cooling to room temperature. Flowing steam (present for the entire procedure) was created by bubbling zero-grade air at 50 cc/min through a heated water saturator (bubbler) upstream of the furnace. Proton form **RTH** samples were steamed at temperatures of 700°C, 800°C, 900°C, and 1000°C, with the bubbler held at 80°C for each sample (corresponding to a steam partial pressure of 47.3 kPa).

4.3.5 MTO Reaction Testing

The calcined materials were then pelletized, crushed, and sieved. Particles between 0.6 mm and 0.18 mm were supported between glass wool beds in an Auto-clave Engineers BTRS, Jr. SS-316 tubular, continuous flow reactor.

All catalysts were dried at 150°C in situ in a 30 cm^3/min flow of 5% Ar/95% He for 4 h prior to the reaction. The reactions were conducted at 400°C in a 10% methanol/inert flow. Methanol was introduced via a liquid syringe pump at 5.4 µL/min, into a gas stream of the inert blend at 30 cm^3/min. The reactant flow had a weight hourly space velocity of 1.3 h−1. In a typical run, 200 mg of dry catalyst was loaded. Effluent gases were evaluated using an on-stream GC/ MS (Agilent GC 6890/MSD5793N) with a Plot-Q capillary column installed. Conversions and selectivities were computed on a carbon mole basis.

4.3.6 Molecular Modelling

The location and the van der Waals (vdW) interaction energy of the OSDA within the **RTH** framework were studied by molecular mechanics simulations using the Materials Studio 6 software.[15] The CVFF forcefield[16] was selected for the calculation, and the most stable locations for the OSDA molecules were obtained by simulated annealing. The zeolite framework was assumed to be pure silicate, because the distribution of the Al atoms in the framework is not clear. We limited the modeling strictly to vdW interaction energies between the OSDAs and the framework, and did not include inorganic cations and water molecules to the calculation. The unit cell and the framework atoms were fixed during the calculation, and in this case, there is no need to generate a supercell. The geometry of the OSDA molecule was first optimized using the CVFF forcefield, and then allowed to change after it was docked to the zeolite framework. Initially, two OSDA molecules were docked per unit cell (as there are two cages per unit cell), and then the number was increased. The results indicated that the most stable situation was when there were four imidazolium OSDA molecules per unit cell, or in the case of the OSDA in Figure 4-1, two OSDAs per unit cell.

4.4 Results and Discussions
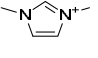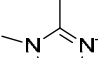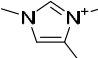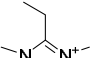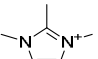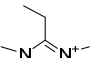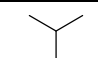
4.4.1 Synthesis of aluminosilicate RTH

Results of the imidazolium screening reactions are given in Table 4-2. It was found that nearly all of the imidazolium cations screened in this study led to the formation of **RTH**-type materials. The simplest imidazolium OSDA, **1**, did not produce **RTH** and was found to decompose under many of the conditions tested in this study. However, **1** led to framework materials in fluoride-mediated reactions, and these results are consistent with previous reports.[17,18] Additionally, OSDA **7** was also unstable under many of the conditions tested in these screening reactions, and was not found to

lead to **RTH** under any conditions tested. Other than OSDAs **1** and **7**, all of the other OSDAs

tested were able to produce aluminosilicate **RTH** under a majority of the inorganic conditions

employed in this study. The formation of aluminosilicate **RTH** using pentamethylimidazolium was

first observed in fluoride-mediated, aluminosilicate conditions, and OSDAs **2-6, 8** were all able to

produce **RTH** under this condition, without the use of seeds. Under more conventional, hydroxide-

mediated conditions, they also formed **RTH** across a wide range of compositions. In some cases,

such as with OSDAs **2-4**, the use of seeds was found to be necessary to cause the formation of

RTH. It is likely that these organics were less directing to **RTH**, but are still able to form the

material when nucleation to **RTH** is induced through seeding (discussed further in section 3.2). The

OSDAs found to be the most strongly directing to **RTH** are **2, 5,** and **8**. (We have previously

reported OSDA **8** to produce aluminosilicate **RTH**.[8]) The ability to obtain **RTH** using a variety of

imidazolium cations may open possibilities for OSDA availability. Industrially, imidazoles are

produced using the Radziszewski reaction or by dehydrogenation of imidazolines, and are

available in high purity; quaternary imidazoliums can then be prepared by standard alkylation

methods.[19]

Table 4-2. Results from synthesis experiments and molecular modelling calculations. All syntheses that produced RTH-type materials are shaded.

Organic	Number	Pure-silica fluoride, H_2O/SiO_2 =4	Pure-silica fluoride, H_2O/SiO_2	Si/Al=20 fluoride	Si/Al=15 Seeds	Si/Al=15 no seeds	CBV 720, seeds	CBV 720, no seeds	CBV 760, seeds	CBV 760, no seeds	Si/Al=50, seeds	Interaction energy (4 OSDAs/cell)
(structure)	1	TON 4 days		FER 11 days	X		X	X	TON 12 days	TON 12 days		-15.94
(structure)	2	ITW 5 days	ITW 5 days	RTH Si/Al=9 12 days (S1)	RTH 3 days	RTH Si/Al=9 6 days (S2)		RTH Si/Al=14 5 days (S3)	RTH Si/Al=18 28 days (S4)	X	RTH + dense 30 days	-18.29
(structure)	3	ITW 5 days	ITW 12 days	RTH Si/Al=10 7 days (S5)	RTH Si/Al=9 3 days (S6)	MOR 20 days	X	X	TON 12 days	X	TON 31 days	-17.40
(structure)	4	CIT-7, ITW, STW, STF, MTW >4 days	ITW 29 days	RTH Si/Al=12 20 days (S7)	RTH Si/Al=8 7 days (S8)	RTH Si/Al=9 8 days (S9)	RTH Si/Al=14 14 days (S10)	X	X	X	MTW 11 days	-17.90
(structure)	5	STW 4 days	STW 4 days	RTH Si/Al=10 5 days (S11)	RTH 10 days	RTH + MOR 12 days	RTH Si/Al=13 5 days (S12)	RTH 5 days	RTH Si/Al=27 12 days (S13)	RTH 12 days		-18.62
(structure)	6	STW 16 days	HPM-2 20 days	RTH Si/Al=13 20 days (S14)	RTH Si/Al=9 15 days (S15)	MOR + RTH 16 days	X	X	X	X	MTW 13 days	-15.00
(structure)	7	STF 9 days	Unknown 21 days	Unknown 45 days	MOR 16 days	MOR 16 days	X	X	X			-16.45
(structure)	8	STW 5 days	STW 7 days	RTH Si/Al=8 10 days (S16)	RTH Si/Al=9 4 days (S17)	RTH Si/Al=4 10 days	RTH Si/Al=17 10 days	RTH Si/Al=15 20 days (S18)	RTH Si/Al=29 13 days	RTH Si/Al=22 20 days (S19)	RTH Si/Al=45 9 days	-20.02

X=Organic Decomposed
Interaction Energy (kJ/mol per T-atom) = vdW energy values shown in the table were averaged from 3 repeated runs.
Synthesis times are reported in days.
Material Si/Al ratios were determined using EDS.
Samples with numbers in parentheses refer to SEM images that can be found in the Supporting Information.

The morphology and composition of the samples that that produced **RTH** were studied using SEM and EDS. The SEM images can be found in the Supplementary Information. In general fluoride-mediated reactions led to larger crystals than the hydroxide-mediated syntheses. However, there was a large amount of variability found between OSDAs using the same inorganic conditions.

4.4.2 Molecular Modelling

To gain deeper insight into the ability of the imidazolium cations used in this study to structure direct **RTH-**type materials, molecular modelling calculations were performed and the results are shown in Figure 4-2. In these calculations, 4 OSDAs were populated per unit cell based on energy optimizations for the framework space filling. The results of the predicted interaction energies agree well with the observed experimental results. The OSDAs with the most favorable interaction energies, **5** and **8**, were found to produce **RTH** under many inorganic conditions, with and without seeds. However, OSDAs with less favorable interaction energies compared to **8** did not lead to the formation of **RTH** as readily and generally required seeds to favor the formation of **RTH**. These results were then compared to the stabilization energy for the original **RTH** OSDA (Figure 4-1), that was found to be -11.10 kJ/mol (for 2 OSDAs per unit cell, the optimal packing). It was surprising that this interaction energy is much less favorable than any of the imidazoliums in this study. One possible explanation for the large energy difference is that the imidazoliums all required two OSDAs per cage while the OSDA in Figure 4-1 only has a single molecule per cage, requiring less ordering between OSDAs. The positions of the OSDAs within the cages are shown in Figure 4-2, as determined by molecular modelling.
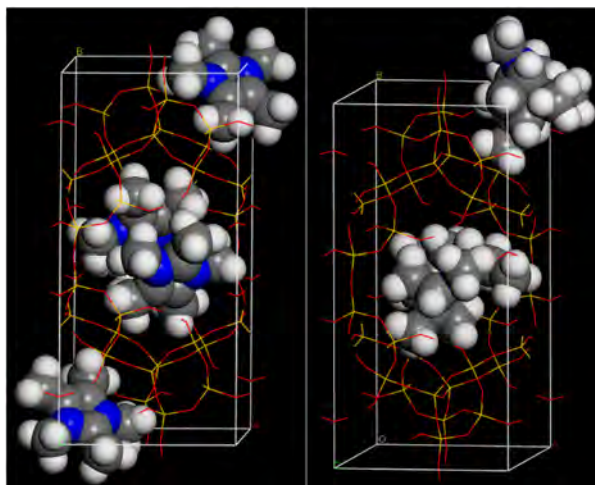
Figure 4-2. Positions of OSDAs within the **RTH** framework for pentamethylimidazolium (left) and the original SSZ-50 OSDA (right).

4.4.3 Hydrothermal Stability

The hydrothermal stability of **RTH-**type zeolites prepared from CBV 720 was assessed by steaming the proton form of the material to various temperatures, and then characterizing the solids thus obtained by PXRD, ^{27}Al MAS NMR, nitrogen adsorption isotherms, and the MTO reaction to test for catalytic activity. The material was steamed to temperatures ranging from 700 to 1000°C, and details of the steaming procedure can be found in the experimental section. The PXRDs of the steamed materials (Figure 4-3) show that the framework structure is intact until at least 900°C, but that the structure essentially collapses by 1000°C. The ^{27}Al MAS NMRs of the proton form and steamed materials are shown in Figure 4-6, and the distribution of aluminum coordination environments for the various samples is given in Table 4-3. As the results from the ^{27}Al quantification show, higher temperature steam treatment decreases the amount of tetrahedral (framework) aluminum in the samples, consistent with framework damage. Nitrogen adsorption isotherms of the proton form sample as well as the material after steaming to 900°C (the highest steaming temperature with the structure intact) are shown in

Figure 4-4. The proton form of the material has a micropore volume of 0.24 cc/g while the

steamed material has a micropore volume of 0.19 cc/g. The reduced micropore volume of the

steamed material indicates that some framework destruction has occurred.

Table 4-3. Distribution of aluminum coordination in steamed samples from ^{27}Al MAS NMR

	Tetrahedral	Pentacoordinated	Octahedral
Proton Form	100%	--	--
Steamed 700°C	55%	8%	38%
Steamed 800°C	15%	15%	70%
Steamed 900°C	14%	21%	64%
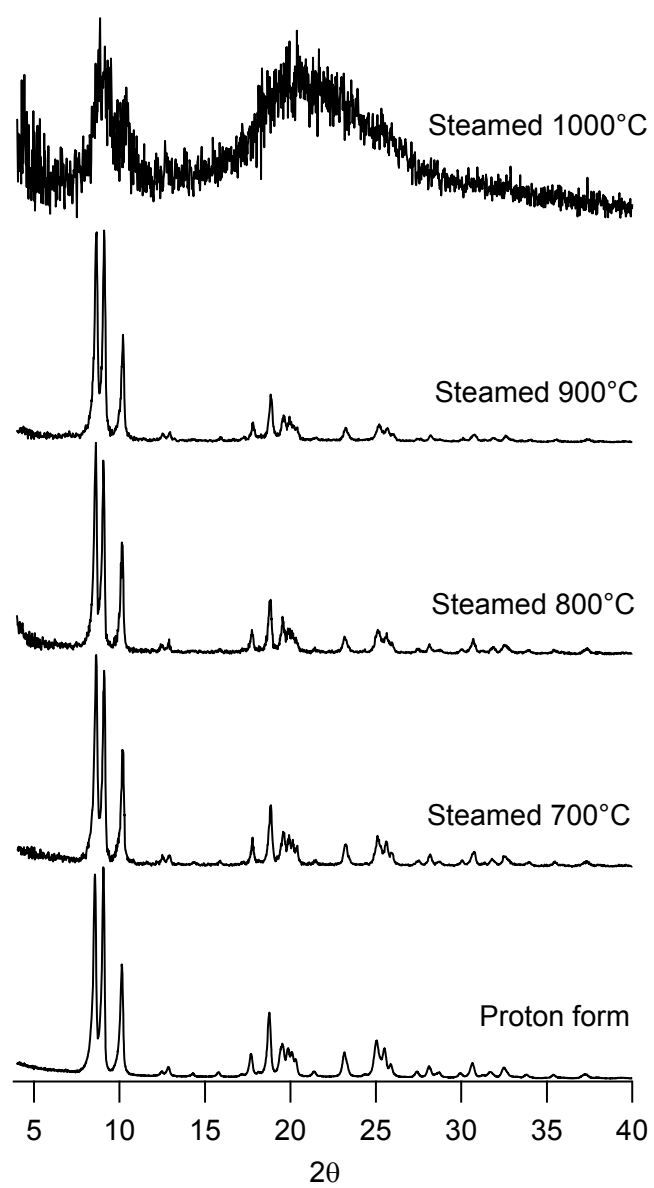
Figure 4-3. PXRDs of steamed and proton form **RTH**
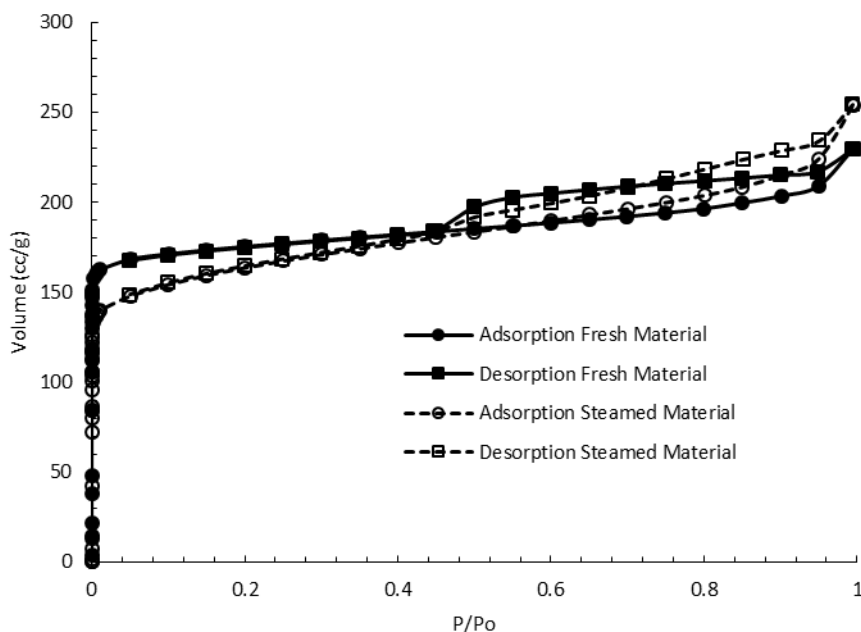
Figure 4-4. Nitrogen isotherms of fresh and steamed RTH

The steamed materials were also studied as catalysts using the MTO reaction, and the results

are shown in Figure 4-5. The fresh **RTH** sample has a significantly longer lifetime than the steamed

samples. However, the purpose of this test was to assess the effects of hydrothermal treatment

on MTO reactivity, and the MTO results show that these materials are catalytically active after

severe steam treatments. The sample steamed to 1000°C was also tested for MTO reactivity, and

showed no catalytic activity, consistent with the severe degradation evident from PXRD. The

steaming studies demonstrate that the **RTH**-type materials are highly resistant to degradation,

even under severe hydrothermal conditions.
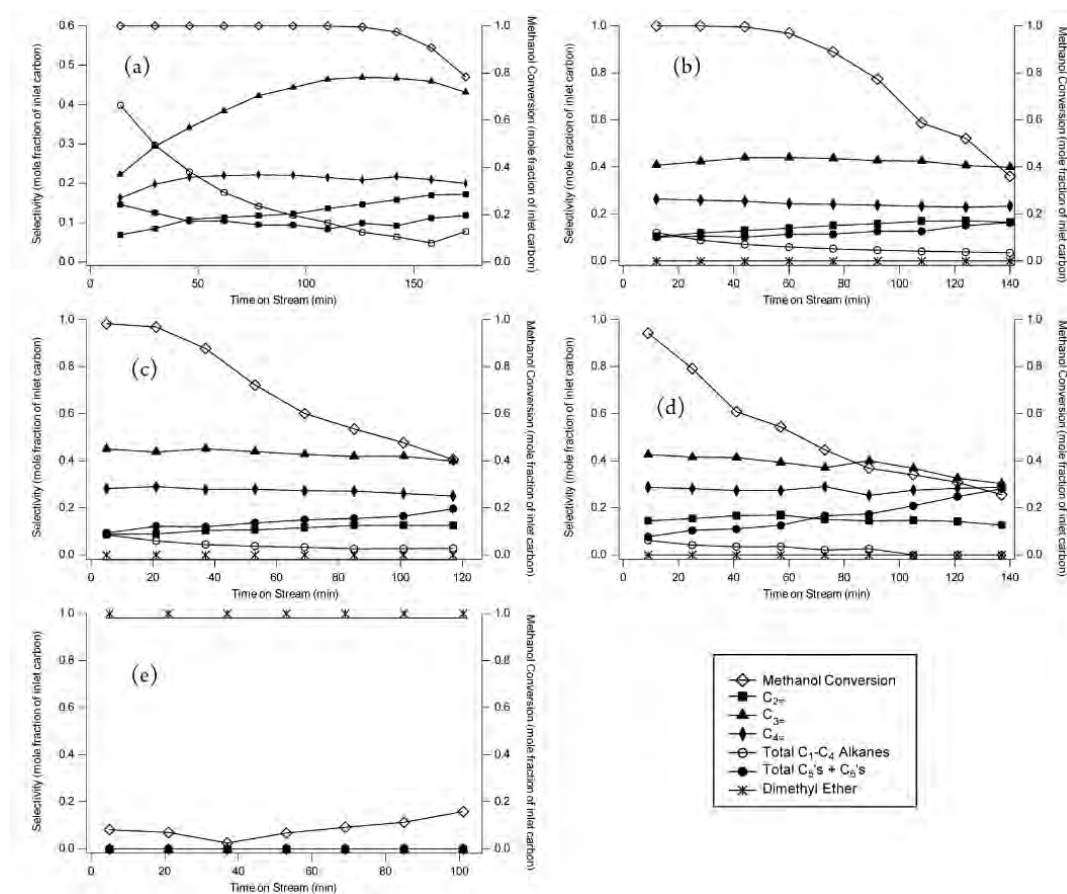
Figure 4-5. MTO reaction data for (a) fresh **RTH** catalyst, (b) steamed to 700°C, (c) steamed to 800°C, (d) steamed to 900°C, and (e) steamed to 1000°C
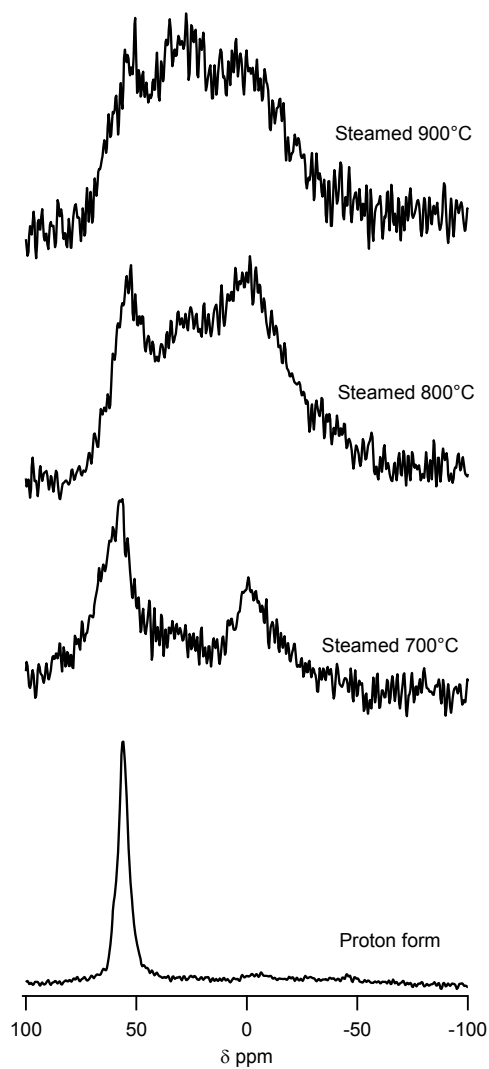
Figure 4-6. ^{27}Al MAS NMRs of proton form and steamed **RTH**

4.5 Conclusions

RTH-type zeolites can be produced by a wide-range of imidazolium cations, diversifying the methods for its synthesis. The structure directing ability of the OSDAs used here agrees well with the results predicted by molecular modelling for the stabilization energies of the organics in the **RTH** framework. Additionally, the **RTH** framework is found to be stable to steaming to 900°C,

demonstrating potential for utility under demanding process conditions.

4.6 Funding Sources

4.7 Acknowledgements

4.8 References

(1) Bravo-suárez, J. J.; Chaudhari, R. V; Subramaniam, B. Design of Heterogeneous Catalysts for Fuels and Chemicals Processing: An Overview. In *Novel Materials for Catalysis and Fuels Processing*; Bravo-Suárez, J. J., Kidder, M. K., Schwartz, V., Eds.; ACS Symposium Series; American Chemical Society: Washington, DC, 2013; Vol. 1132, pp 3–68.

(2) Yilmaz, B.; Müller, U. Catalytic Applications of Zeolites in Chemical Industry. *Top. Catal.* **2009**, *52* (6-7), 888–895.

(3) Zones, S. I. Translating New Materials Discoveries in Zeolite Research to Commercial Manufacture. *Microporous Mesoporous Mater.* **2011**, *144* (1-3), 1–8.

(4) Pophale, R.; Daeyaert, F.; Deem, M. W. Computational Prediction of Chemically Synthesizable Organic Structure Directing Agents for Zeolites. *J. Mater. Chem. A* **2013**, *1* (23), 6750–6760.

(5) Zones, S. I.; Hwang, S.-J. Synthesis of High Silica Zeolites Using a Mixed Quaternary

Ammonium Cation, Amine Approach: Discovery of Zeolite SSZ-47. *Chem. Mater.* **2002**, *14* (1), 313–320.

(6) Zones, S. I.; Lee, H.; Davis, M. E.; Casci, J.; Burton, A. W. Strategies in Developing Routes to Commercialization of Novel High Silica Zeolites. *Stud. Surf. Sci. Catal.* **2005**, *158*, 1–10.

(7) Iyoki, K.; Itabashi, K.; Okubo, T. Progress in Seed-Assisted Synthesis of Zeolites without Using Organic Structure-Directing Agents. *Microporous Mesoporous Mater.* **2013**, *8* (7), 1419–1427.

(8) Schmidt, J. E.; Deimund, M. A.; Davis, M. E. Facile Preparation of Aluminosilicate RTH across a Wide Composition Range Using a New Organic Structure-Directing Agent. *Chem. Mater.* **2014**, *26* (24), 7099–7105.

(9) Lee, G. S.; Zones, S. I. Polymethylated [4.1.1] Octanes Leading to Zeolite SSZ-50. *J. Solid State Chem.* **2002**, *167* (2), 289–298.

(10) Kim, C.; Hwang, S.-J.; Burton, A. W.; Zones, S. I. A Case Study of Divergent Structure Directing Effects of Geometric Isomers: The Discovery of a New Structure Directing Agent for an All-Silica RTH Zeolite Prepared in Fluoride Media. *Microporous Mesoporous Mater.* **2008**, *116* (1-3), 227–232.

(11) Yokoi, T.; Yoshioka, M.; Imai, H.; Tatsumi, T. Diversification of RTH-Type Zeolite and Its Catalytic Application. *Angew. Chem. Int. Ed. Engl.* **2009**, *48* (52), 9884–9887.

(12) Yoshioka, M.; Yokoi, T.; Liu, M.; Imai, H.; Inagaki, S.; Tatsumi, T. Preparation of RTH-Type Zeolites with the Amount And/or Kind of Organic Structure-Directing Agents (OSDA): Are OSDAs Indispensable for the Crystallization? *Microporous Mesoporous Mater.* **2012**, *153*, 70–78.

(13) Schmidt, J. E.; Deem, M. W.; Davis, M. E. Synthesis of a Specified, Silica Molecular Sieve by Using Computationally Predicted Organic Structure-Directing Agents. *Angew. Chem. Int. Ed.*

Engl. **2014**, *53* (32), 8372–8374.

(14) Wagner, P.; Nakagawa, Y.; Lee, G. S.; Davis, M. E.; Elomari, S.; Medrud, R. C.; Zones, S. I. Guest/Host Relationships in the Synthesis of the Novel Cage-Based Zeolites SSZ-35, SSZ-36, and SSZ-39. *J. Am. Chem. Soc.* **2000**, *122* (2), 263–273.

(15) Materials Studio 6.0, Accelrys, Inc.: San Diego, CA, 2012.

(16) Dauber-Osguthorpe, P.; Roberts, V. A.; Osguthorpe, D. J.; Wolff, J.; Genest, M.; Hagler, A. T. Structure and Energetics of Ligand Binding to Proteins: Escherichia Coli Dihydrofolate Reductase-Trimethoprim, a Drug-Receptor System. *Proteins* **1988**, *4* (1), 31–47.

(17) Rojas, A.; Martínez-Morales, E.; Zicovich-Wilson, C. M.; Camblor, M. A. Zeolite Synthesis in Fluoride Media: Structure Direction toward ITW by Small Methylimidazolium Cations. *J. Am. Chem. Soc.* **2012**, *134* (4), 2255–2263.

(18) Archer, R. H.; Zones, S. I.; Davis, M. E. Imidazolium Structure Directing Agents in Zeolite Synthesis: Exploring Guest/host Relationships in the Synthesis of SSZ-70. *Microporous Mesoporous Mater.* **2010**, *130* (1-3), 255–265.

(19) Ebel, K.; Koehler, H.; Gamer, A.; Jackh, R. Imidazole and Derivatives. In *Ullmann's Encyclopedia of Industrial Chemistry*; Wiley-VCH Verlag GmbH & Co. KGaA: Weinheim, Germany, 2000; pp 637–645.

4.9 Supporting Information for Chapter 4

Representative SEM images of selected samples (see Table 4-2)

Si/Al=20, fluoride media

S1   S5

S7   S11

S14   S16
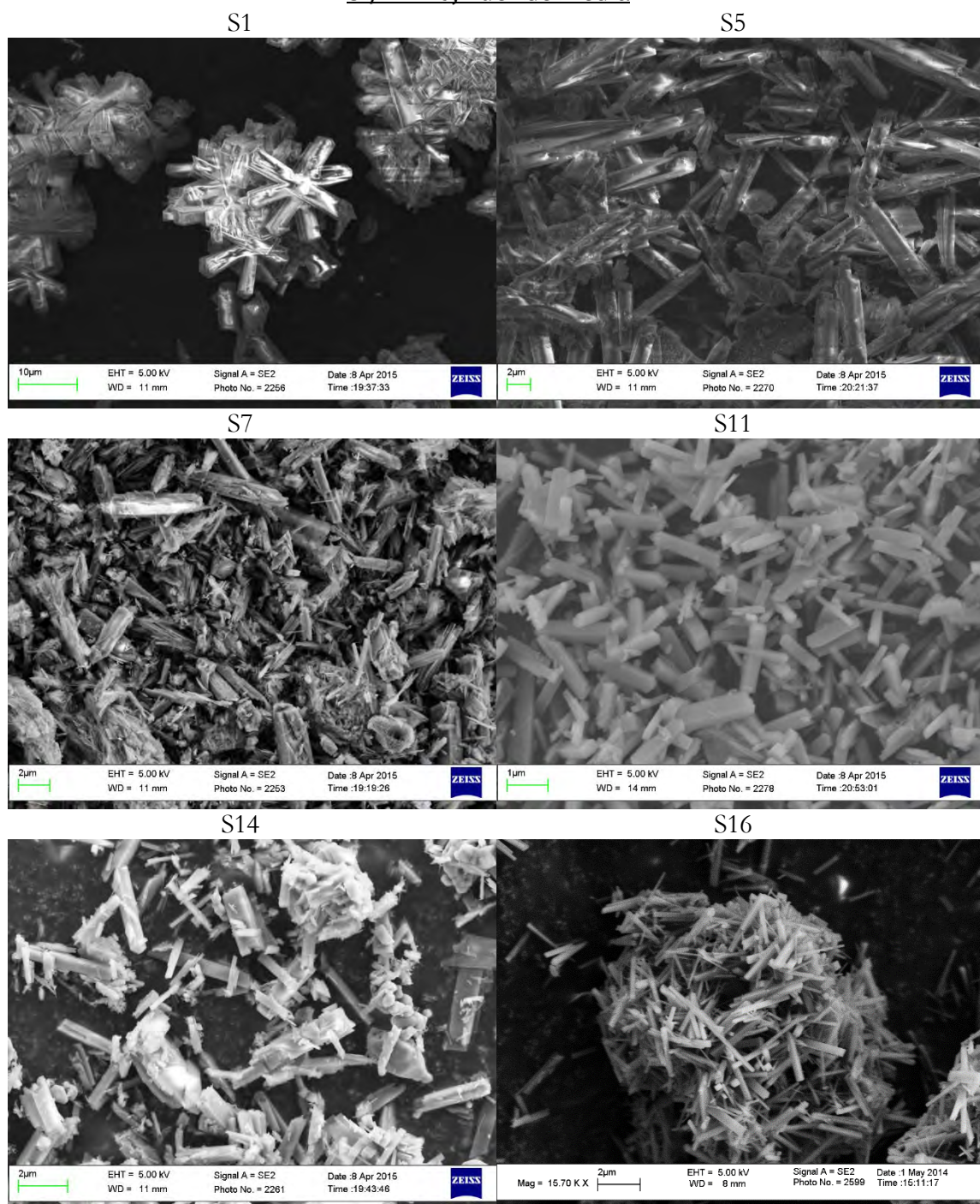
Si/Al=15, seeds

S6
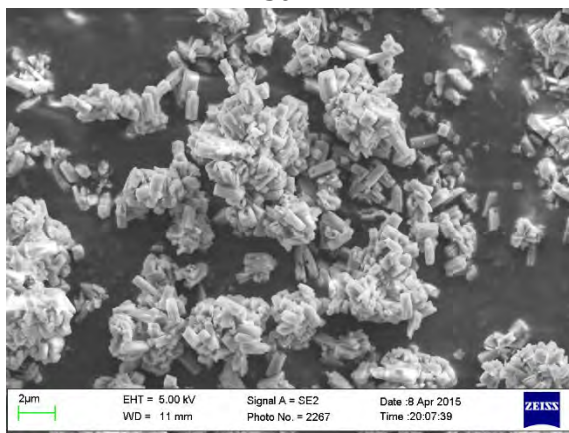
S8
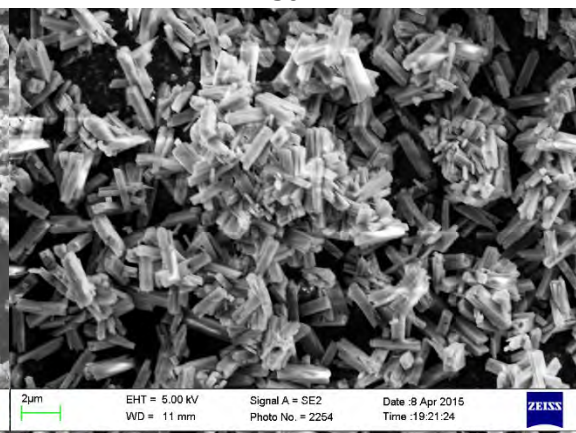
S15
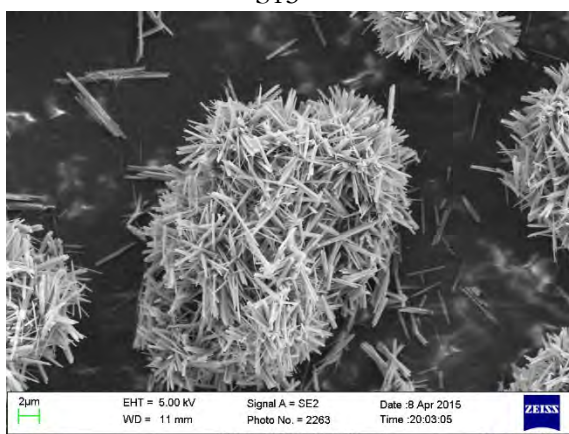
S17
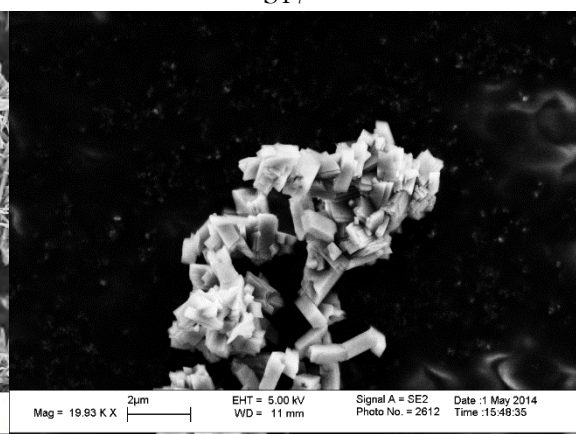
Si/Al=15, no seeds

S2
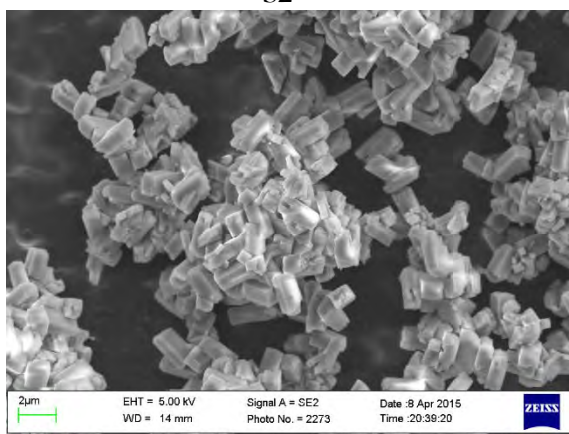
S9
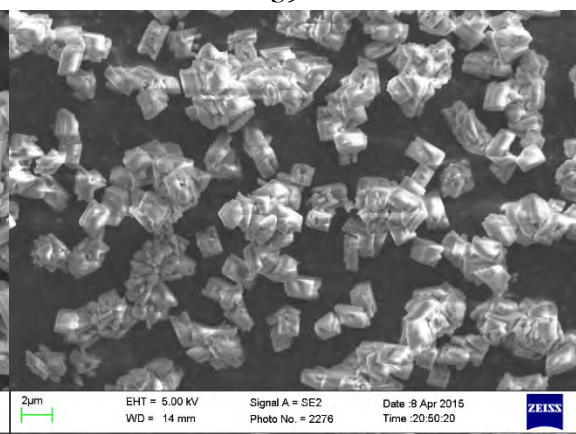
CBV720, seeds
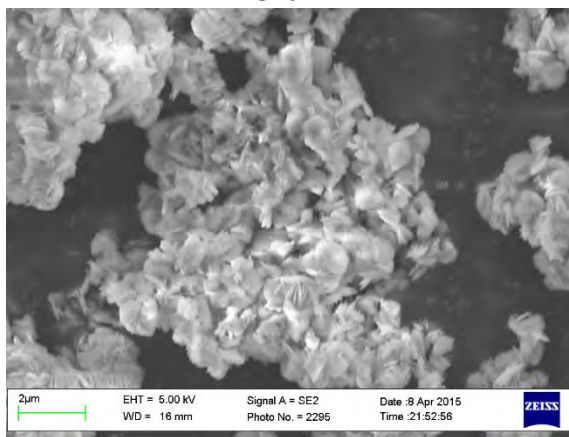
S10 · S12
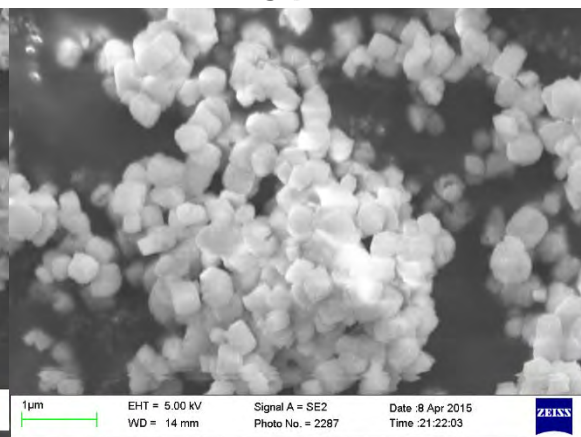
CBV720, no seeds
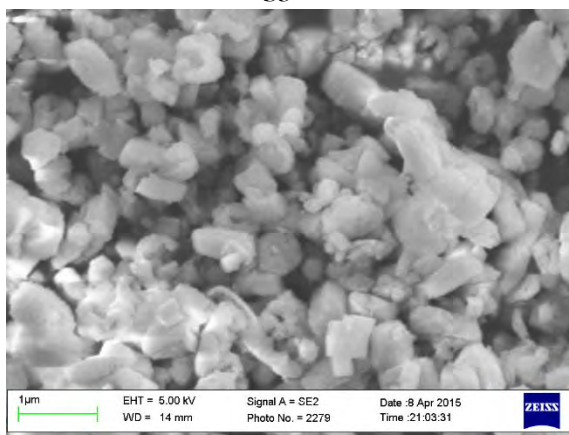
S3 · S18
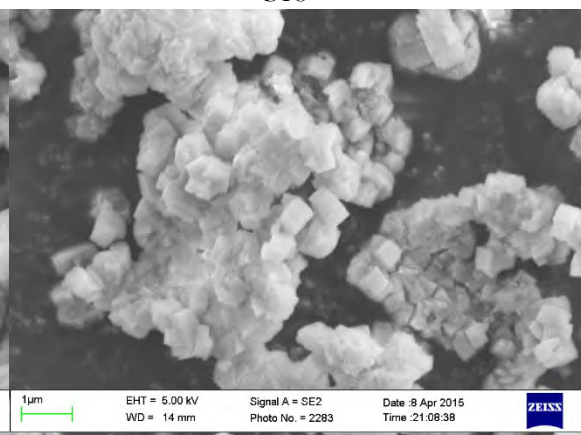
CBV760, seeds
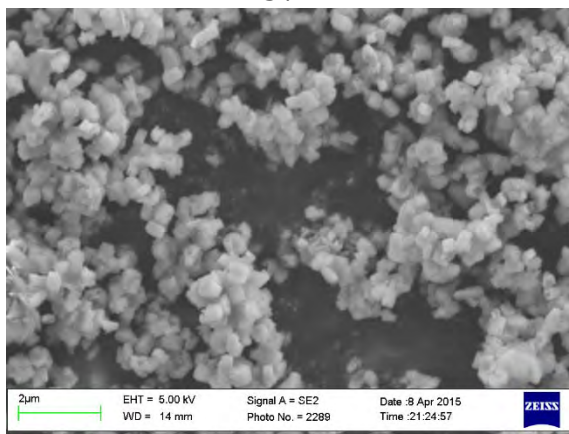
S4 · S13
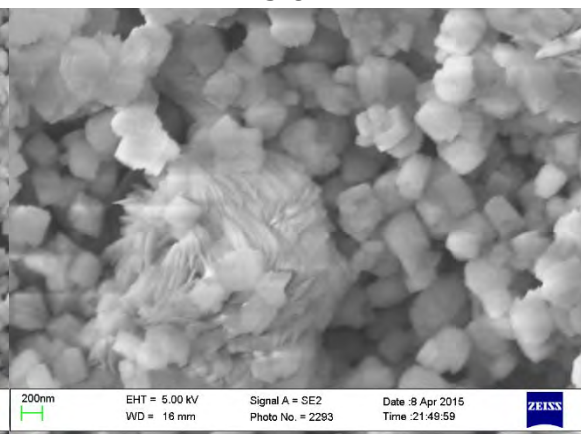
CBV760, no seeds

S19
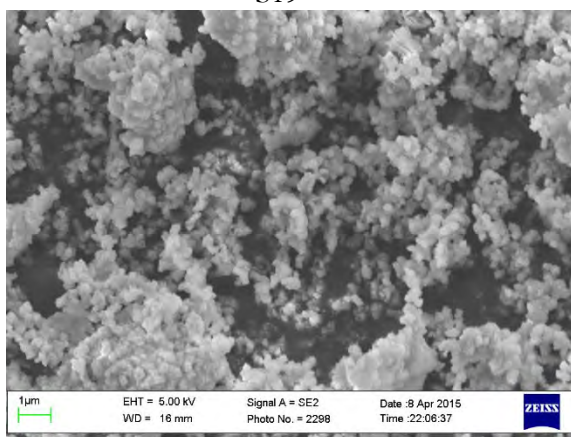
Chapter 5. Synthesis of the RTH-Type Layer: The First Small-Pore, Two Dimensional Layered Zeolite Precursor

Chapter 5 previously appeared as: Schmidt, J. E.; Xie, D.; Davis, M. E. Synthesis of the RTH-Type

  Layer: The First Small-Pore, Two Dimensional Layered Zeolite Precursor. *Chem. Sci.*

  Submittted.

5.1 Abstract

There are several distinct two-dimensional zeolite building layers that can condense through different stacking arrangements of the layers to form various three-dimensional framework materials. All known building layers are dense layers in that they do not contain 8-membered ring (MR) or larger pores perpendicular to the two-dimensional layers. Herein, we report a new material (CIT-10) that consists of a two-dimensional layer (termed "rth" layer) that contains an 8MR perpendicular to the layer. Calcination of CIT-10 forms pure-silica **RTH** (SSZ-50). CIT-10 can be pillared to form a new framework material with a three-dimensional pore system of 8 and 10 MRs, denoted CIT-11, that can be calcined to form a new microporous material, denoted CIT-12.

5.2 Introduction

The rate of discovery of new microporous materials has accelerated in recent years due to factors including new organic structure directing agents, the use of fluoride as a mineralizing agent as well as germanium as a heteroatom in syntheses.[1–6] Much of this discovery is motivated by the fact that a single framework and composition are normally found to achieve optimal performance in a process.[7] Another synthesis strategy that has received increased attention is that of

synthesizing layered silicates that can directly form microporous materials via topotactic condensation, or can be pillared using silyating agents, forming structures with larger pores (generally larger by 2 tetrahedral atoms) than would be formed via topotactic condensation. [8–14]

In a topotactic condensation, a three-dimensional (3D) framework structure is formed from a two-dimensional (2D) layered silicate by condensation of surface silanol groups (Si-OH), releasing water. Some of the initial framework materials prepared via topotactic condensation were **FER,** formed from the layered precursor denoted PREFER,[15] and **MWW**, formed from the layered precursor MCM-22(P).[16] After these pioneering efforts, several additional frameworks have been prepared using topotactic condensation, and they include (layered precursor given in parentheses): **AST** (β-helix-layered silicate),[17] **CAS-NSI** intermediate (EU-19, NU-6(1)),[18–20] **CDO** (PLS-1, RUB-36),[19,21] **FER** (PREFER),[15] **MTF** (HPM-2),[22] **MWW** (MCM-22),[16] **PCR** (IPC-4 prepared by disassembly of **UTL**),[23] **RRO** (RUB-39),[24] **RWR** (RUB-18)[25], and **SOD** (RUB-15).[26] The layered materials that form 3D frameworks can be built by different stacking arrangements of a few 2D building layers (such as cas, fer, heu, mww and rwr).[8,9] Additionally, methods have been developed to prepare **MFI** nanosheets that are a single unit cell thick;[27,28] however, this material generally is not considered to be a building layer.[29]

The silanol groups of the layered zeolite precursors can also be used to prepare larger pore materials through a pillaring process. This process normally uses dichlorodimethylsilane or diethoxydimethylsilane to react with the silanol groups to form pillars that are coordinated to two methyl groups (or two hydroxyl groups after calcination). This process is typically carried out in acidic media under hydrothermal conditions. Some of the layered materials that have been pillared include PREFER, MWW(P), PLS-1, MCM-47, RUB-36, RUB-39, and Nu-6(1).[8,30,31] Additionally, related strategies to prepare porous materials include delamination or exfoliation. Recently, it has also been shown to be possible to introduce catalytic activity in the pillars.[32,33]

Excellent reviews of the above strategies are available.[8,9]

All of the previously reported layered zeolite precursors are dense layers, that is, they contain no pores (8-membered ring (MR) or larger) that are perpendicular to the layers. The **MWW** layer contains a sinusoidal 10MR channel parallel to the *ab*-plane, but it is still dense as this channel is not perpendicular to the layer. However, the nanosheets of **MFI** that are single unit cell thick do contain a 10MR perpendicular to the layer, a medium size pore.[27] We recently reported a method to prepared high-silica heulandite (denoted CIT-8) via topotactic condensation from a layered precursor (denoted CIT-8P), that was prepared using a diquaternary organic structure directing agent (OSDA) in fluoride-mediated syntheses.[34] In that case, the building layer that forms CIT-8 (**HEU**) is the same as that of RUB-41 (**RRO**), but is formed from a different stacking of the heu building layer: AA stacking gives the **RRO** structure while AA' stacking (where the A'-layer is related to the A-layer by a 180 degree rotation) gives the **HEU** structure.[25] CIT-8 was prepared from fluoride-mediated, aluminosilicate inorganic conditions across a relatively narrow composition range. It is interesting to note with this material that the OSDA used was considerably larger than what is normally found in preparing topotactic materials such as piperdines,[15] as well as methyl, ethyl, and propyl substituted ammoniums.[31]

In the absence of aluminium, we have found conditions to prepare the layered precursor to pure-silica **RTH**, denoted CIT-10. This layered material can be directly calcined to prepare pure-silica **RTH** (SSZ-50[35]) or can be pillared, leading to a new microporous material (denoted CIT-11), that is stable to calcination (calcined material denoted CIT-12). CIT-10 is a layered material composed of a new type of 2D building layer (termed "rth", according to the nomenclature defined in Ref. 9) containing an 8MR channel going through the layer (8MR pore dimensions of 5.6 x 2.5 Å). The discovery of CIT-10 adds a new group of layered zeolite precursors and is the first to contain an 8MR through the 2D layer. Pure-silica **RTH** is now the sixth known microporous

material that can be obtained by both direct synthesis and topotactic condensation.

5.3 Experimental

5.3.1 OSDA Synthesis

The diquaternary OSDA used in this work (shown in Figure 5-1) was synthesized by reacting 200 mmol of 1,2,4,5-tetramethylimidazole (TCI Chemicals) with 100 mmol of 1,5-dibromopentane (Aldrich) at reflux in methanol overnight. The solvent was then removed using rotary evaporation and the product washed with ether. The product was verified using ^{13}C NMR in D_2O with methanol added as an internal standard. ^{13}C-NMR (125 MHz, D_2O): δ 7.76, 7.82, 9.61, 22.82, 28.58, 31.42, 44.72, 124.84, 126.03, 141.95. The product was ion exchanged to hydroxide form using Dowex Marathon A exchange resin and the final product concentration was determined using a Mettler-Toledo DL22 autotitrator using 0.01 M HCl as the titrant.
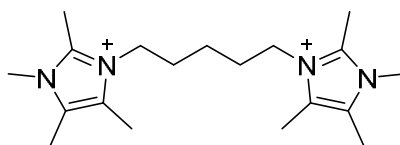
Figure 5-1. OSDA used to prepare CIT-10

5.3.2 Synthesis of CIT-10

Tetraethylorthosilicate was added to the OSDA in its hydroxide form in a Teflon Parr Reactor. The container was closed and stirred overnight to allow for complete hydrolysis. The lid was then removed, and the ethanol and some water were allowed to evaporate under a stream of air. Once the gel was dry, a small amount of water was added to obtain a homogenous liquid. Then aqueous HF was added and the mixture was stirred by hand. A second evaporation step was then used to give a final gel molar ratio of $1SiO_2:0.5R_{1/2}(OH):0.5HF:4H_2O$. Seeds of CIT-10 were then added and the autoclave was sealed and placed in a rotating oven (43 rpm) at 175°C. Aliquots of the material

were taken periodically by first quenching the reactor in water and then removing enough material for powder X-ray diffraction (PXRD). Synthesis times for pure silica RTH were on the order of 20 days when no seeds were added and 10 days when seeds were added. The product was recovered via centrifugation and was washed with water three times and a final time with acetone, and dried in air at 100°C.

5.3.3 Pure-silica RTH

The as-made material prepared in section 2.2 was calcined in breathing grade air. The material was heated to 150°C at 1°C/min, held for three hours, then heated to 580°C at 1°C/min and held for six hours to assure complete combustion of the organic.

5.3.4 Pillaring of CIT-10 to obtain CIT-11

The procedure that led to the pillared product with the highest crystallinity (judged using PXRD) was found to be as follows. 500 mg of CIT-10 were placed in a 45 mL Teflon Parr Reactor., then 20 g of a 1.25 M solution of HCl in ethanol were added. Finally 500 mg of silyating agent (dichlorodimethylsilane or diethoxydimethylsilane, both were found to produce a similar product) were added. The reactor was sealed and place in a rotating oven at 175°C for 24 hours. The product was recovered via centrifugation and was washed one time with absolute ethanol, three times with water, and finally one time with acetone and then dried in air at 100°C.

5.3.5 CIT-12

CIT-12 was obtained by the calcination of CIT-11 using the procedure described in section 2.3.

5.3.6 Characterizations

Liquid NMR spectra were recorded with a 500 MHz spectrometer. ^{13}C and and ^{29}Si solid-state NMR were performed using a Bruker DSX-500 spectrometer (11.7 T) and a Bruker 4mm MAS probe. The spectral operating frequencies were 500.2 MHz, 125.721 MHz and 99.325 MHz for ^{1}H,

[13]C and [29]Si nuclei, respectively. Spectra were referenced to external standards as follows:

tetramethylsilane (TMS) for ^{1}H and [29]Si and adamantane for ^{13}C as a secondary external standard

relative to tetramethylsilane. Samples were spun at 8 kHz for ^{13}C and ^{29}Si MAS and CPMAS NMR

experiments. Thermogravimetric analysis was performed on a PerkinElmer STA 6000 with a ramp

of 1 °C/min to 900 °C under air atmosphere. Argon physical adsorption isotherms were performed

at 87 K using a Quantachrome Autosorb iQ and were conducted using a quasi-equilibrium,

volumetric technique.[36] PXRD data were collected on a Rigaku MiniFlex II with Cu Kα radiation.

Variable temperature Powder x-ray diffraction (PXRD) patterns were collected from 30°C to 580°C

at increments of 50°C under ambient conditions, using a PANalytical Empyrean powder

diffractometer (Cu Kα radiation) equipped with an Anton Paar HTK 1200N high-temperature

chamber. The sample was stabilized at each measurement temperature for 15 min before starting

each measurement. The temperature ramp between two consecutive temperatures was 5°C/min.

Scanning electron microscope (SEM) images were acquired on a ZEISS 1550 VP FESEM, equipped

with in-lens SE. Energy-dispersive X-ray spectroscopy (EDS) spectra were acquired with an Oxford

X-Max SDD X-ray Energy Dispersive Spectrometer system. Three-dimensional electron diffraction

data were collected using the rotation electron diffraction (RED) technique.[37,38] The RED software

was installed on a JEOL 2010 microscope operating at 200 kV, and data were collected over a tilt

range of ±50° with a tilt step of 0.50°, with an exposure time of 3 seconds per tilt step.

5.4 Results and Discussions

5.4.1 Synthesis of CIT-10 and calcination to produce pure-silica RTH

We have recently been investigating imidazolium OSDAs in the synthesis of microporous

materials, and have found that they are able to produce a wide range of phases including **LTA**,[39]

RTH,[40,41] **STW**,[42] CSV,[43] and **HEU**[34] in addition to a number of additional phases discussed in the

previous references. While the majority of these products are microporous materials that were made with OSDAs intact inside the framework, the high-silica **HEU** (CIT-8) could be prepared from a layered precursor (CIT-8P). CIT-8P was synthesized in fluoride-media from a gel containing a relatively high amount of aluminum (gel Si/Al=15 or 20). The result of finding a layered material in these conditions led us to continue to explore similar inorganic conditions. In aluminum-free syntheses, we have reported that diquats formed from tetramethylimidazole can be used to prepare pure-silica **CSV** (CIT-7).[43] However, under similar conditions, we found that the diquat containing a five-carbon chain linker length led to a phase that could not be identified (shown in Figure 5-2). Upon calcination, this material yielded a phase that was easily identified as pure-silica **RTH** (Figure 5-2). This is the second reported method to synthesize pure-silica **RTH,** and may broaden its evaluation in applications, as previously the synthesis of this type of material required a difficult to prepare OSDA.[35] SEM images of CIT-10 and pure-silica **RTH** are shown in Figure 5-3. These images do not show solids with regular morphologies that are commonly observed in highly crystalline materials, but instead show morphologies resembling thick plates. Plate-like morphology is common in layered materials; however, the thickness of the plates in these samples is unusual.
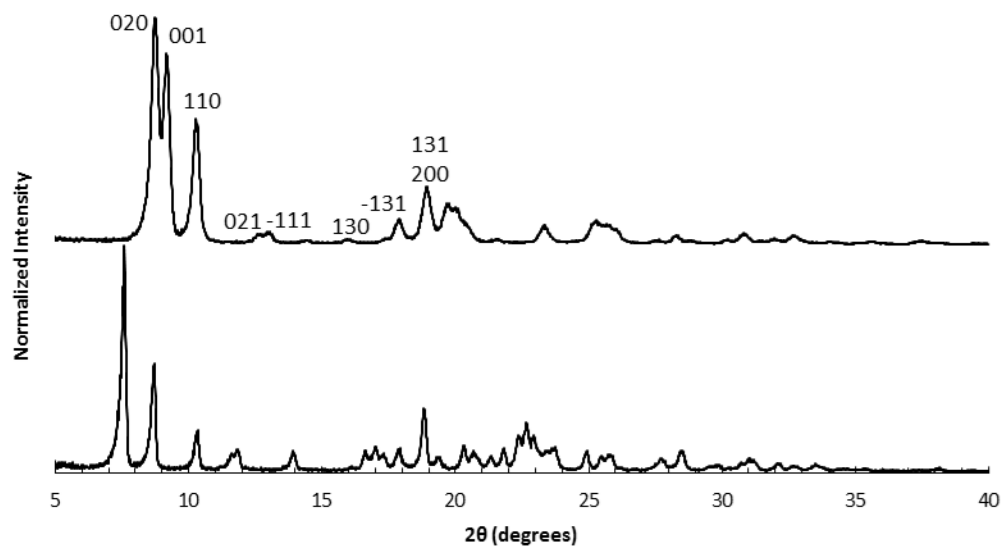
Figure 5-2. PXRD of CIT-10 (lower) and calcined CIT-10 (pure silica **RTH**, upper) with selected

crystallographic indices
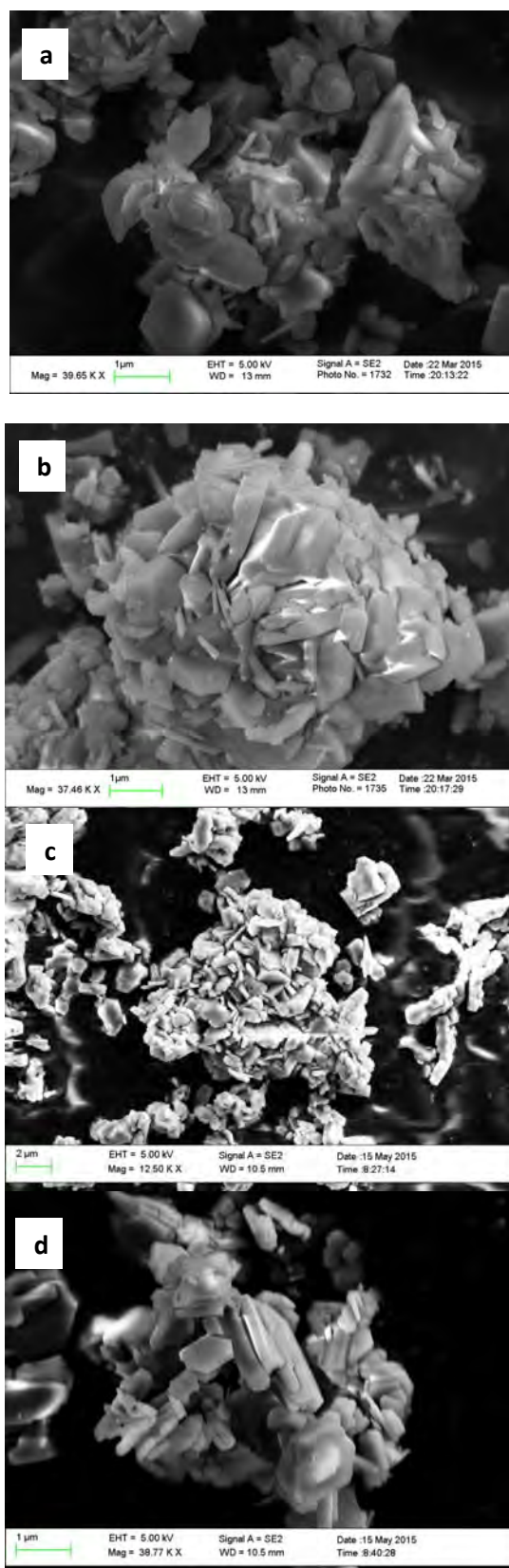
Figure 5-3. SEM images of a) CIT-10, b) Si-RTH, c) CIT-11 and d) CIT-12

To determine the mechanism of formation of pure-silica **RTH**, the materials were studied using ^{13}C CPMAS NMR, ^{29}Si MAS and CPMAS NMR, and variable temperature PXRD. The ^{13}C CPMAS NMR of CIT-10 (Figure 5-4) shows that the diquat OSDA was occluded intact in the material. It is interesting to note that many of the peaks in this spectrum are split, indicating that otherwise equivalent carbon atoms are present in non-equivalent environments; this has been previously reported in layered materials.[10] The ^{29}Si MAS and CPMAS NMRs of CIT-10 are shown in Figure 5-5. CIT-10 was studied using CPMAS NMR in addition to MAS NMR to confirm the resonances (organic-containing materials often exhibit a poor signal-to-noise ratio). In the as-made material there are three resonances at -113, -107, and -102 ppm with approximate area ratios of 8:5:3. The signals at -113 and -107 ppm are assigned to Q^4 silicon, $Si(OSi)_4$ coordination, while the signal at -102 ppm is assigned to Q^3 silicon, $Si(OSi)_3(OH)$ coordination. The presence of Q^3 silicon is expected in a layered material. The ratio of $Q^3/(Q^3 + Q^4)$ silicon in the as made material is 0.23, which is very close to the theoretical value of 0.25 (see the Supporting Information Figure S1 for additional details). Upon calcination, the ^{29}Si MAS NMR spectrum no longer shows the presence of any Q^3 silicon and instead shows 3 resonances in the Q^4 region at -116, -114, and -109 ppm, with area ratios of 1:2:1. These area ratios agree with the crystal structure of **RTH**, as it contains 4 independent T-sites.
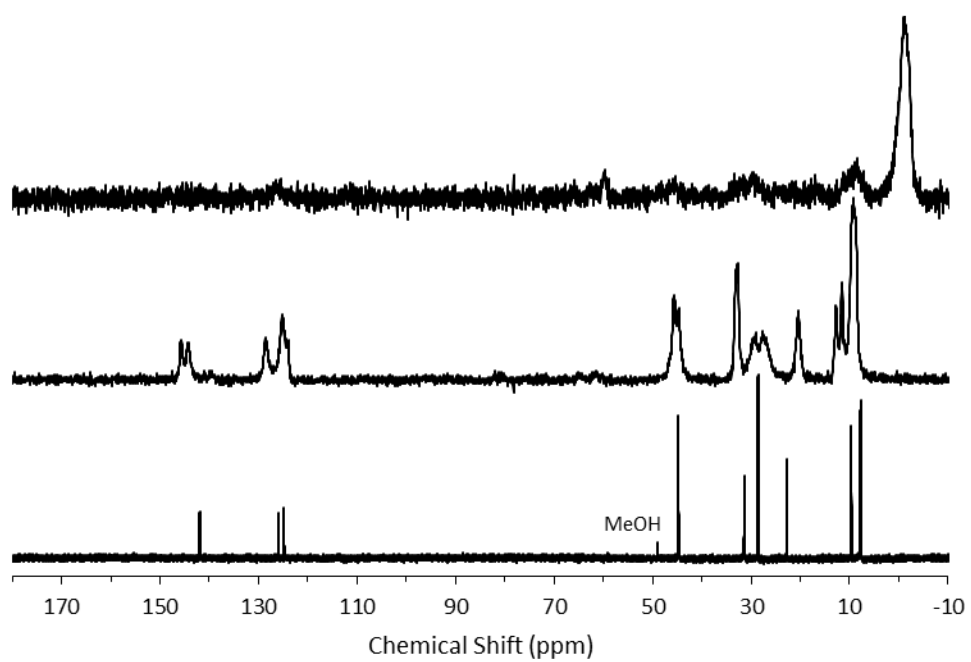
Figure 5-4. ^{13}C NMR of the diquat in D$_2$O (lower, methanol added as an internal standard), ^{13}C CPMAS NMR of CIT-10 showing the occluded diquat (middle), and ^{13}C CPMAS NMR of CIT-11 (upper)
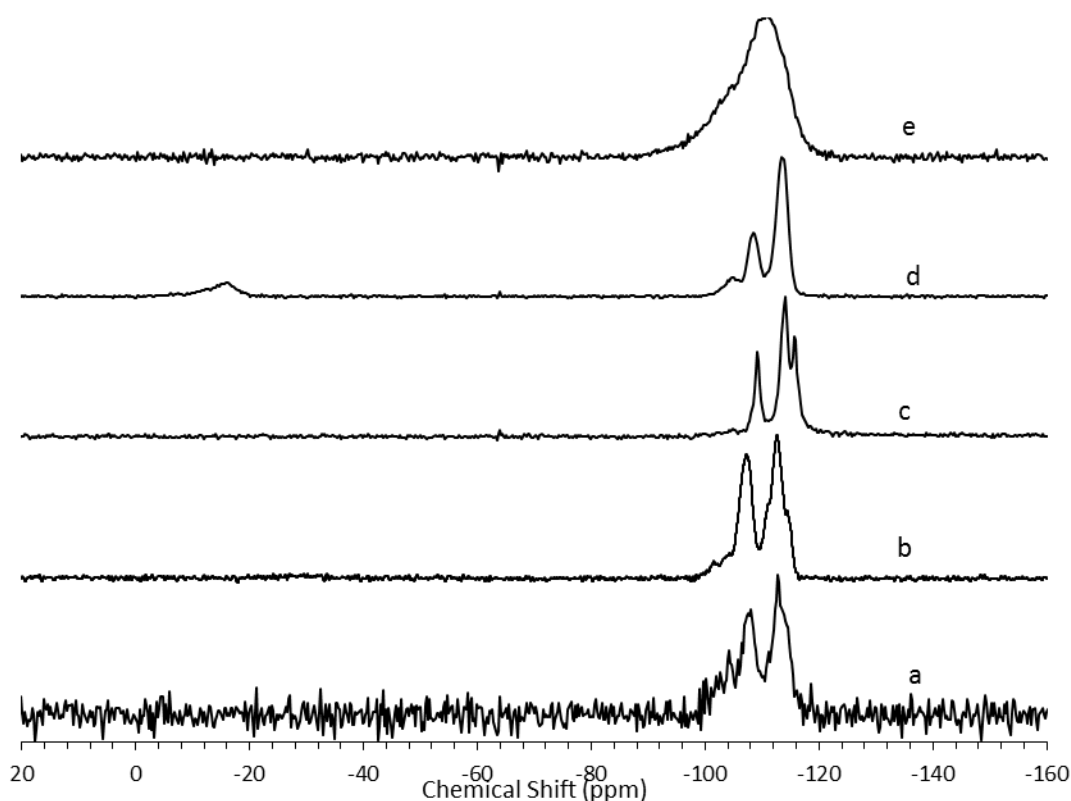
Figure 5-5. ^{29}Si a) MAS NMR of CIT-10, b) CPMAS NMR of CIT-10, c) MAS NMR of pure-silica **RTH**

prepared by calcination of CIT-10, d) MAS NMR of CIT-11, and e) MAS NMR of CIT-12

The structural mechanism of condensation was determined by using variable temperature

PXRD as well as RED. The variable temperature PXRD of CIT-10 is shown in Figure 5-7. When

compared with the PXRD patterns of **RTH** in Figure 5-2 (labelled with the crystallographic indices),

it is apparent that peak positions for *hk*0 reflections remain during heating, while the peak

positions for the *hkl* (*l* ≠0) reflections are shifted to higher 2θ angles (i.e., lower *d*-spacing). This

result indicates that the 3D **RTH** structure forms via topotactic condensation along the *c*-axis, and

that the *a* and *b* axes are intact in the layered material. The structural change was further

confirmed by studying CIT-10 using RED (Figure 5-6). The RED clearly shows that CIT-10 is ordered

in the *a* and *b* directions (indicated by clearly defined diffraction spots), but that some disorder

is present in the *c* direction (indicated by diffraction streaks between diffraction spots). Thus,

results from using both techniques confirm that CIT-10 contains 2D sheets in the *a* and *b* directions

that are separated by a disordered organic in the *c* direction.

The TGA data are consistent with the condensation temperature observed in the variable

temperature PXRD. In the variable temperature PXRD, the structure of the layered material is

intact until 330°C, then the low angle peak corresponding to the 001 direction abruptly disappears.

This reflection is absent at the PXRD pattern taken at 380°C, then begins to emerge around 430°C.

From the TGA trace in Figure 5-8, a sharp mass loss occurring around 375°C is seen, and is in the

same temperature range where the low angle peak disappeared in the variable temperature

PXRD. The rapid change observed with RTH is in contrast to the TGA trace and structural changes

observed with CIT-8P, where a gradual shift in position of the low-angle peak was observed along

with the gradual decrease in mass.[34]
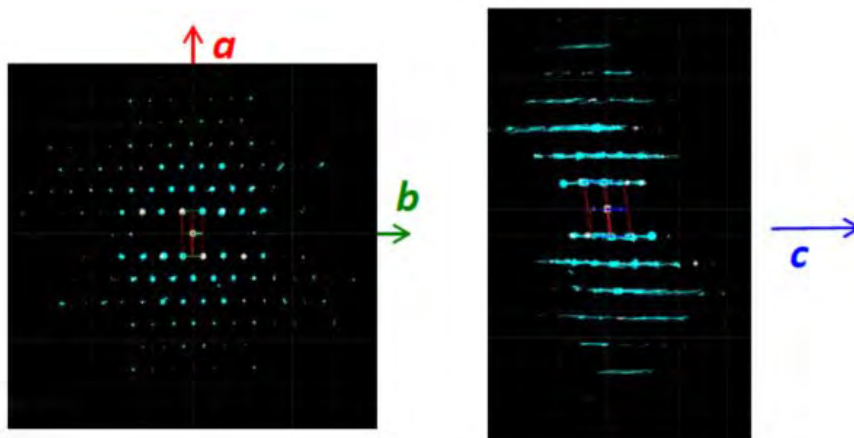
Figure 5-6. RED structure analysis of CIT-10
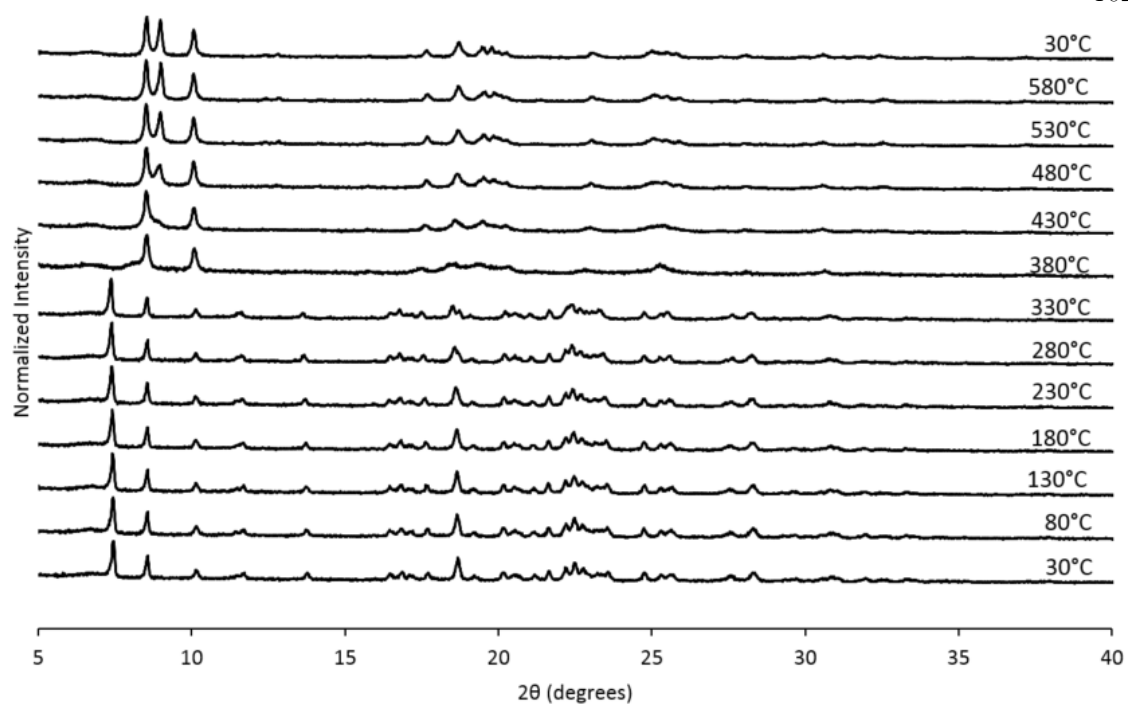
Figure 5-7. Variable temperature PXRD of CIT-10
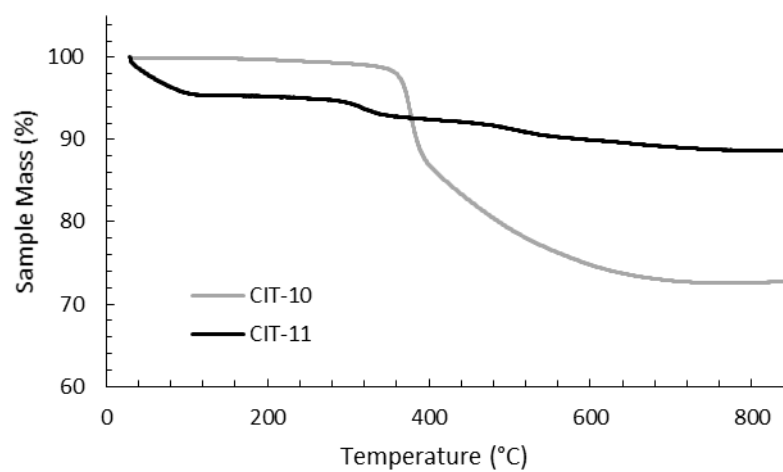
Figure 5-8. TGA of CIT-10 and CIT-11

A detailed analysis of the structural changes occurring during the topotactic condensation

process for RUB-39 have been reported as a series interconnected endothermic (OSDA

decomposition and condensation of silicate layers) and exothermic (OSDA combustion) processes

that are dominated by combustion of the OSDA.[44] It was found that as soon as the OSDA was removed, the condensation occurred. Attempts to stabilize the intermediate material were not successful. The sharp mass loss over a narrow temperature range observed with CIT-10 is similar to what is reported with RUB-39, and for the latter the loss was ascribed to a fast series of connected processes that include OSDA decomposition and combustion as well as condensation of the silicate layers.

CIT-10 has an 8MR channel running through the layer along the c axis, with dimensions of 2.5 x 5.6 Å. As the structure condenses along the c-axis, a second 8MR channel system running through the a-axis is formed, and a cavity is created at the intersection of the two 8MR channels, forming the **RTH** framework structure. The condensation process is shown schematically in Figure 5-9. As the schemes in the figure depict, the **RTH** layer is actually a half unit cell thick compared to the final **RTH** framework unit cell.

Table 5-1. Comparisons of the d-spacing corresponding to the first and most intense PXRD peak for known 2D layered materials, and the corresponding d-spacing shrinkage after topotactic condensation to form 3D framework materials.

2D zeolite	d-spacing (Å)	3D zeolite	Corresponding d-spacing (Å)	d-spacing Shrinkage (Å)	Ref.
CIT-10	11.8	Siliceous RTH	9.8	2.0	this work
RUB-36	11.1	RUB-37 (CDO)	9.2	1.9	44
MCM-22P	26.9	MCM-22 (MWW)	24.9	2.0	16,45
HPM-2	17.5	MCM-35 (MTF)	15.4	2.1	22
RUB-39	10.8	RUB-41 (RRO)	8.7	2.1	24
R-RUB-18	9.1	RUB-24 (RWR)	6.8	2.3	25
EU-19	11.5	EU-20 (CAS-NSI)	8.3	3.2	19
PREFER	13.1	FER	9.4	3.7	15
CIT-8P	12.8	CIT-8 (HEU)	8.9	3.9	34

Table 5-1 shows the comparisons of the *d*-spacing corresponding to the first and most intense PXRD peak for known 2D layered materials, and the corresponding *d*-spacing shrinkage after topotactic condensation to form 3D framework materials. In most of the cases (including CIT-10) the *d*-spacing shrinkage due to topotactic condensation is around 2 Å, an observation that has been discussed by Roth *et. al*. [45] It is also interesting to note that although the OSDAs used to make CIT-10 and CIT-8P are very similar, the latter demonstrated a *d*-spacing contraction nearly twice that of the former.
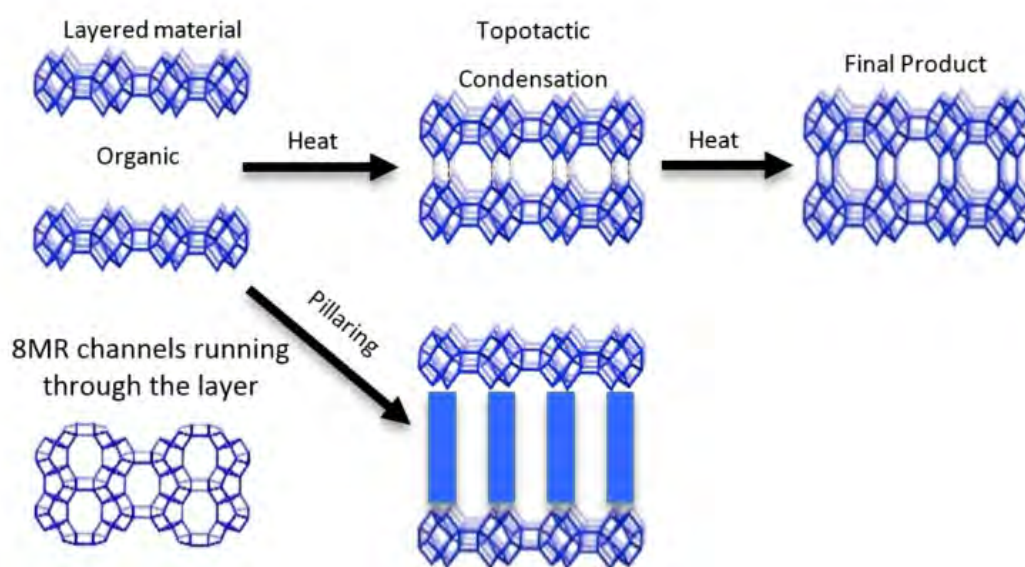
Figure 5-9. Depiction of the topotactic condensation and pillaring of CIT-10

5.4.2 Pillaring of CIT-10

In some cases it is possible to pillar layered materials using a monomeric silane in order to prepare materials with pores larger than would have been formed by topotactic condensation. These materials are commonly referred to as interlayer expanded zeolites (IEZ), and they have been prepared from precursors such as PREFER, MWW(P), PLS-1, MCM-47, RUB-36, RUB-39, and

Nu-6(1).[8,30,31] Pillaring is normally carried out in acidic media, under hydrothermal conditions,

and two of the most common pillaring agents are dichlorodimethylsilane and

diethoxydimethylsilane.

In attempting to pillar CIT-10, a wide range of conditions were explored including acid type,

aqueous versus ethanolic acid, silane source, and reaction temperature and time. The optimal

conditions to pillar CIT-10 were found to be 1.25 M HCl in ethanol with either

dichlorodimethylsilane or diethoxydimethylsilane at 175°C for 24 hours. Other conditions lead to

what appeared to be pillared materials (based on PXRD), but these materials exhibited very weak

x-ray reflections. We interpret these results as indicating framework destruction, and these solids

were often not stable to calcination. This phenomenon has been observed before, i.e., that acidic

ethanol is the only effective medium to carry out pillaring. It has been postulated that the reason

for this is that effective pillaring takes place when the rate of removal of OSDA is well matched by

the rate of silylation.[30] It should be noted that while we made no special efforts to preclude trace

amounts of water in these syntheses (such as working in a glovebox or using a Schlenk line), the

water content was likely very low.

The X-ray diffraction results of pillared CIT-10 are shown in Figure 5-10. As can be observed

from the PXRD patterns, pillaring causes a shift in the most intense reflection from 7.5° 2θ in CIT-

10 to 6.8° 2θ in CIT-11 (i.e., 1.1 Å expansion). This peak continues to shift to 7.7° 2θ in CIT-12 (after

calcination). The ^{13}C CPMAS NMR of CIT-11 (Figure 5-4) shows that the majority of the organic was

removed under acidic conditions (while CPMAS NMR is not quantitative this was confirmed by

TGA, shown in Figure 5-8). This result was expected as a change in color of the acidic medium was

observed. The strong resonance observed near -1 ppm is consistent with $(CH_3)_2Si$ carbon that is

expected from the pillaring. (Prior to NMR analysis it was necessary to degas the material under

vacuum at 150°C to remove any residual ethanol or acetone.) The TGA analysis of CIT-11

(Figure 5-8) shows several distinct mass loss regions. The first mass loss of 5% is attributed to the

loss of water and possibly residual ethanol or acetone (material was dried in air at 100°C prior to

analysis but not under vacuum as was done with the NMR sample). The second sharp mass loss

begins around 300°C, and is attributed to removal of residual organic (present in ^{13}C CPMAS NMR).

There is a third, distinct region of mass loss that begins around 500°C and is attributed to

combustion of the Si-CH$_3$ groups to form hydroxyl groups.

The ^{29}Si NMR spectra are consistent with a pillared material (Figure 5-5). In CIT-10, both Q^4

and Q^3 silicon environments are observed, consistent with a layered material (vide supra). In the

pillared material, CIT-11, ^{29}Si NMR resonances are observed at -113.5, -108.4, -104.5, and -15.3

ppm with approximate area ratios of 20:8:2:5. The resonances at -113.5 and -108.4 are assigned to

Q^4 silicon and the resonance at -104.5 is assigned to residual Q^3 silicon. The Q^3/(Q^3 + Q^4) ratio in

the pillared material is 0.07, a significant decrease from 0.23 in CIT-10, indicating that a substantial

amount of Q^3 species have been consumed in linking the layers of the material. The resonance at -

15.3 is assigned to bridging silanol groups bonded to two methyl groups, that is Si(CH$_3$)$_2$(OSi)$_2$

coordination. The ratio of (Q^2 + Q^3)/(Q^2 + Q^3 + Q^4) is 0.25, consistent with the expected value from

the RTH layer (see Supporting Information). Upon calcination the material exhibits a broad

resonance around -110 ppm. A single broad resonance has been observed in other pillared,

calcined materials such as PLS-4.[46] No obvious peak for Q^2 silicon can be seen near -90 ppm, but it

is likely obscured by the much broader resonance.

The structure of CIT-11/12 is a 3D pore system consisting of 8 and 10MRs, shown in Figure 5-

9. The 8MR running the in the *c*-direction perpendicular to the **RTH** layer remains intact. The pillars

form two new ring sizes as the previous 8MR along the *a*-direction expands to a 10MR and the

6MR along the *b*-direction expands to an 8MR. This means that the previous 2D ring system in

RTH expands be a 3D ring system in CIT-11/12.

The pore system of CIT-12 was confirmed using argon adsorption. The results from this

analysis are shown in Figure S2 compared to pure-silica **RTH** as well as zeolite 5A and pure-silica

BEA. We chose to plot all of these isotherms on the same graph as the shape of the isotherm in

the low pressure regime is an indication of the pore size distribution. The comparison of the low

pressure region of the argon adsorption isotherms indicates that this material has a pore system

that has expanded compared to pure-silica **RTH** (8MRs) but is smaller than pure-silica **BEA**

(12MRs), consistent with the structure solution.
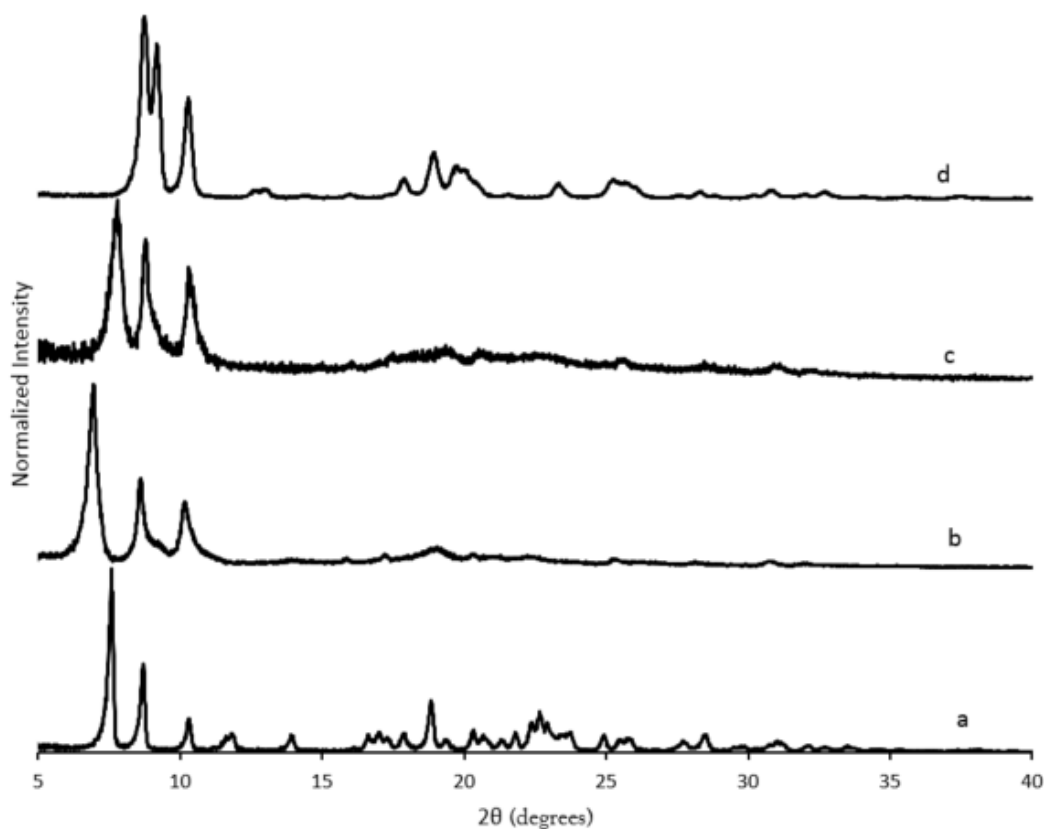
Figure 5-10. PXRD patterns of a) CIT-10, b) CIT-11, c) CIT-12 and d) pure-silica **RTH**

5.5 Conclusions

A new 2D building layer has been synthesized, the rth type layer, denoted CIT-10. This is the first reported 2D building layer that contains small pores that are perpendicular to the layer. Upon calcination, this material forms pure-silica **RTH**, making pure-silica **RTH** accessible without using a difficult to synthesize organic. CIT-10 can be pillared, forming CIT-11, that can then be calcined, forming CIT-12. CIT-12 contains a 3D pore system of 8 and 10MRs. As CIT-10 contains a new 2D layer there are many further studies to be conducted with this material such as swelling, exfoliation, and delamination as well as heteroatom introduction to introduce sites for ion exchange and catalysis. CIT-10 is the first material to contain small pores running through the layer; it is possible this material could find use in separations, especially of small molecules. Such possibilities have already been explored with other microporous material frameworks such as **LTA** and **MFI**. However, the **RTH** layers are only half a unit cell thick compared to a full unit cell with **MFI**[27] (which has medium pores) and multiple unit cells with **LTA**[47–49] (small pores). Additionally, the **RTH** layers have elliptical pores running through them, which may offer additional size discrimination compared to other small pore materials with circular pores, such as **LTA**.

5.6 Acknowledgements

5.7 Notes and References

(1)   Moliner, M.; Martínez, C.; Corma, A. Multipore Zeolites: Synthesis and Catalytic Applications. Angew. Chemie Int. Ed. 2015, 54 (12), 3560–3579.

(2)   Moliner, M.; Rey, F.; Corma, A. Towards the Rational Design of Efficient Organic Structure-Directing Agents for Zeolite Synthesis. Angew. Chem. Int. Ed. Engl. 2013, 52 (52), 13880–13889.

(3)   Wang, Z.; Yu, J.; Xu, R. Needs and Trends in Rational Synthesis of Zeolitic Materials. Chem. Soc. Rev. 2012, 41 (5), 1729–1741.

(4)   Corma, a. State of the Art and Future Challenges of Zeolites as Catalysts. J. Catal. 2003, 216 (1-2), 298–312.

(5)   Davis, M. E. Zeolites from a Materials Chemistry Perspective. Chem. Mater. 2014, 26 (1), 239–245.

(6)   Jiang, J.; Yu, J.; Corma, A. Extra-Large-Pore Zeolites: Bridging the Gap between Micro and Mesoporous Structures. Angew. Chem. Int. Ed. Engl. 2010, 49 (18), 3120–3145.

(7)   Pophale, R.; Daeyaert, F.; Deem, M. W. Computational Prediction of Chemically Synthesizable Organic Structure Directing Agents for Zeolites. J. Mater. Chem. A 2013, 1 (23), 6750–6760.

(8)   Díaz, U.; Corma, A. Layered Zeolitic Materials: An Approach to Designing Versatile Functional Solids. Dalton Trans. 2014, 43 (27), 10292–10316.

(9)   Marler, B.; Gies, H. Hydrous Layer Silicates as Precursors for Zeolites Obtained through

Topotactic Condensation: A Review. Eur. J. Mineral. 2012, 24 (3), 405–428.

(10) Wu, P.; Ruan, J.; Wang, L.; Wu, L.; Wang, Y.; Liu, Y.; Fan, W.; He, M.; Terasaki, O.; Tatsumi, T. Methodology for Synthesizing Crystalline Metallosilicates with Expanded Pore Windows through Molecular Alkoxysilylation of Zeolitic Lamellar Precursors. J. Am. Chem. Soc. 2008, 130 (26), 8178–8187.

(11) Mochizuki, D.; Shimojima, A.; Imagawa, T.; Kuroda, K. Molecular Manipulation of Two- and Three-Dimensional Silica Nanostructures by Alkoxysilylation of a Layered Silicate Octosilicate and Subsequent Hydrolysis of Alkoxy Groups. J. Am. Chem. Soc. 2005, 127 (19), 7183–7191.

(12) Suib, S. L. Zeolitic and Layered Materials. Chem. Rev. 1993, 93 (2), 803–826.

(13) Roth, W. J.; Nachtigall, P.; Morris, R. E.; Cejka, J. Two-Dimensional Zeolites: Current Status and Perspectives. Chem. Rev. 2014, 114 (9), 4807–4873.

(14) Díaz, U. Layered Materials with Catalytic Applications: Pillared and Delaminated Zeolites from MWW Precursors. ISRN Chem. Eng. 2012, 2012 (Figure 1), 1–35.

(15) Schreyeck, L.; Caullet, P.; Mougenel, J. C.; Guth, J. L.; Marler, B. PREFER: A New Layered (alumino) Silicate Precursor of FER-Type Zeolite. Microporous Mater. 1996, 6 (5-6), 259–271.

(16) Leonowicz, M. E.; Lawton, J. a; Lawton, S. L.; Rubin, M. K. MCM-22: A Molecular Sieve with Two Independent Multidimensional Channel Systems. Science 1994, 264 (5167), 1910–1913.

(17) Asakura, Y.; Takayama, R.; Shibue, T.; Kuroda, K. Topotactic Conversion of B-Helix-Layered Silicate into AST-Type Zeolite through Successive Interlayer Modifications. Chemistry 2014, 20 (7), 1893–1900.

(18) Blake, A. J.; Franklin, K. R.; Lowe, B. M. Preparation and Properties of Piperazine Silicate (EU-19) and a Silica Polymorph (EU-20). J. Chem. Soc. Dalt. Trans. 1988, No. 10, 2513.

(19) Marler, B.; Camblor, M. a.; Gies, H. The Disordered Structure of Silica Zeolite EU-20b,

Obtained by Topotactic Condensation of the Piperazinium Containing Layer Silicate EU-19. *Microporous Mesoporous Mater.* **2006,** *90* (1-3), 87–101.

(20) Zanardi, S.; Alberti, A.; Cruciani, G.; Corma, A.; Fornés, V.; Brunelli, M. Crystal Structure Determination of Zeolite Nu-6(2) and Its Layered Precursor Nu-6(1). *Angew. Chem. Int. Ed. Engl.* **2004,** *43* (37), 4933–4937.

(21) Ikeda, T.; Akiyama, Y.; Oumi, Y.; Kawai, A.; Mizukami, F. The Topotactic Conversion of a Novel Layered Silicate into a New Framework Zeolite. *Angew. Chem. Int. Ed. Engl.* **2004,** *43* (37), 4892–4896.

(22) Rojas, A.; Camblor, M. a. HPM-2, the Layered Precursor to Zeolite MTF. *Chem. Mater.* **2014,** *26* (2), 1161–1169.

(23) Roth, W. J.; Nachtigall, P.; Morris, R. E.; Wheatley, P. S.; Seymour, V. R.; Ashbrook, S. E.; Chlubná, P.; Grajciar, L.; Položij, M.; Zukal, A.; Shvets, O.; Cejka, J. A Family of Zeolites with Controlled Pore Size Prepared Using a Top-down Method. *Nat. Chem.* **2013,** *5* (7), 628–633.

(24) Wang, Y. X.; Gies, H.; Marler, B.; Müller, U. Synthesis and Crystal Structure of Zeolite RUB-41 Obtained as Calcination Product of a Layered Precursor: A Systematic Approach to a New Synthesis Route. *Chem. Mater.* **2005,** *17* (1), 43–49.

(25) Marler, B.; Ströter, N.; Gies, H. The Structure of the New Pure Silica Zeolite RUB-24, Si32O64, Obtained by Topotactic Condensation of the Intercalated Layer Silicate RUB-18. *Microporous Mesoporous Mater.* **2005,** *83* (1-3), 201–211.

(26) Moteki, T.; Chaikittisilp, W.; Shimojima, A.; Okubo, T. Silica Sodalite without Occluded Organic Matters by Topotactic Conversion of Lamellar Precursor. *J. Am. Chem. Soc.* **2008,** *130* (47), 15780–15781.

(27) Zhang, X.; Liu, D.; Xu, D.; Asahina, S.; Cychosz, K. a; Agrawal, K. V.; Al Wahedi, Y.; Bhan, A.; Al

Hashimi, S.; Terasaki, O.; Thommes, M.; Tsapatsis, M. Synthesis of Self-Pillared Zeolite Nanosheets by Repetitive Branching. Science 2012, 336 (6089), 1684–1687.

(28) Tsapatsis, M. 2-Dimensional Zeolites. AIChE J. 2014, 60 (7), 2374–2381.

(29) Díaz, U.; Corma, A. Layered Zeolitic Materials: An Approach to Designing Versatile Functional Solids. Dalton Trans. 2014, 43 (27), 10292–10316.

(30) Jiang, J.; Jia, L.; Yang, B.; Xu, H.; Wu, P. Preparation of Interlayer-Expanded Zeolite from Lamellar Precursor Nu-6 (1) by Silylation. Chem. Mater. 2013, 6 (1).

(31) Gies, H.; Müller, U.; Yilmaz, B.; Feyen, M.; Tatsumi, T.; Imai, H.; Zhang, H.; Xie, B.; Xiao, F. S.; Bao, X.; Zhang, W.; Baerdemaeker, T. De; De Vos, D. Interlayer Expansion of the Hydrous Layer Silicate Rub-36 to a Functionalized, Microporous Framework Silicate: Crystal Structure Analysis and Physical and Chemical Characterization. Chem. Mater. 2012, 24 (8), 1536–1545.

(32) De Baerdemaeker, T.; Gies, H.; Yilmaz, B.; Müller, U.; Feyen, M.; Xiao, F.-S.; Zhang, W.; Yokoi, T.; Bao, X.; De Vos, D. E. A New Class of Solid Lewis Acid Catalysts Based on Interlayer Expansion of Layered Silicates of the RUB-36 Type with Heteroatoms. J. Mater. Chem. A 2014, 2 (25), 9709.

(33) De Baerdemaeker, T.; Vandebroeck, W.; Gies, H.; Yilmaz, B.; Müller, U.; Feyen, M.; De Vos, D. Shape-Selective Organic–inorganic Zeolitic Catalysts Prepared via Interlayer Expansion. Catal. Today 2014, 235, 169–175.

(34) Schmidt, J. E.; Xie, D.; Davis, M. E. High-Silica, Heulandite-Type Zeolites Prepared by Direct Synthesis and Topotactic Condensation. J. Mater. Chem. A 2015, 3, 12890–12897.

(35) Lee, G. S.; Zones, S. I. Polymethylated [4.1.1] Octanes Leading to Zeolite SSZ-50. J. Solid State Chem. 2002, 167 (2), 289–298.

(36) Hathaway, P. E.; Davis, M. E. High Resolution, Quasi-Equilibrium Sorption Studies of

Molecular Sieves. Catal. Letters 1990, 5 (4-6), 333–347.

(37) Zhang, D.; Oleynikov, P.; Hovmöller, S.; Zou, X. Collecting 3D Electron Diffraction Data by the Rotation Method. Zeitschrift für Krist. 2010, 225 (2-3), 94–102.

(38) Wan, W.; Sun, J.; Su, J.; Hovmöller, S.; Zou, X. Three-Dimensional Rotation Electron Diffraction: Software RED for Automated Data Collection and Data Processing. J. Appl. Crystallogr. 2013, 46 (Pt 6), 1863–1873.

(39) Schmidt, J. E.; Zones, S. I.; Xie, D.; Davis, M. E. The Synthesis of Aluminophosphate and Germanosilicate LTA Using a Triquaternary Structure Directing Agent. Microporous Mesoporous Mater. 2014, 200 (3), 132–139.

(40) Schmidt, J. E.; Deimund, M. A.; Davis, M. E. Facile Preparation of Aluminosilicate RTH across a Wide Composition Range Using a New Organic Structure-Directing Agent. Chem. Mater. 2014, 26 (24), 7099–7105.

(41) Schmidt, J. E.; Deimund, M. A.; Xie, D.; Davis, M. E. Synthesis of RTH-Type Zeolites Using a Diverse Library of Imidazolium Cations. Chem. Mater. 2015, 27 (10), 3756–3762.

(42) Schmidt, J. E.; Deem, M. W.; Davis, M. E. Synthesis of a Specified, Silica Molecular Sieve by Using Computationally Predicted Organic Structure-Directing Agents. Angew. Chem. Int. Ed. Engl. 2014, 53 (32), 8372–8374.

(43) Schmidt, J. E.; Xie, D.; Rea, T.; Davis, M. E. CIT-7, a Crystalline, Molecular Sieve with Pores Bounded by 8 and 10-Membered Rings. Chem. Sci. 2015, 6, 1728–1734.

(44) Song, J.; Gies, H. Zeolites Synthesis in the System N(CH3)(C2H5)3F-SiO2-H2O. Stud. Surf. Sci. Catal. 2004, 154 (Part A), 295–300.

(45) Roth, W. J.; Dorset, D. L.; Kennedy, G. J. Discovery of New MWW Family Zeolite EMM-10: Identification of EMM-10P as the Missing MWW Precursor with Disordered Layers.

Microporous Mesoporous Mater. 2011, 142 (1), 168–177.

(46) Ikeda, T.; Kayamori, S.; Mizukami, F. Synthesis and Crystal Structure of Layered Silicate PLS-3 and PLS-4 as a Topotactic Zeolite Precursor. J. Mater. Chem. 2009, 19 (31), 5518.

(47) Huang, A.; Caro, J. Highly Oriented, Neutral and Cation-Free AlPO4 LTA: From a Seed Crystal Monolayer to a Molecular Sieve Membrane. Chem. Commun. (Camb). 2011, 47 (14), 4201–4203.

(48) Tiscornia, I.; Valencia, S.; Corma, A.; Téllez, C.; Coronas, J.; Santamaría, J. Preparation of ITQ-29 (Al-Free Zeolite A) Membranes. Microporous Mesoporous Mater. 2008, 110 (2-3), 303–309.

(49) Hunt, H. K. DEVELOPMENT OF FACILE ROUTE TO FLUORIDE-MEDIATED, PURE-SILICA ZEOLITE THIN FILMS, PhD Thesis, California Insititue of Technology, 2010.

5.8 Supporting Information
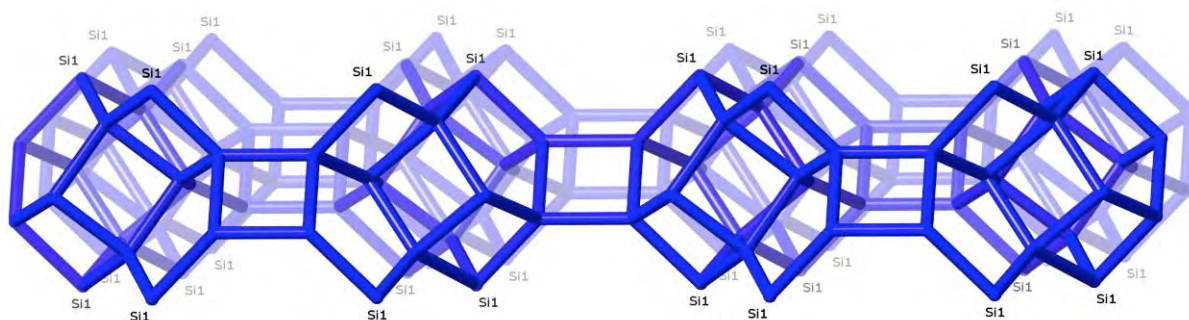
Figure S1. RTH building layer showing *4 independent T atoms*. As *a*ll 4 have the same multiplicity

and only T-1 atoms are on the surface, *ideally $Q^3/Q^4 = 1/4 = 0.25$.*
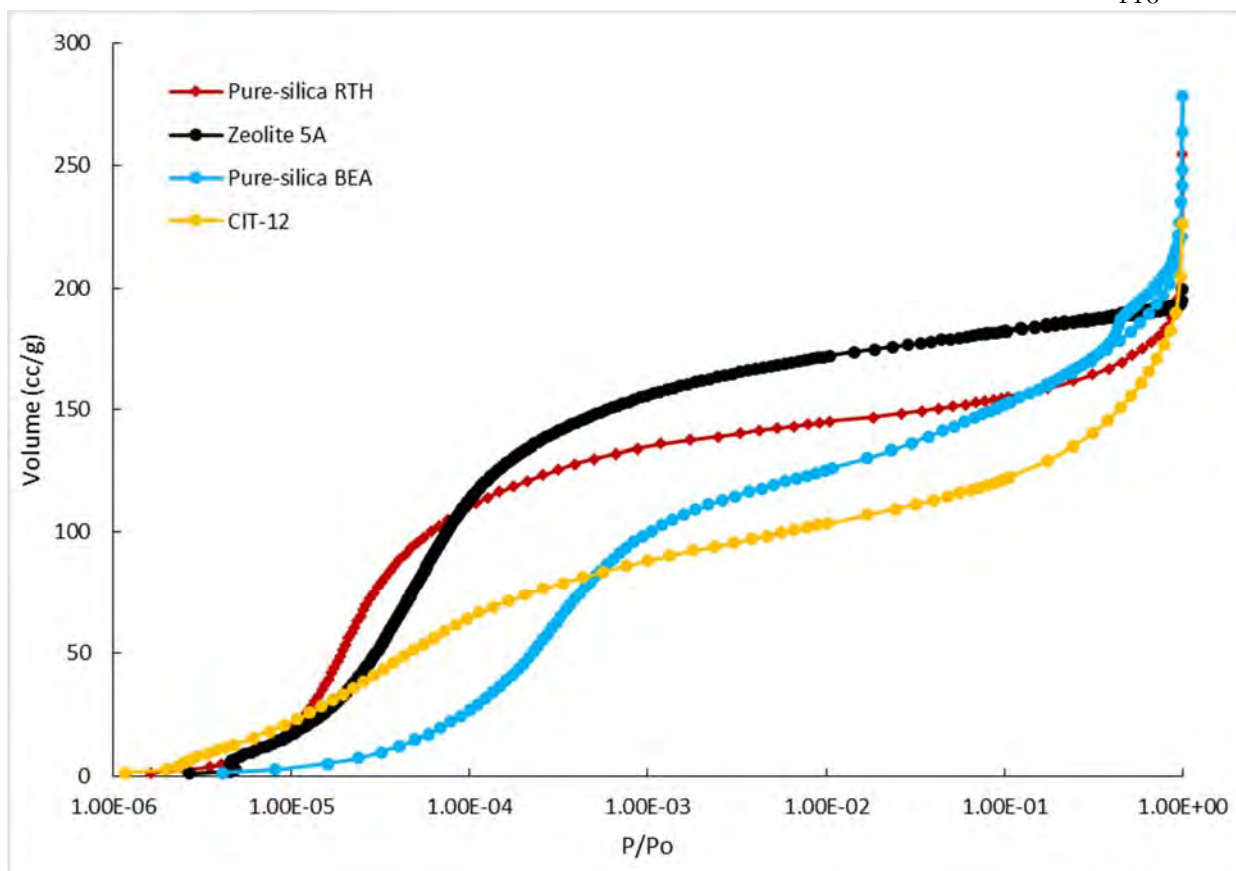
Figure S2. Argon adsorption isotherms.

Chapter 6. CIT-7, a Crystalline, Molecular Sieve with Pores Bounded by 8 and 10-Membered Rings

Chapter 6 previously appeared as: Schmidt, J. E.; Xie, D.; Rea, T.; Davis, M. E. CIT-7, a Crystalline, Molecular Sieve with Pores Bounded by 8 and 10-Membered Rings. *Chem. Sci.* **2015**, *6*, 1728–1734. doi: 10.1039/C4SC03935A

6.1 Abstract

A new crystalline molecular sieve, denoted CIT-7, is synthesized using an imidazolium-based diquaternary organic structure directing agent (OSDA). The framework structure is determined from a combination of rotation electron diffraction and synchrotron X-ray powder diffraction data. The structure has 10 crystallographically unique tetrahedral atoms (T-atoms) in the unit cell, and can be described as an ordered arrangement of the $[4^2 5^4 6^2]$ *mtw* building unit and a previously unreported $[4^4 5^2]$ building unit. The framework contains a 2-dimensional pore system that is bounded by 10 T-atom rings (10-ring, 5.1 Å * 6.2 Å opening) that are connected with oval 8-rings (2.9 Å * 5.5 Å opening) through medium-sized cavities (7.91 Å) at the channel intersections. CIT-7 can be synthesized over a broad range of compositions including pure-silica and heteroatom, e.g., aluminosilicate and titanosilicate, containing variants.

6.2 Introduction

The commercial utility of a molecular sieve arises from the combination of properties such as pore size, composition and hydrothermal stability that each structure can possess.[1–3] The unique nature of each framework and properties often enables a single material to achieve optimal performance for a given application. Because of this phenomenon, there remains a strong

motivation for creating new molecular sieve materials with new properties.[4] One synthetic

method that has been quite successful in the creation of new molecular sieves is the use of

organic structure directing agents (OSDAs). Beginning with the pioneering work of Barrer and

Denny,[5] numerous mono-, di-, and polyquaternary OSDAs have been examined in the synthesis of

microporous materials.[6–16] The properties of OSDAs that show the greatest successes have been

enumerated and the design of new OSDAs is now instrumental in the discovery of new molecular

sieves; many have provided enhanced material properties, e.g., catalytic activity and stability.

Recently, we reported a computational method that was used to identify

pentamethylimidazolium as being strongly directing towards pure-silica HPM-1 (**STW** framework

type[17,18]).[19] Based on the success of using pentamethylimidazolium, the simplest fully substituted

imidazolium, we began with 1,2,4,5-tetramethylimidazole to prepare diquaternary (diquat) OSDAs.

Here, we show that the diquat prepared using a 4-carbon chain length linker (Figure 6-1) can be

used to synthesize a new microporous material framework in pure-silica, fluoride mediated

reactions. That same framework can be produced in aluminosilicate fluoride and hydroxide

mediated reactions with product compositions of Si/Al=9-∞, as well as a titanosilicate material in

fluoride-mediated syntheses. The structure of the new material, denoted CIT-7, is determined

using a combination of synchrotron powder diffraction and rotation electron diffraction data.

6.3 Experimental

6.3.1 Organic Structure Directing Agent

In a typical synthesis 200 mmol (24.8 g) of 1,2,4,5-teteramethylimidazole (TCI Chemicals) was

dissolved in methanol. 100 mmol (21.6 g) of 1,4-dibromobutane (Sigma-Aldrich) was then added

and the solution was refluxed overnight. The methanol was removed using rotary evaporation and

the product was washed with ether to remove unreacted starting materials. The product was

characterized using carbon NMR in D_2O with methanol added as an internal standard, ^{13}C-NMR

(125 MHz, D_2O): δ 7.83, 7.88, 9.67, 26.12, 31.48, 44.39, 124.81, 126.19, 142.10. HRMS-FAB (*m/z*):

[M+H] calculated for $C_{18}H_{31}N_4$, 303.25; found, 303.26. The product was converted from the iodide

to the hydroxide form using hydroxide exchange resin (Dowex Marathon A) in water (all water

used in these experiments was doubly-distilled deionized water from a MEGA-PURE® 6A Water

Still) and the final concentration was determined using titration with a Mettler-Toledo DL22

autotitrator using 0.01 M HCl as the titrant.
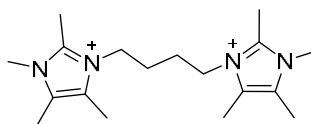
Figure 6-1. Diquaternary OSDA used to synthesize CIT-7.

6.3.2 Microporous Materials Synthesis

6.3.2.1. Fluoride-Mediated Syntheses

A general synthesis procedure was as follows. First, tetraethylorthosilicate (Aldrich) was added

to the OSDA in its hydroxide form. For aluminosilicates, aluminum isopropoxide (Aldrich) was then

added and for titanosilicates, titanium(IV) butoxide (Aldrich) was added. The container was closed,

and stirred for at least 12 h to allow for complete hydrolysis. The lid was then removed, and the

alcohol and an appropriate amount of water were allowed to evaporate under a stream of air.

Composition was monitored gravimetrically. Additional water was added as necessary, and then

aqueous HF (48 wt%, Aldrich) was added and the mixture was stirred by hand until a homogenous

gel was obtained. (Caution: Use appropriate personal protective equipment, ventilation, and other

safety measures when working with HF.) If necessary, a second evaporation step was used after

the addition of HF to reach the necessary water level. The final molar ratios are given in Table S1.

The autoclave was sealed and placed in a rotating oven at 175°C. Aliquots of the material were taken periodically by first quenching the reactor in water and then removing enough material for X-ray powder diffraction (XPD).

6.3.2.2. Hydroxide-Mediated Syntheses

The molar ratios used for hydroxide-mediated syntheses are given in Table S2. In general, the OSDA in its hydroxide form, sodium hydroxide, any necessary water and sodium aluminate (Pfaltz & Bauer) were combined and stirred until the sodium aluminate completely dissolved. Ludox AS-40 (Aldrich) was then added and stirred until a homogenous gel was obtained. The gel pH was measured and then it was placed in a rotating oven at 160°C. Aliquots were taken periodically and crystallization was monitored by both XPD and pH, as a jump in pH was generally observed when the product crystallized. After the product crystallized, the material was washed with water and then collected via centrifugation; this process was repeated at least three times and a final wash was performed using acetone. The product was dried at 100°C in air.

For the synthesis using CBV 760 (dealuminated Y-zeolite with $SiO_2/Al_2O_3 = 60$, Zeolyst International), 3 mmol of OSDA (based on charge) was mixed with 1 g of 1 M NaOH and water was added to bring the total mass to 7 g. Then 1 g of CBV 760 was added. The mixture was heated at 175°C tumbling and monitored the same way as the other hydroxide reactions.

6.3.2.3. Calcination

Products were calcined in breathing grade air. The material was heated to 150°C at 1°C /min, held for three hours, then heated to 580°C at 1°C /min and held for six hours to assure complete combustion of the organic

6.3.3 Characterizations

Liquid NMR spectra were recorded with a 500 MHz Spectrometer. The ^{13}C CP-MAS NMR was

recorded using a Bruker Avance 200 MHz spectrometer with a 7 mm rotor at a spinning rate of

4 kHz and were conducted in a 4.7 T magnetic field corresponding to Larmor frequencies of 200

MHz and 50.29 MHz for ^{1}H and ^{13}C, respectively. The ^{13}C NMR spectra are referenced to

adamantane as a secondary external standard relative to tetramethylsilane. ^{29}Si and ^{19}F NMR were

performed using a Bruker DSX-500 spectrometer (11.7 T) and a Bruker 4mm MAS probe. The

spectral frequencies were 500.2 MHz, 99.4 MHz, and 470.7 MHz for ^{1}H, ^{29}Si, and ^{19}F nuclei,

respectively, and spectra were referenced to external standards as follows: tetramethylsilane

(TMS) for ^{1}H and ^{29}Si, and $CFCl_3$ for ^{19}F. The ^{27}Al MAS NMR were recorded using a Bruker AM 300

MHz spectrometer with a 4 mm rotor at a spinning rate of 8 kHz, and were conducted in a 7.0 T

magnetic field corresponding to a Larmor frequency of 78.172 MHz. The ^{27}Al NMR spectra are

referenced to 1.1 M $Al(NO_3)_3$ as an external standard.

Thermogravimetric analysis measurements were performed with a Netzsch STA 449C Jupiter.

Samples were heated in air to 900°C at a rate of 1°C/min.

Argon physical adsorption isotherms were performed at 87.45 K using a Quantachrome

Autosorb iQ and conducted using a quasi-equilibrium, volumetric technique.[20]

XPD data were collected on a Rigaku MiniFlex II with Cu Kα radiation.

Scanning electron micrographs (SEM) were recorded on a Hitachi S-570 instrument. EDS

spectra were acquired with an Oxford X-Max SDD X-ray Energy Dispersive Spectrometer system on

a ZEISS 1550 VP FESEM equipped with in-lens SE.

Diffuse reflectance UV–visible (DRUV) spectra were recorded using a Cary 3G

spectrophotometer equipped with a diffuse reflectance cell; zeolite samples were calcined using

the method in section 2.2.3 prior to data collection.

Details on the synchrotron XPD data collection can be found in the Supporting Information,

Section 3.2. Three-dimensional electron diffraction data were collected on 2 crystals of CIT-7

using the rotation electron diffraction (RED) technique.[21,22] The RED software was installed on a

JEOL 2010 microscope operating at 200 kV, and data were collected over a tilt range of ±55° with a

tilt step of 0.50° for the first set and 0.35° for the second set, with the exposure time set at 3

seconds per tilt step.

6.4 Results and Discussion

6.4.1 Synthesis and Characterization of Pure-Silica CIT-7

Complete experimental results for fluoride-mediated, pure-silica syntheses can be found in

Table S1. With $H_2O/SiO_2=7$, the product was pure-silica **STW**. This phase has already been reported

using several different imidazolium based OSDAs.[19,23,24] When the water contents of the reactions

were decreased to $H_2O/SiO_2=4$, the OSDA led to the formation of a previously unknown phase. The

XPD of the calcined material is shown in Figure S1. This material is denoted CIT-7 (California

Institute of Technology number 7). Under these synthesis conditions, CIT-7 was found to crystallize

along with **STW** as a competing phase, so care had to be taken to avoid the formation of **STW**.

Once a pure-phase CIT-7 was obtained, seeds of CIT-7 were used in subsequent reactions to favor

its formation over that of **STW**.

To demonstrate that the OSDA shown in Figure 6-1, and not a decomposition product, formed

CIT-7, the pure-silica material was analyzed with ^{13}C CP-MAS NMR. The ^{13}C CP-MAS NMR spectrum

is compared to the liquid phase ^{13}C NMR of the OSDA in Figure S2, and these data confirm that the

OSDA is occluded intact in the material. The as-made, pure-silica material was stable to calcination

in air at 580°C to remove the OSDAs, and the TGA showed an organic content of 22.5wt%. An

argon adsorption isotherm of the calcined material is shown in Figure S3, and the micropore

volume was found to be 0.19 cm^3/g (t-plot method, log plot of the data is provided in Figure

S4). The ^{19}F NMR of the as-made material is shown in Figure S5 and reveals resonances at -45 ppm

and -128 ppm. The resonance at -128 ppm can be assigned to a small amount of SiF$_6$ in the

sample, and the resonance at -45 ppm is consistent with fluoride being occluded in a pure-silica

material.[25] The ^{29}Si NMR of the calcined material is shown in Figure 6-2. All of the resonances in

this material are assigned to Q^4 silicon, that is Si(OSi)$_4$ environments. The lack of any significant

resonances in the Q^3 region shows that this pure-silica framework has very low defects, and

suggests that in the as-made material, the charge of the organic was compensated by occluded

fluoride anions (shown to be present by ^{19}F NMR).[25]
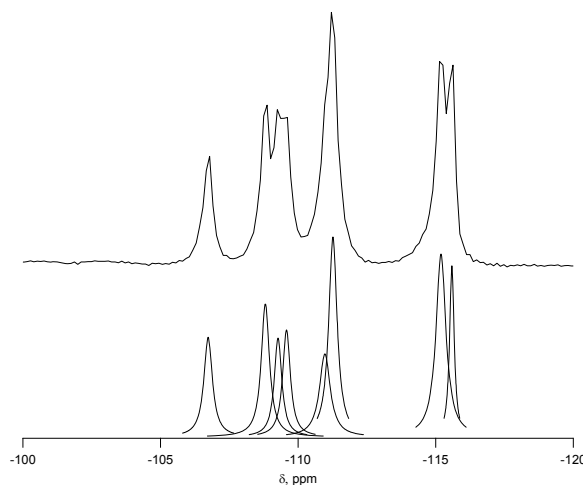
Figure 6-2. ^{29}Si NMR of calcined CIT-7 (upper) with the peak deconvolution (lower).

6.4.2. Structure Determination of CIT-7

The structure of the calcined, pure-silica material was determined using a combination of

synchrotron XPD and RED data. The calcined, pure-silica CIT-7 powder sample was packed into a

0.5 mm glass capillary and sealed. High-resolution XPD data were then collected on the 2-1

Powder Diffraction beamline at the Stanford Synchrotron Radiation Lightsource (SSRL).

The XPD pattern could be indexed with a triclinic unit cell (a = 13.020 Å, b = 11.205 Å, c = 9.375

Å, α = 92.8°, β = 107.2°, γ = 103.3°), using the program *TREOR*[26] implemented in the software

CMPR[27]. No indexing solutions on higher symmetry crystal systems could be found. Individual

reflection intensities were extracted from the powder pattern to a minimum d-spacing of 0.90 Å

(ca. 67.5° 2θ) using the program *EXTRACT*[28] in the *XRS-82* suite of programs[29]. Structure solution

using these data was then attempted using both the zeolite-specific structure-solution program

Focus[30], and the powder charge-flipping algorithm[31] in the program *Superflip*[32]. Unfortunately,

neither approach yielded a reasonable structural model.

Therefore, the RED technique[21,22] was applied to the CIT-7 sample to obtain 3-dimensional

single-crystal data (See Supporting Information Section 3.1). Two independent RED data sets were

collected on two tiny crystallites, and both could be indexed on triclinic unit cells that are similar to

the one found for the XPD pattern. Reflection intensities (*ca.* 1.0 Å resolution) were then extracted

for each data set using the RED software[22], and were further analyzed by the program *Triple*[33].

Although both datasets gave data completeness of only ca. 55%, one did provide better quality

over the other, i.e., the agreement factor of the reflection intensities for Friedel pairs is 11.7%

versus 22.1%. Therefore, a structure solution attempt using the better RED dataset for *Focus*

structure solution (assuming the centro-symmetric space group *P*-1) was performed. Many

framework topologies were proposed by *Focus*, but none were chemically reasonable. Luckily, the

two available RED datasets covered different areas of reciprocal space, and therefore by merging

them, the data completeness could be improved to 86%. With the merged dataset included in the

Focus runs, the structure solution became surprisingly straightforward. A model with 10 unique

framework T-atoms, clearly showing a 2-dimensional channel system of intersecting 10- and 8-

rings, was revealed. Indeed, this was the only solution proposed by the structure solution

program.

The geometry of the CIT-7 framework structure model from the *Focus* run was optimized using the program DLS-76[34], and then served as a starting point for Rietveld refinement[35], using the synchrotron XPD data. Geometric restraints were applied on the bond distances and bond angles of the framework atoms, and their positions refined. These restraints were imposed throughout the refinement, but their relative weighting with respect to the XPD data was reduced as the refinement progressed. The structural model finally converged with R_F = 0.055 and R_{wp} = 0.077 (R_{exp} = 0.068). All atoms were refined isotropically using scattering factors for neutral atoms. The displacement parameters for similar atoms were constrained to be equal to keep the number of parameters to a minimum. Details of the refinement and selected bond distances and angles are given in Table 6-1 and Table S3, and a *cif* file with the final atomic parameters is provided in the Supporting Information. The fit of the profile calculated from the final model to the experimental data is shown in Figure 6-3.

Table 6-1. Crystallographic data for pure-silica CIT-7.

Chemical composition			$[Si_{20}O_{40}]$
Unit cell			
a (Å)			13.0187(1)
B (Å)			11.2063(1)
c (Å)			9.3758(1)
α (°)			92.8224(6)
β (°)			107.2048(5)
γ (°)			103.2565 (5)
Space group			P-1
Number of observations			8001
Number of contributing reflections			3703
Number of geometric restraints			120
Number of structural parameters			98
Number of profile parameters			12
R_F			0.041
R_{wp}			0.077
R_{exp}			0.068
Selected bond distances (Å) and angles (°)			
Si – O (Å)	min: 1.59	max: 1.62	avg: 1.61
O - Si – O (°)	min: 106.4	max: 112.2	avg: 109.5
Si – O – Si (°)	min: 142.1	max: 157.3	avg: 148.9
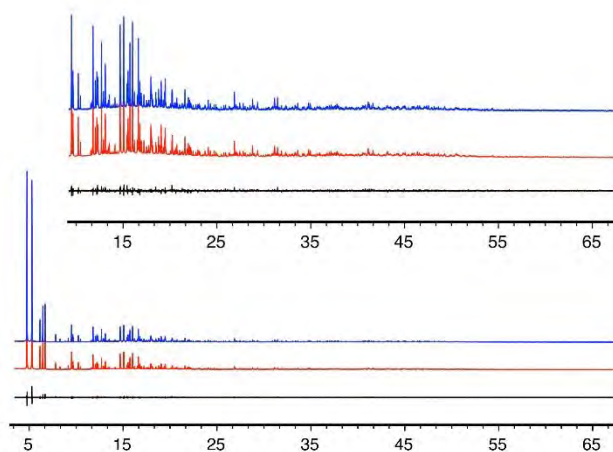
Figure 6-3. Observed (top), calculated (middle), and difference (bottom) profiles for the Rietveld refinement of pure-silica CIT-7. The profiles in the inset have been scaled up by a factor of 6 to

show more detail.

6.4.3 Description and Experimental Support of CIT-7 Structure

The framework structure of CIT-7 can be described as an ordered arrangement of a building block consisting of the $[4^2 5^4 6^2]$ mtw composite building unit (CBU), and a new $[4^4 5^2]$ building unit that has not been reported previously (i.e., it is not found in either the list of selected CBUs from the Database of Zeolite Structures[17] or the exhaustive lists from Smith[36] and van Koningsveld[37]) (Figure 6-4a, b). The building unit could be connected to the same neighbouring building unit to form a chain (Figure 6-4c) and the chain repeats itself to form a layer (Figure 6-4d, e). As a result, oval 8-rings are created (2.9Å × 5.5Å opening, with the oxygen diameter of 2.70Å subtracted). The layer that has 8-rings could again link to itself and form 10-ring channels (5.1Å × 6.2Å opening, with the oxygen diameter of 2.70Å subtracted) that are running perpendicular to the layer and intersected by 8-ring channels (Figure 6-4f). At each intersection, a $[4^8 5^4 6^8 8^2 10^2]$ cavity is created (Figure 6-4g). Alternatively, the CIT-7 framework structure could be described by natural tiling[38] with a transitivity of [(10)(20)(16)4]. Four different types of tiles (i.e., $[4^{4\cdot}5^2]$, $[5^{2\cdot}6^2]$, $[4^{2\cdot}5^{4\cdot}6^2]$ and $[4^{8\cdot}5^{4\cdot}6^{8\cdot}8^{2\cdot}10^2]$), derived by the program Topos[39], could be used to build the whole framework (see Supporting Information Section 4.1). The projection view along the three main crystallographic axes and the two-dimensional channel system are shown in Figure 6-5 and 6, respectively.
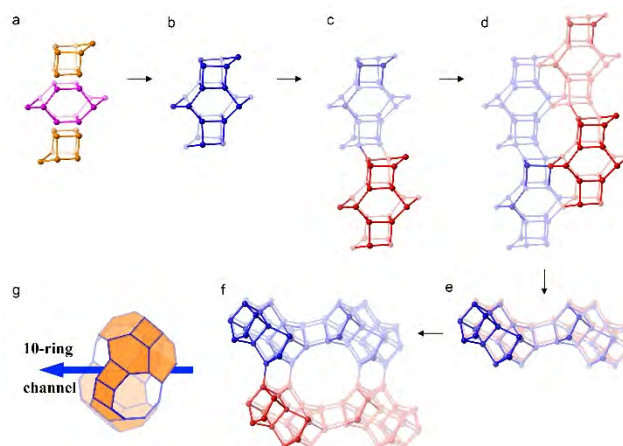
Figure 6-4. The construction of the framework structure CIT-7. (a) The mtw (in purple) and the new [4^45^2] (in yellow) composite building units assembled to form (b) a repeating building unit. (c) The connection of the building units in (b) to form a chain. (d) The arrangement of the chain (c) to form a layer with distorted 8-rings. (e) A different view of the layer in (d). (f) The connection of the layers in (d) to form 10-ring channels that are intersected with the 8-ring channels. (g) The [$4^85^46^88^210^2$] cavity that can be accessed by 10-ring and 8-ring windows.
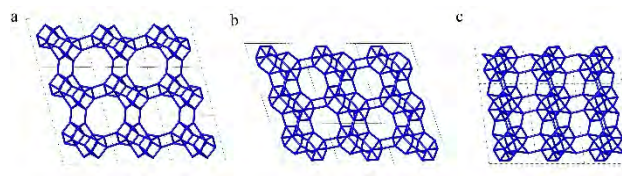
Figure 6-5. Framework structure of CIT-7. Projection view (3×3×3 unit cells) along the main crystallographic axis (a) [001], (b) [010], and (c) [100]. Framework O atoms have been omitted for clarity.
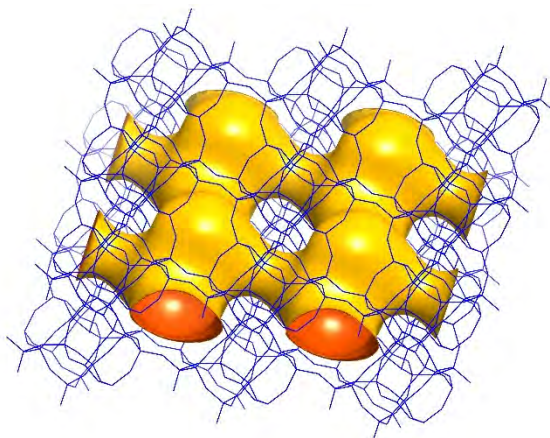
Figure 6-6. A structure envelope[44] (yellow) highlighting the 10-/8-ring 2-dimensional channel system in the CIT-7 framework structure (blue).[45]

It should be noted that the structure of CIT-7 is not predicted in any hypothetical zeolite framework databases, as these databases only contain structures having less than 10 unique T atoms per unit cell. The optimized framework energy of pure-silica CIT-7 relative to α-quartz, *i.e.*, 16.63 kJ/mol per Si atom, calculated by the program GULP[40] that is implemented in the software Materials Studio 6.1[41], clearly demonstrates that this structure is energetically favorable[42]. On the other hand, Li *et. al.*[43] recently proposed a set of criteria for evaluating the chemical feasibility of zeolite frameworks based on the statistics of the local interatomic distances (LIDs) rather than energy values. Calculations on the GULP-optimized CIT-7 structure indicated that this structure also fulfils all the LID criteria quite well.

The ^{29}Si NMR spectrum of the calcined material is shown in Figure 6-2 along with the deconvolution into 8 separate peaks. The chemical shifts, peak areas, and T-site assignments are given in Table 6-2. The spectrum was deconvoluted into eight different resonances, with approximate area ratios of 1:2:2:1:1:1:1:1. The number of resonances and their area ratios are

consistent with the structure solution having ten T-sites (there are ten unique T-sites in CIT-7,

each with a site multiplicity of 2 as the space group is P-1), and the chemical shifts and their area

ratios correspond well with the average Si-O-Si bond angles. SEM images showing the morphology

of the calcined, pure-silica material are provided in Figure S6. The observed low symmetry of the

crystals is consistent with the low-symmetry found for the structure. Based on the structure

solution, the TGA mass loss of 22.5wt% corresponds well with 1 molecule of organic and 2 fluoride

anions per unit cell. This organic content is also in agreement with the measured micropore

volume.

Table 6-2. Chemical shifts from ^{29}Si NMR of calcined pure silica CIT-7 along with the normalized

peak areas and assigned T sites.

Shift (ppm)	Normalized Area	Assigned T site	Average Si-O-Si Angle[a]
-115.6	0.92	Si10	152.2
-115.2	2.14	Si3 + Si8	151.7, 151.6
-111.3	1.97	Si1 + Si5	149.4, 149.1
-111.0	1.06	Si6	148.3
-109.6	0.97	Si9	147.2
-109.3	0.88	Si4	147.2
-108.8	1.28	Si7	146.8
-106.7	1.00	Si2	145.6
[a]From structure determination			

6.4.4. Heteroatom Incorporation

6.4.4.1 Aluminosilicate CIT-7

In fluoride-mediated reactions, CIT-7 was produced with gel compositions of Si/Al=15, 25, 50,

100, 250 using seeded syntheses with pure-silica CIT-7 seeds (see Supporting Information for

synthesis details and results in Table S1 and a representative XPD in Figure S7). Of more

importance to any practical application would be aluminosilicate materials produced in hydroxide

mediated reactions. At Si/Al=15 (see Supporting Information for complete results in Table S2), without the addition of seeds, **IWV** was found as the product (Figure S8). **IWV** is a 2-dimenionsal, 12-membered ring material that contains 14-membered rings that are only accessible through 12-membered rings. The aluminosilicate was first reported as ITQ-27, and was made using diphenyldimethylphosphonium as the OSDA. The synthesis is only reported at a difficult to achieve composition of: $1SiO_2:0.014Al_2O_3:0.50Me_2Ph_2POH:0.50HF:4.2H_2O$, and takes 59 days to form, the addition of seeds only shortens this by one week.[46, 47]

With the addition of pure-silica CIT-7 seeds to the aluminosilicate syntheses in hydroxide media, CIT-7 was produced instead of ITQ-27 (see XPD in Figure S9). Aluminosilicate CIT-7 could be easily obtained in hydroxide media at gel compositions of Si/Al=5-15. Higher silica compositions led to products containing CIT-7 along with dense phases or ITQ-27. It is likely that optimizing these synthesis conditions will lead to higher silica products using a hydroxide mediated synthesis; however, these compositions are already accessible using the fluoride method. To demonstrate that the aluminum was in the framework, the calcined samples with the highest aluminum contents in both fluoride and hydroxide media were investigated by using ^{27}Al NMR (Figure S10). In the sample prepared in hydroxide media, 95% of the aluminum was tetrahedral, and in the sample synthesized in fluoride media 88% was in tetrahedral coordination. In both of these samples, the majority of the aluminum was in tetrahedral coordination, demonstrating incorporation in the framework. The Si/Al range over which CIT-7 can be produced will allow for a wide variety of catalytic testing to be performed.

6.4.4.2. Titanosilicate CIT-7

The ability of the CIT-7 framework to incorporate heteroatoms besides aluminum was tested by adding titanium to fluoride syntheses. Synthesis conditions are given in Table S1. In the

titanosilicate material, both Si/Ti=50 and 100 were synthesized. DRUV of the as-made and calcined titanosilicate materials was used to show that the titanium was present in tetrahedral coordination (Figure S11), indicating framework incorporation.

6.4.5. Additional OSDAs

In addition to the OSDA shown in Figure 6-1, we found that 2-ethyl-1,3-dimethylimidazolium can form CIT-7. However, this OSDA was not as strongly directing as the diquat as it was very difficult to produce a pure-phase sample, as the product was often contaminated with **ITW**, **MTW**, **STF**, and **STW**. In our investigations of diquats of varying linker length using tetramethylimidazole, we have found that linkers of 3 and 5 carbons can also form CIT-7, but these are not as strongly directing towards this framework. Further studies on diquats of varying linker lengths are in progress .

6.4.6. Comparison to Known Materials

Four other zeolite frameworks, i.e., **FER** (e.g., NU-23, ZSM-35), **MFS** (e.g., ZSM-57), **RRO** (e.g., RUB-41), and **STI** (e.g., TNU-10, SSZ-75), have a 2-dimensional 10-/8-ring channel systems. CIT-7 distinguishes itself from these known materials by some unique structural features. As shown in Figure 6-7, CIT-7 is the only system that has a large cavity in the intersection region. The maximum included sphere diameter for the idealized CIT-7 framework (i.e., the one after distance-angle least-square refinement[34]) is calculated to be 7.91 Å, significantly larger than those for the other four idealized frameworks (Table 6-3). Also, it should also be noted that CIT-7 can be made across a very wide Si/Al ratio (9-∞) as well as a titanium (and we suspect other heteroatoms) containing material. This compositional flexibility, when combined with the medium-/small-pore channels and intersecting cavities, could be of interest in a broad spectrum of applications.
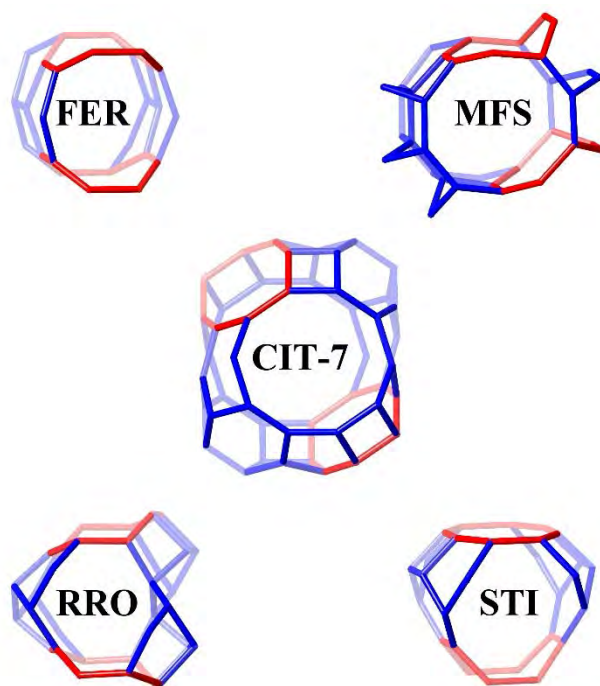
Figure 6-7. The 10-/8-ring channel intersections for CIT-7, **FER**, **MFS**, **RRO**, and **STI**. The 8-rings are highlighted in red. Bridging O atoms have been omitted for clarity.

Table 6-3. Comparison of the channel and pore characteristics for the five 2D 10-/8-ring

zeolites. For the 4 known zeolite frameworks, the channel characteristics are taken from the

literature[48], and the pore characteristics are taken from the Database of Zeolite Structures[17]. The

channel characteristics for CIT-7 are calculated using the program "Sphere Viewer"[49]. All data are

in Å.

Framework	D_M	D_a	D_b	D_c	Material	10R opening	8R opening
Idealized CIT-7	7.91	1.87	2.92	4.67	CIT-7	5.1 × 6.2	2.9 × 5.5
MFS	6.71	5.31	3.14	1.51	ZSM-57	5.1 × 5.4	3.3 × 4.8
FER	6.25	1.50	3.34	4.63	Ferrierite	4.2 × 5.4	3.5 × 4.8
STI	6.23	4.88	2.90	1.79	SSZ-75	4.7 × 5.0	2.7 × 5.6
RRO	4.40	4.03	1.48	3.07	RUB-41	4.0 × 6.5	2.7 × 5.0
Note: D_M means the maximum included sphere diameters, D_a, D_b and D_c are the maximum free sphere diameters that can diffuse along a-, b- and c-axis, respectively.							

Other materials with 2-dimensional 10-/8-ring channel systems have been proposed for

applications including carbonylation, NO_X reduction, methanol-to-olefins, amine synthesis, and gas

separations.[50–52] Among these materials, it has been reported that ferrierite has been

commercialized for isomerization of butenes and pentenes in the Isomplus process (Shell and

Lyondell Petrochemical) on a 10,000 BPD butene feed at the Equistar Chemicals facility in

Channelview, TX.[2,53] A modified ferrierite is also used as a catalyst in olefin skeletal isomerization in

the Isotex process by Texaco.[53-55] These examples illustrate the potential utility of 2-dimensional

10-/8-ring channel systems. Thus, it will be interesting to compare CIT-7 to these known materials,

and we are currently testing them in a number of catalytic reactions.

6.5 Conclusions

We have reported here the synthesis, structural solution and characterization of a new microporous material with a 10-/8-ring, 2-dimensional channel system, with large cages at the intersections. This material can be prepared across a wide range of compositions and exhibits good stability. As microporous materials with a similar 2-dimensional 10-/8-ring channel systems have already been commercialized, we are currently investigating the catalytic applications of CIT-7 to find the influence of the unique features of this framework, such as the large cage at channel intersections.

6.6 Acknowledgements

6.7 Notes

Electronic Supplementary Information (ESI) available: Details of the synthesis and characterization of all materials as well as details on the synchrotron and RED data collection and structure determination (with CIF file) are available in the Supporting Information.

6.8 References

(1)   Davis, M. E. Ordered Porous Materials for Emerging Applications. *Nature* **2002**, *417* (6891), 813–821.

(2)   Vermeiren, W.; Gilson, J.-P. Impact of Zeolites on the Petroleum and Petrochemical Industry. *Top. Catal.* **2009**, *52* (9), 1131–1161.

(3)   Cundy, C. S.; Cox, P. A. The Hydrothermal Synthesis of Zeolites: History and Development from the Earliest Days to the Present Time. *Chem. Rev.* **2003**, *103* (3), 663–702.

(4)   Pophale, R.; Daeyaert, F.; Deem, M. W. Computational Prediction of Chemically Synthesizable Organic Structure Directing Agents for Zeolites. *J. Mater. Chem. A* **2013**, *1* (23), 6750–6760.

(5)   Barrer, R. M.; Denny, P. J. 201. Hydrothermal Chemistry of the Silicates. Part IX. Nitrogenous Aluminosilicates. *J. Chem. Soc.* **1961**, 971–9825.

(6)   Burton, A.; Zones, S. Organic Molecules in Zeolite Synthesis: Their Preparation and Structure-Directing Effects. *Stud. Surf. Sci. Catal.* **2007**, *168*, 137–179.

(7)   Zones, S. I.; Burton, A. W.; Lee, G. S.; Olmstead, M. M. A Study of Piperidinium Structure-Directing Agents in the Synthesis of Silica Molecular Sieves under Fluoride-Based Conditions. *J. Am. Chem. Soc.* **2007**, *129* (29), 9066–9079.

(8)   Jones, W.; Rao, C. Towards the Rational Design of Zeolite Frameworks. In *Supramolecular organization and materials design*; Cambridge University Press: Cambridge, UK, 2002; pp 83–102.

(9)   Zones, S. I.; Hwang, S. A Novel Approach to Borosilicate Zeolite Synthesis in the Presence of Fluoride. *Microporous Mesoporous Mater.* **2011**, *146* (1-3), 48–56.

(10)   Moini, A.; Schmitt, K.; Valyocsik, E.; Polomski, R. The Role of Diquaternary Cations as Directing Agents in Zeolite Synthesis. *Zeolites* **1994**, *14* (7), 504–511.

(11) Ren, L.; Wu, Q.; Yang, C.; Zhu, L.; Li, C.; Zhang, P.; Zhang, H.; Meng, X.; Xiao, F.-S. Solvent-Free Synthesis of Zeolites from Solid Raw Materials. *J. Am. Chem. Soc.* **2012**, *134* (37), 15173–15176.

(12) Camblor, M.; Villaescusa, L.; Diaz-Cabanas, M. Synthesis of All-Silica and High-Silica Molecular Sieves in Fluoride Media. *Top. Catal.* **1999**, *9*, 59–76.

(13) Zones, S. I.; Hwang, S.-J.; Elomari, S.; Ogino, I.; Davis, M. E.; Burton, A. W. The Fluoride-Based Route to All-Silica Molecular Sieves; a Strategy for Synthesis of New Materials Based upon Close-Packing of Guest–host Products. *Comptes Rendus Chim.* **2005**, *8* (3-4), 267–282.

(14) Camblor, M. A.; Barrett, P. A.; Díaz-Cabañas, M.-J.; Villaescusa, L. A.; Puche, M.; Boix, T.; Pérez, E.; Koller, H. High Silica Zeolites with Three-Dimensional Systems of Large Pore Channels. *Microporous Mesoporous Mater.* **2001**, *48* (1-3), 11–22.

(15) Jiang, J.; Yu, J.; Corma, A. Extra-Large-Pore Zeolites: Bridging the Gap between Micro and Mesoporous Structures. *Angew. Chem. Int. Ed. Engl.* **2010**, *49* (18), 3120–3145.

(16) Takewaki, T.; Beck, L. W.; Davis, M. E. Zeolite Synthesis Using 1,4-diazabicyclo[2,2,2]octane (DABCO) Derivatives as Structure-Directing Agents. *Microporous Mesoporous Mater.* **1999**, *33* (1-3), 197–207.

(17) Baerlocher, C.; Mccusker, L. B. Database of Zeolite Structures, <http://www.iza-structure.org/databases/>. Accessed December 8, 2014.

(18) Three-Letter Framework Type Codes (boldface Capital Letters) for All Zeolites Mentioned in the Text Are given in Parentheses.

(19) Schmidt, J. E.; Deem, M. W.; Davis, M. E. Synthesis of a Specified, Silica Molecular Sieve by Using Computationally Predicted Organic Structure-Directing Agents. *Angew. Chem. Int. Ed. Engl.* **2014**, *53* (32), 8372–8374.

(20) Hathaway, P. E.; Davis, M. E. High Resolution, Quasi-Equilibrium Sorption Studies of Molecular Sieves. *Catal. Letters* **1990**, *5* (4-6), 333–347.

(21) Zhang, D.; Oleynikov, P.; Hovmöller, S.; Zou, X. Collecting 3D Electron Diffraction Data by the Rotation Method. *Zeitschrift für Krist.* **2010**, *225* (2-3), 94–102.

(22) Wan, W.; Sun, J.; Su, J.; Hovmöller, S.; Zou, X. Three-Dimensional Rotation Electron Diffraction: Software RED for Automated Data Collection and Data Processing. *J. Appl. Crystallogr.* **2013**, *46* (Pt 6), 1863–1873.

(23) Rojas, A.; Camblor, M. A. A Pure Silica Chiral Polymorph with Helical Pores. *Angew. Chem. Int. Ed. Engl.* **2012**, *51* (16), 3854–3856.

(24) Rojas, A.; Arteaga, O.; Kahr, B.; Camblor, M. a. Synthesis, Structure, and Optical Activity of HPM-1, a Pure Silica Chiral Zeolite. *J. Am. Chem. Soc.* **2013**, *135* (32), 11975–11984.

(25) Mafra, L.; Vidal-moya, J. A.; Blasco, T. Structural Characterization of Zeolites by Advanced Solid State NMR Spectroscopic Methods. In *Annual Reports on NMR Spectroscopy*; 2012; Vol. 77, pp 259–351.

(26) Werner, P. E.; Eriksson, L.; Westdahl, M. TREOR, a Semi-Exhaustive Trial-and-Error Powder Indexing Program for All Symmetries. *J. Appl. Crystallogr.* **1985**, *18* (5), 367–370.

(27) Toby, B. H. CMPR – a Powder Diffraction Toolkit. *J. Appl. Crystallogr.* **2005**, *38* (6), 1040–1041.

(28) Baerlocher, C. EXTRACT. A Fortran Program for the Extraction of Integrated Intensities from a Powder Pattern; Institut Für Kristallographie, ETH Zürich, Switzerland, 1990.

(29) Baerlocher, C.; Hepp, A. XRS-82. The X-Ray Rietveld System; Institut Für Kristallographie, ETH Zürich, Switzerland, 1982. *Baerlocher, C.; Hepp, A. XRS-82. X-ray Rietveld Syst. Inst. für Krist. ETH Zürich, Switzerland, 1982.*

(30) Grosse-Kunstleve, R. W.; McCusker, L. B.; Baerlocher, C. Powder Diffraction Data and Crystal

Chemical Information Combined in an Automated Structure Determination Procedure for Zeolites. *J. Appl. Crystallogr.* **1997**, *30* (6), 985–995.

(31) Baerlocher, C.; McCusker, L. B.; Palatinus, L. Charge Flipping Combined with Histogram Matching to Solve Complex Crystal Structures from Powder Diffraction Data. *Zeitschrift für Krist.* **2007**, *222* (2), 47–53.

(32) Palatinus, L.; Chapuis, G. SUPERFLIP – a Computer Program for the Solution of Crystal Structures by Charge Flipping in Arbitrary Dimensions. *J. Appl. Crystallogr.* **2007**, *40* (4), 786–790.

(33) Triple: Http://www.calidris-Em.com/triple.php. Accessed December 8, 2014. *Triple http//www.calidris-em.com/triple.php. Accessed December 8, 2014.*

(34) Baerlocher, C.; Hepp, A.; Meier, W. M. DLS-76; Institut Für Kristallographie, ETH Zürich, Switzerland, 1976. *Baerlocher, C.; Hepp, A.; Meier, W. M. DLS-76; Inst. für Krist. ETH Zürich, Switzerland, 1976.*

(35) Rietveld, H. M. A Profile Refinement Method for Nuclear and Magnetic Structures. *J. Appl. Crystallogr.* **1969**, *2* (2), 65–71.

(36) Román-Leshkov, Y.; Moliner, M.; Davis, M. E. Impact of Controlling the Site Distribution of Al Atoms on Catalytic Properties in Ferrierite-Type Zeolites †. *J. Phys. Chem. C* **2011**, *115* (4), 1096–1102.

(37) Tijsebaert, B.; Yilmaz, B.; Müller, U.; Gies, H.; Zhang, W.; Bao, X.; Xiao, F.-S.; Tatsumi, T.; De Vos, D. Shape-Selective Synthesis of Methylamines over the RRO Zeolite Al-RUB-41. *J. Catal.* **2011**, *278* (2), 246–252.

(38) Jr, A. B.; Ong, K.; Zones, S. Molecular Sieve SSZ-75 Composition of Matter and Synthesis Thereof. *US Pat. 7,713,512* **2010**.

6.9 Supporting Information

1. Microporous Material Synthesis Results

Table S1. Fluoride mediated synthesis results.

Gel Ratios							Product Ratios[b]	
Si/Al	Si/Ti	H_2O/SiO_2	Seeds	Temp (°C)	Time (days)	Result	Si/Al	Si/Ti
∞	-	4	None	175	8	STW[a]	-	-
∞	-	4	None	175	6	**STW**+CIT-7[a]	-	-
∞	-	4	None	175	6	CIT-7[a]	-	-
∞	-	4	Silica CIT-7	175	6	CIT-7	-	-
∞	-	7	None	175	6	STW	-	-
15	-	4	Silica CIT-7	175	5	CIT-7	10	-
20	-	4	None	175	20	CIT-7	14	-
20	-	4	None	175	12	CIT-7	13	-
25	-	4	Silica CIT-7	175	5	CIT-7	15	-
25	-	4	Silica CIT-7	175	5	CIT-7	17	-
25	-	4	Silica CIT-7	175	6	CIT-7	14	-
50	-	4	None	175	18	CIT-7	27	-
50	-	4	Silica CIT-7	175	4	CIT-7	28	-
100	-	4	Silica CIT-7	175	4	CIT-7	36	-
250	-	4	Silica CIT-7	175	4	CIT-7	225	-
-	50	4	Silica CIT-7	175	7	CIT-7	-	63
-	100	4	Silica CIT-7	175	7	CIT-7	-	88
[a]Since **STW** and CIT-7 were competing products some syntheses produced pure phase versions (per XPD) of those molecular sieves [b]Determined using EDS of calcined material								

Table S2. Hydroxide mediated synthesis results.

Gel Si/Al	Gel Na/Si	Gel ROH/Si	Gel H₂O/Si	Temp (°C)	Seeds	Time (days)	Product	Product Si/Al
5[a]	0.25	0.16	30	160	Silica CIT-7	35	CIT-7	9
10[a]	0.25	0.16	30	160	None	20	CIT-7	12
15[a]	0.16	0.16	30	160	None	35	IWV	
15[a]	0.16	0.16	30	160	Silica CIT-7	10	CIT-7	18.4 H⁺ form
15[a]	0.16	0.16	30	160	Silica CIT-7	10	CIT-7	9
30[b]				175	None	18	IWV	29
30[b]				175	Silica CIT-7	23	IWV+CIT-7	
[a]Made using Ludox AS-40 and sodium aluminate [b]Made from CBV760								

2. Characterization
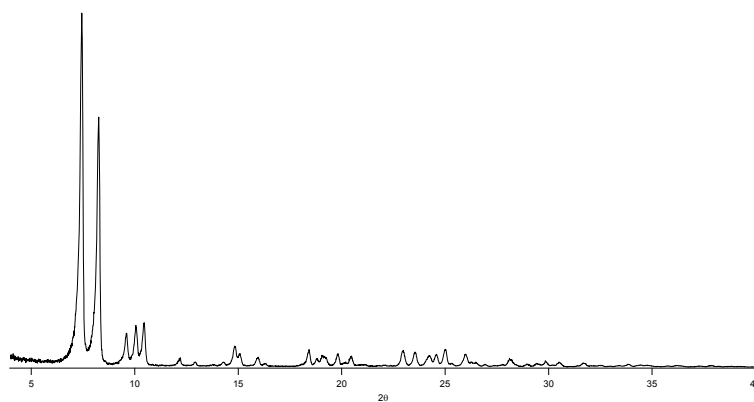
Figure S1. XPD pattern of calcined pure-silica CIT-7 produced in fluoride media.
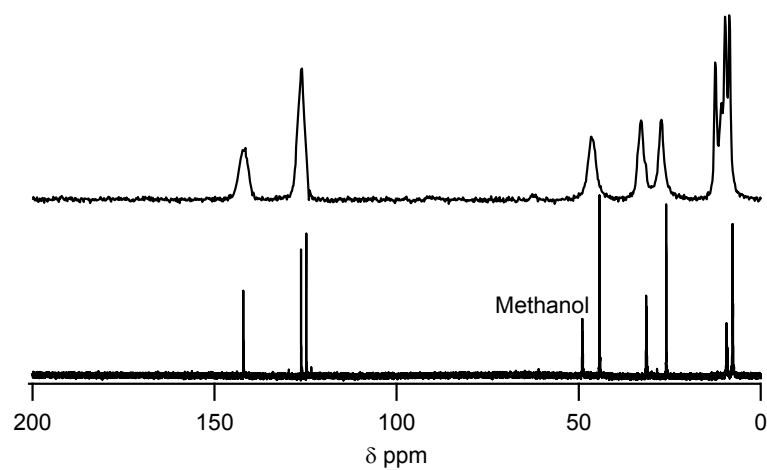
Figure S2. ^{13}C CP-MAS NMR of as-made CIT-7 (upper) showing the occluded OSDA and comparison to the liquid NMR (lower, methanol added as an internal standard).
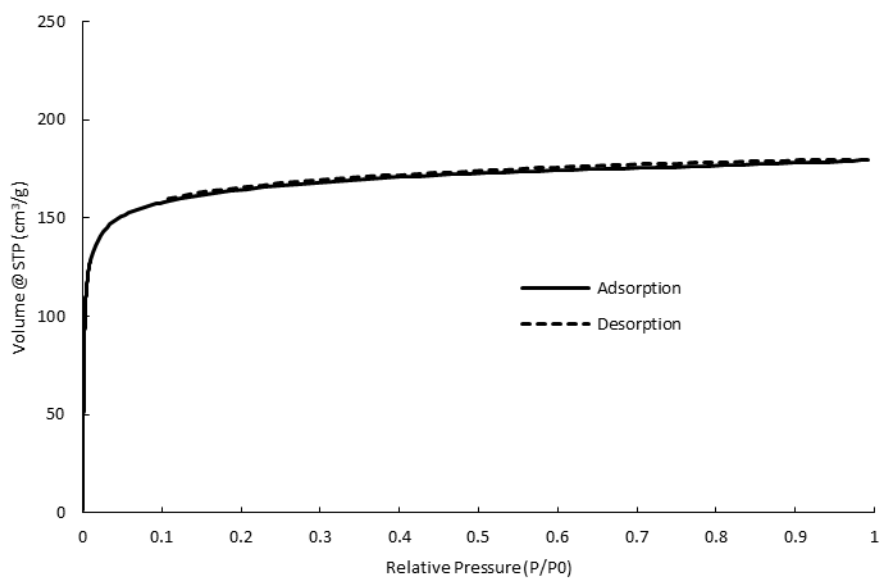
Figure S3. Argon isotherm of CIT-7.
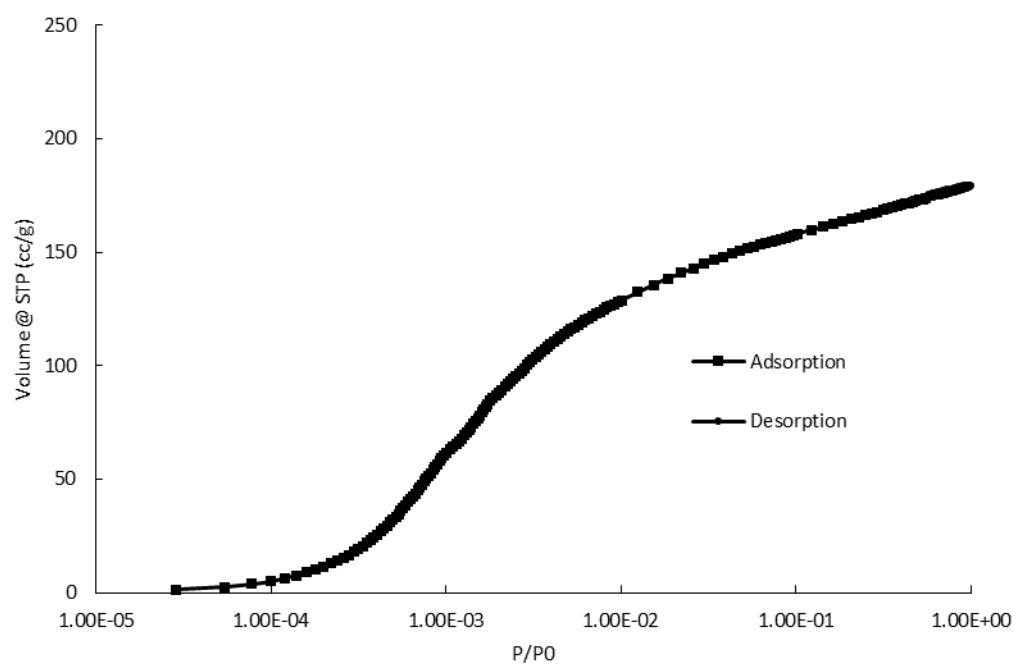
Figure S*4*. Log plot argon adsorption isotherm.
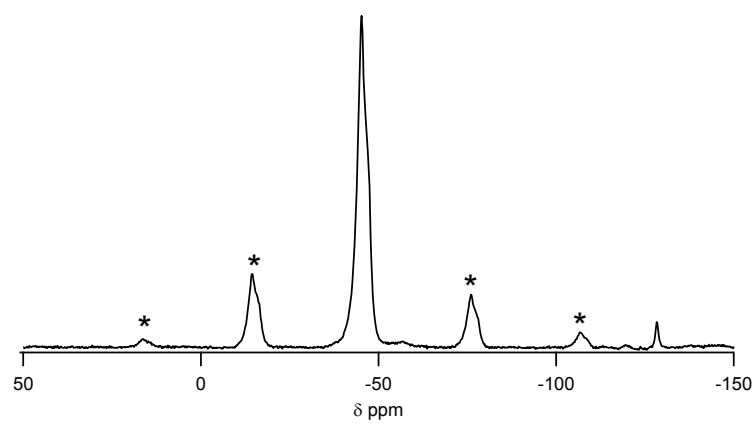
Figure S5. ^{19}F NMR of as-made CIT-7, spinning side bands are marked with an asterisk.
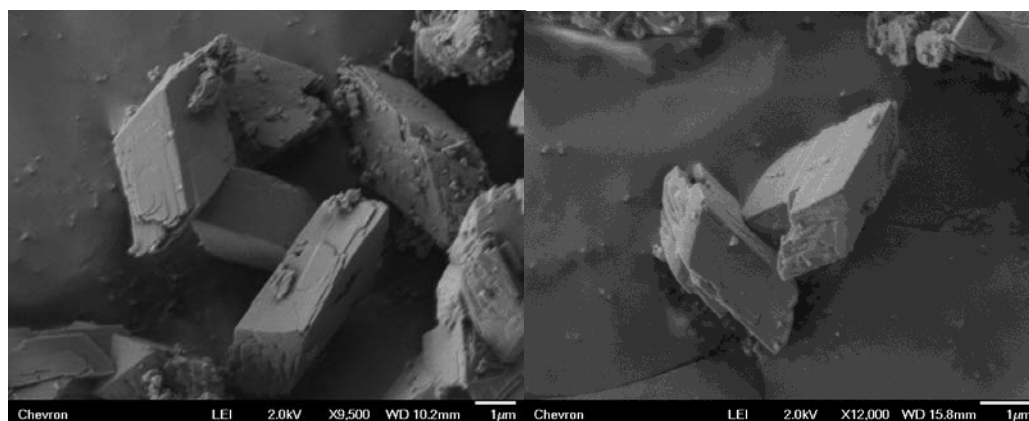
Figure S7. SEM images of calcined, pure-silica CIT-7.
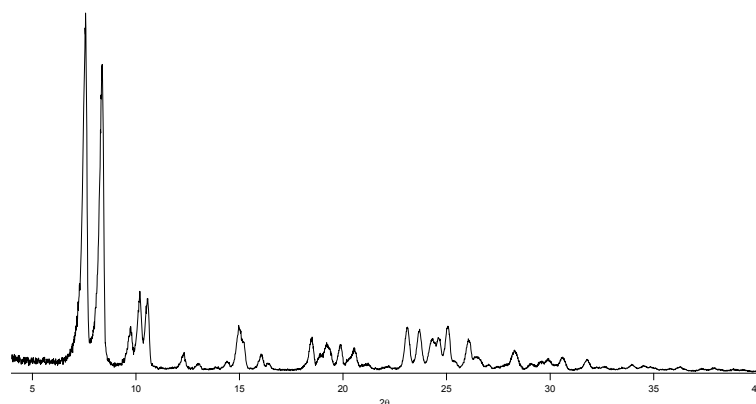
Figure S7. XPD pattern of calcined aluminosilicate CIT-7 produced in fluoride media with gel

Si/Al=50.
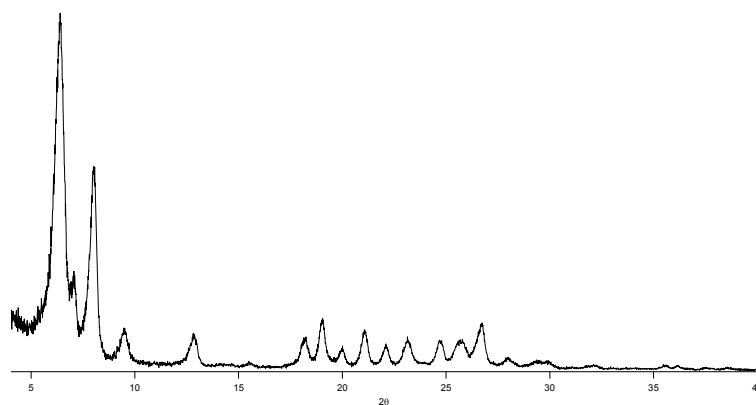
Figure S8. XPD pattern of calcined ITQ-27.
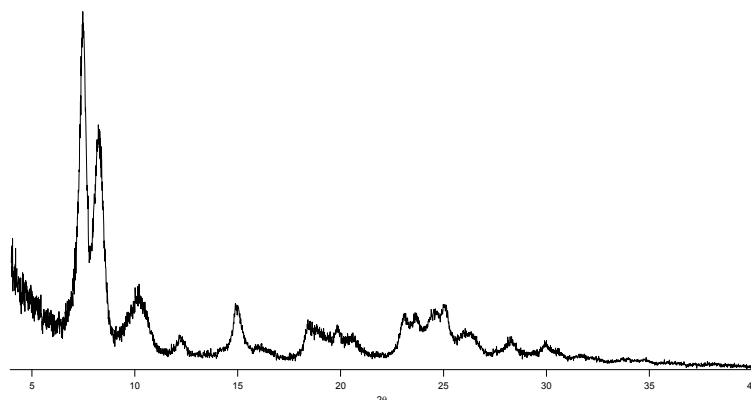
Figure S9. XPD pattern of as-made CIT-7 produced in hydroxide media with gel Si/Al=15.
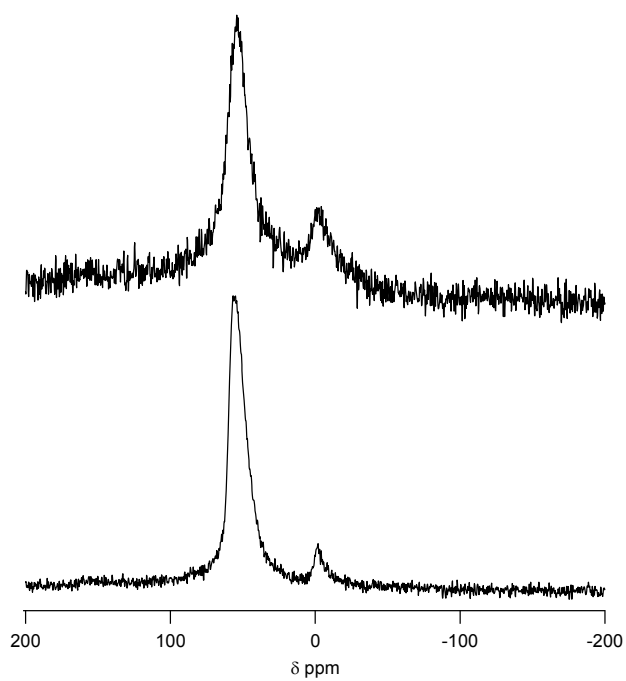
Figure S10. ^{27}Al MAS NMR of aluminosilicate CIT-7. Upper is fluoride mediated synthesis with gel Si/Al=15 and lower is hydroxide mediated synthesis with gel Si/Al=5. The sample made in hydroxide media is 95% tetrahedral aluminum and the sample made in fluoride media is 88% tetrahedral aluminum.
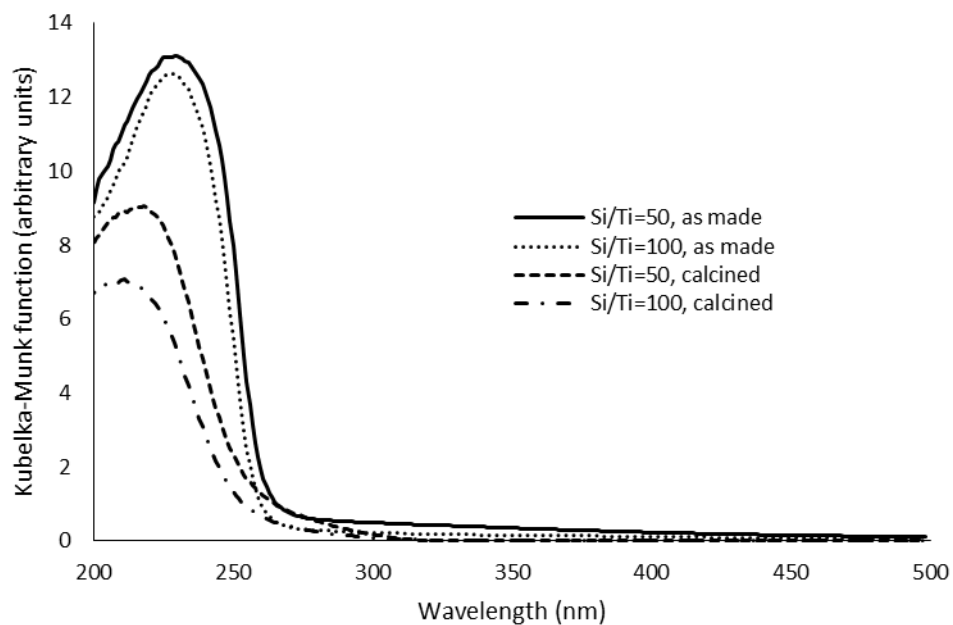
Figure S11. UV-VIS of titanosilicate CIT-7.

3. Structure Determination

3.1 Rotation Electron Diffraction Data Collection

Large tilt steps (0.5º/0.35º) had to be used for these measurements, because the RED

software to perform the finer tilts by tilting the electron beam had not yet been implemented to

the JEOL 2010 TEM. As a result, the RED data were not of optimal quality.

Table S3. RED data collection.

	Dataset 1	Dataset 2	Merged dataset
Tilt range (in º)	-55 -> +60	-55 -> +60	/
Tilt step size (in º)	0.50	0.35	/
Number of 2-dimensional ED images	262	296	/
Collected reflections	2312	2248	3590
Independent reflections	1315	1289	2007
Data resolution (in Å)	1.0	1.0	1.0
Agreement factor of the reflection intensities for Friedel pairs	11.7%	22.1%	16.8%
Data completeness	56.0%	54.9%	85.5%
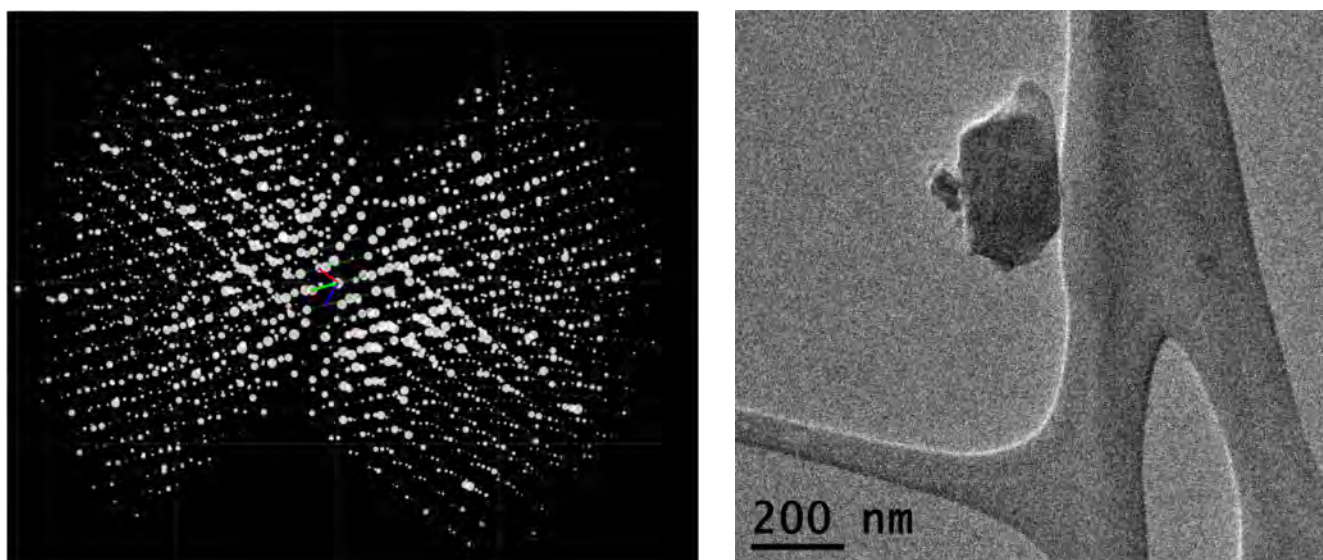
Figure S12. 3D electron diffraction tomography data (left) collected from a calcined, pure-silica

CIT-7 (right).

3.2 Synchrotron XPD Data Collection.

Table S4. Synchrotron XPD data collection.

Synchrotron facility	2-1 Beamline at SSRL
Wavelength	0.99995 Å
Diffraction geometry	Debye-Scherrer
Analyzer crystal	Si 1 1 1
Sample	Rotating 0.5 mm capillary
2θ range	3.5-73.5º
Step size	0.004º2θ
Time per step	
3.5-5.8º2θ	2.0 s
5.8-19.8º2θ	4.0 s
19.8-73.5º2θ	6.0 s

4. Description of The CIT-7 Framework Structure

4.1 Natural Tiling Analysis of the CIT-7 Framework
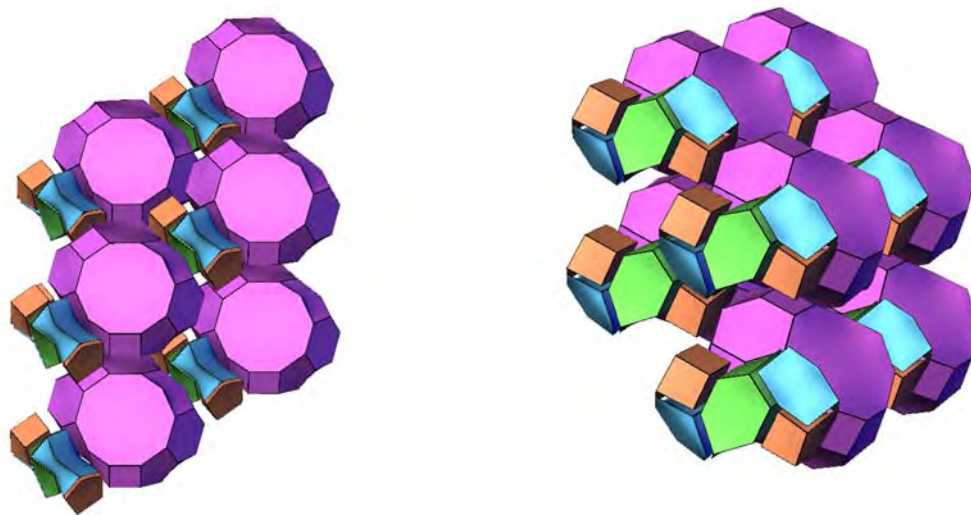
Figure S13. Tiling of the CIT-7 framework built by 4 different types of tiles $[5^2.6^2]$ (blue), $[4^4.5^2]$

(Orange), $[4^2.5^4.6^2]$ (green), and $[4^8.5^4.6^8.8^2.10^2]$ (purple), viewing down the [011] projection (left)

and the [111] projection (right). The software TOPOS [S1] was used to analyze the framework topology, and the software 3dt [S2] was used for visualizing the tiles.

Transitivity: [(10)(20)(16)4]; Natural Tiling Signature:

$2[5^2.6^2]+2[4^4.5^2]+[4^2.5^4.6^2]+[4^8.5^4.6^8.8^2.10^2]$

Coordination Sequences:

Si1: 4 12 17 27 49 79 99 120 146 192	Si2: 4 9 18 30 49 73 100 117 150 203
Si3: 4 10 18 31 47 75 98 124 156 189	Si4: 4 10 19 32 55 70 89 124 160 199
Si5: 4 12 20 29 49 73 100 129 157 186	Si6: 4 10 21 35 46 65 99 134 162 191
Si7: 4 9 19 37 50 66 92 126 164 200	Si8: 4 10 18 30 48 71 105 126 145 193
Si9: 4 9 18 32 48 69 95 131 160 182	Si10: 4 11 19 30 45 73 102 125 156 187

4.2 The crystallographic information file (cif) for the pure-silica CIT-7.

data_all-silica_CIT-7
_chemical_name_systematic
"CIT-7"
_chemical_formula_structural
"[Si20O40]"

_cell_length_a   13.0187(1)
_cell_length_b   11.2063(1)
_cell_length_c   9.3758(1)
_cell_angle_alpha   92.8224(6)
_cell_angle_beta   107.2048(5)
_cell_angle_gamma   103.2565(5)

_symmetry_space_group_name_H-M   'P -1'
_symmetry_Int_Tables_number   2
_symmetry_cell_setting   triclinic
loop_
_symmetry_equiv_pos_as_xyz
'+x,+y,+z'
'-x,-y,-z'

loop_
_atom_site_label
_atom_site_type_symbol
_atom_site_occupancy
_atom_site_fract_x
_atom_site_fract_y
_atom_site_fract_z
_atom_site_U_iso_or_equiv
  O1   O 1.0000   0.2236(2)   0.5059(3)   0.0497(2) 1.07(10)
  O2   O 1.0000   0.3564(1)   0.4201(2)   0.2714(5) 1.07
  O3   O 1.0000   0.3240(2)   0.6411(2)   0.3146(3) 1.07
  O4   O 1.0000   0.1662(1)   0.4463(4)   0.2860(1) 1.07
  O5   O 1.0000   0.3703(1)   0.6646(2)   0.9715(3) 1.07
  O6   O 1.0000   0.1691(1)   0.5937(2)   0.7893(2) 1.07
  O7   O 1.0000   0.2986(1)   0.4377(2)   0.8372(3) 1.07
  O8   O 1.0000   0.3411(3)   0.2514(1)   0.7003(3) 1.07
  O9   O 1.0000   0.4275(3)   0.4816(3)   0.6650(3) 1.07
 O10   O 1.0000   0.2112(2)   0.3738(3)   0.5487(3) 1.07
 O11   O 1.0000   0.1312(2)   0.5669(1)   0.4991(2) 1.07
 O12   O 1.0000   1.0012(2)   0.3462(3)   0.3897(2) 1.07
 O13   O 1.0000   0.3314(3)   0.0139(1)   0.6712(3) 1.07
 O14   O 1.0000   0.5093(1)   0.1725(3)   0.6611(2) 1.07
 O15   O 1.0000   0.4571(2)   0.1536(2)   0.9168(3) 1.07
 O16   O 1.0000   0.4093(5)   0.8471(2)   0.8129(3) 1.07
 O17   O 1.0000   0.2014(1)   0.7903(2)   0.6425(2) 1.07
 O18   O 1.0000   0.3636(1)   0.8314(3)   0.5162(2) 1.07
 O19   O 1.0000   0.4693(2)   0.3106(2)   0.1474(2) 1.07
 O20   O 1.0000   0.4992(2)   0.3135(2)   0.4408(2) 1.07

Si1	Si 1.0000	0.2680(1)	0.5033(1)	0.2286(2)	0.80(5)
Si2	Si 1.0000	0.2646(1)	0.5496(2)	0.9108(1)	0.80
Si3	Si 1.0000	0.3210(2)	0.3874(1)	0.6886(2)	0.80
Si4	Si 1.0000	0.1261(1)	0.4313(1)	0.4305(2)	0.80
Si5	Si 1.0000	0.4105(2)	0.1493(2)	0.7367(1)	0.80
Si6	Si 1.0000	0.3255(1)	0.8692(2)	0.6586(2)	0.80
Si7	Si 1.0000	0.1261(1)	0.6529(1)	0.6366(2)	0.80
Si8	Si 1.0000	0.4754(2)	0.3911(2)	0.2987(2)	0.80
Si9	Si 1.0000	0.4638(2)	0.7620(1)	0.9296(2)	0.80
Si10	Si 1.0000	0.4203(1)	0.7469(2)	0.4335(2)	0.80

5. References

[S1] V. A. Blatov, O. Delgado-Friedrichs, M. O'Keeffe, D. M. Proserpio, *Acta Cryst. A.*, 2007, **63**, 418–425.

[S2] O. Delgado-Friedrichs, M. O'Keeffe, *Acta Cryst. A.*, 2003, **59**, 351-360.

Chapter 7. High-Silica, Heulandite-Type Zeolites Prepared by Direct Synthesis and Topotactic Condensation

7.1 Abstract

There are both natural minerals and synthetic zeolites that possess the HEU framework topology. These materials have a limited compositional range (Si/Al < 6), and the natural zeolites often contain a large amount of impurities such as Fe^{3+}. The preparation of impurity-free HEU-type zeolites with higher Si/Al ratio could open many areas of application, particularly in catalysis. Here, we report the first high-silica HEU-type zeolite that can be prepared via two different procedures. In the first method high-silica HEU (denoted CIT-8) is prepared using a topotactic condensation mechanism (layered precursor denoted CIT-8P); CIT-8P is obtained from a low-water synthesis in fluoride media. CIT-8 prepared in this manner has a product Si/Al ratio of 9.8 +/- 0.7 and a micropore volume of 0.10 cc/g (measured by nitrogen adsorption). The variable temperature powder X-ray diffraction shows that CIT-8 forms via topotactic condensation from CIT-8P along the *b* axis. Additionally, high-silica heulandite can be synthesized directly from a hydroxide-mediated reaction mixture (denoted CIT-8H), and has a Si/Al ratio of 6.4 +/- 0.3 and a micropore volume of 0.10 cc/g. Both synthesis methods produce zeolites that expand the compositional range of HEU-type zeolites. These synthetic methods allow for the addition of other heteroatoms, and titanium-containing CIT-8 is prepared as an illustrative example.

7.2 Introduction

Natural zeolites form under hydrothermal processes, normally near volcanic deposits, and according to the International Mineralogical Association definition, there were known to be 93 different mineral species belonging to 44 different framework types as of 2014.[1] Approximately 2.5 million metric tons of natural zeolites are consumed per year, compared to 1.7-2 million metric tons of synthetic zeolites.[2] Natural zeolites are employed in applications such as separations, impurity removal (such as ammonia), and as additives in paper, consumer products, and animal feed.[3] Many natural zeolites are known to have synthetic analogs that can be produced at different compositions than the natural material. Additionally, natural zeolites often have large amounts of impurities, making them unsuitable for many applications. Natural zeolites commonly occur at compositions (typically low Si/Al ratio, e.g., below 5) that are not thermally or hydrothermally stable, further rendering them unusable in demanding process conditions, such as catalytic applications. Therefore, discovery of synthetic methods to produce analogs of natural zeolites that result in desired frameworks free of impurities and exhibiting robust thermal and hydrothermal stability (typically Si/Al ratio higher than 5) are highly desired. One recent example of this approach is that of the synthetic analogue of the mineral boggsite (**BOG**[4]), recently prepared as ITQ-47.[5] The **BOG** framework has a 2-dimensional system of intersecting 10- and 12-membered rings (MRs) and was prepared synthetically using an organic structure directing agent based on phosphazenes, as a silicoborate framework material instead of the aluminosilicate material that is the rare natural zeolite. ITQ-47 has been evaluated for catalytic applications including the production of cumene by the alkylation of benzene with propylene, where it shows better product selectivities to cumene than ***BEA**, the current industrial standard material for this

reaction.[5]

Zeolites with the **HEU** framework exist as both natural minerals as well as their synthetic analogs. The natural materials can be excavated from quarries at low cost, and are used in applications including building materials, paper fillers, livestock feed supplements, water purification, dehydration, and gas separations.[3] The **HEU** framework contains a pore channel system with openings consisting of 10-MRs in the [001] direction that are 3.1 x 7.5 Å as well as 8-MRs with dimensions of 3.6 x 4.6 Å in the [001] direction. Additionally, there is another set of 8-MRs along the [100] direction with dimensions of 2.8 x 4.7 Å.[6] Materials with the **HEU** framework are divided into two distinct classes based on Si/Al ratio. Those with Si/Al of less than 4 are known as heulandite and those with Si/Al greater than 4 are known as clinoptilolite, or silica-rich heulandite. The key difference in these materials is that those with Si/Al of less than 4 are not thermally stable to calcination above 350°C (though the literature contains some ambiguity about the definition).[7] Natural heulandites are often encountered containing Ba, Ca, Na, K, and Sr in addition to a significant amount of iron as Fe^{3+} (up to 1.5% of the tetrahedra).[3]

A synthetic method to produce a high-silica heulandite was first reported by removing aluminum from natural clinoptilolite to make a material with Si/Al ≥ 5.5, known as LZ-219.[8] Later, methods were developed to produce synthetic heulandites across a range of Si/Al=2.5-6 using various sources of silica and alumina and a wide range of inorganic cations (Ca, K, Li, Na, Ca, Sr) under hydrothermal synthesis conditions.[7,9–12] These materials have been considered for applications such as gas cleaning and separations, ion exchange, isomerization of 1-butene and xylene, methanol dehydration, acetylene hydration, and the separation of nitrogen from natural gas.[7,13] In any of these applications, the ability to tailor the framework composition is important for material properties such as exchange capacity, and thermal and hydrothermal stability as well as

pore accessibility.

Herein, we report methods to prepare high-silica heulandite. High-silica heulandite is prepared via topotactic condensation of a layered aluminosilicate material (layered material denoted CIT-8P, condensation product denoted CIT-8) formed using an organic structure directing agent (OSDA). High-silica heulandite can also be prepared by direct synthesis in hydroxide media using an OSDA that is found to be occluded in the product (material prepared in hydroxide media denoted CIT-8H).

7.3 Experimental

7.3.1 Organic structure directing agent

The diquaternary OSDAs used in this work (shown in Figure 7-1) were synthesized by reacting 200 mmol of 1,2,4,5-tetramethylimidazole (TCI Chemicals) with 100 mmol of dibromoalkane (Aldrich) at reflux in methanol overnight. The solvent was then removed using rotary evaporation and the product washed with ether. The product was verified using ^{13}C NMR in D_2O with methanol added as an internal standard and the characterization results for the diquats are given in Table 7-1. The product was ion exchanged to hydroxide form using Dowex Marathon A exchange resin and the final product concentration was determined using a Mettler-Toledo DL22 autotitrator using 0.01 M HCl as the titrant.
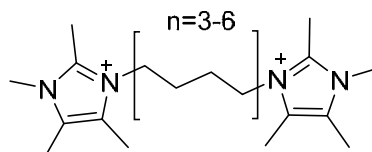

Figure 7-1. Diquats of varying carbon chain linker

Table 7-1. Carbon NMR shifts for the diquats

Dibromoalkane	^{13}C-NMR (125 MHz, D_2O)
1,3-dibromopropane	7.93, 7.98, 9.96, 29.02, 31.70, 41.81, 124.62, 126.42, 142.05
1,4-dibromobutane	7.56, 9.35, 21.21, 25.88, 30.17 , 44.14, 124.60, 126.00, 141.89
1,5-dibromopentane	7.76, 7.82, 9.61, 22.82, 28.58, 31.42, 44.72, 124.84, 126.03, 141.95
1,6-dibromohexane	7.88, 7.95, 9.72, 25.42, 28.88, 31.51, 44.97, 124.96, 126.08, 142.01

7.3.2 Microporous materials synthesis

7.3.2.1 Characterization

Liquid NMR spectra were recorded with a 500 MHz spectrometer.

^{13}C, ^{27}Al and ^{29}Si solid-state NMR were performed using a Bruker DSX-500 spectrometer (11.7 T) and a Bruker 4mm MAS probe. The spectral operating frequencies were 500.2 MHz, 125.721 MHz, 130.287 MHz, and 99.325 MHz for ^1H, ^{13}C, ^{27}Al, and ^{29}Si nuclei, respectively. Spectra were referenced to external standards as follows: tetramethylsilane (TMS) for ^1H and ^{29}Si, adamantane for ^{13}C as a secondary external standard relative to tetramethylsilane, and 1.0 M $Al(NO_3)_3$ aqueous solution for ^{27}Al. Samples were spun at 14 kHz for ^1H and ^{27}Al MAS NMR and 8 kHz for ^{13}C and ^{29}Si MAS and CPMAS NMR experiments. For detection of ^{27}Al signal, a short 0.5µs - π/18 pulse was used before FID was recorded in order to make quantitative comparison among resonances.

Thermogravimetric analysis measurements were performed on Netzsch STA 449C Jupiter. Samples were heated in air to 900°C at a rate of 1°C/min.

Nitrogen physical adsorption isotherms were performed at 77 K using a Quantachrome Autosorb iQ and the micropore volume was determined using the t-plot method.[14]

Powder X-ray diffraction data (PXRD) data were collected on a Rigaku MiniFlex II with Cu Kα

radiation.

Variable temperature PXRD patterns were collected from 30°C to 580°C at increments of 50°C

under ambient conditions, using a PANalytical Empyrean powder diffractometer (Cu Kα radiation)

equipped with an Anton Paar HTK 1200N high-temperature chamber. The sample was stabilized at

each measurement temperature for 15 min before starting each measurement. The temperature

ramp between two consecutive temperatures was 5°C/min.

Scanning electron micrographs (SEM) were recorded on a Hitachi S-570 instrument. EDS

spectra were acquired with an Oxford X-Max SDD X-ray Energy Dispersive Spectrometer system on

a ZEISS 1550 VP FESEM, equipped with in-lens SE.

Diffuse reflectance UV–visible (DRUV) spectra were recorded using a Cary 3G

spectrophotometer equipped with a diffuse reflectance cell; zeolite samples were calcined prior to

data collection.

Three-dimensional electron diffraction data were collected using the rotation electron

diffraction (RED) technique.[15,16] The RED software was installed on a JEOL 2010 microscope

operating at 200 kV, and data were collected over a tilt range of ±50° with a tilt step of 0.50°, with

an exposure time of 3 seconds per tilt step.

A general synthesis procedure for the microporous materials can be found below. In all

situations where a rotating oven was used, the samples were spun at 43 rpm.

7.3.2.2 Fluoride-mediated reactions

Tetraethylorthosilicate, aluminum isopropoxide, and titanium(IV) butoxide (if necessary) were

added to the OSDA in its hydroxide form in a Teflon Parr Reactor. The container was closed and

stirred overnight to allow for complete hydrolysis. The lid was then removed, and the ethanol and

an appropriate amount of water were allowed to evaporate under a stream of air. Once the

appropriate mass was reached, aqueous HF was added and the mixture was stirred by hand until a

homogenous gel was obtained. In the syntheses with $H_2O/SiO_2=4$, a second evaporation step was

normally used. The final gel molar ratios can be found in Table 7-2. Seeds were then added (see

section 3.1) and the autoclave was sealed and placed in a rotating oven at 175°C. Aliquots of the

material were taken periodically by first quenching the reactor in water and then removing

enough material for PXRD.

7.3.2.3 Hydroxide-mediated reactions

Molar ratios used in all hydroxide mediated reactions are given in Table 7-3. In these syntheses

sodium aluminate (Pfaltz & Bauer) was combined with the OSDA in hydroxide form, 1 M NaOH,

and any necessary water and stirred until the solution cleared. Finally, Ludox AS-40 (Aldrich) was

added and stirred until a homogenous gel was obtained. Seeds were added and then the gel was

heated at 160°C in a rotating oven.

7.3.3 Calcination and ammonium exchange

All products were calcined in breathing grade air. The material was heated to 150°C at

1°C/min, held for three hours, then heated to 580°C at 1°C/min and held for six hours to assure

complete combustion of the organic. After calcination, materials prepared in hydroxide media

were exchanged to ammonium form using 1 M NH_4NO_3 (100 mL of solution per gram of catalyst)

at 95°C with stirring for three hours, this was done a total of three times per sample. After

ammonium exchange the materials were washed with water and dried and then calcined to

proton form using the standard method.

7.4 Results and discussion

7.4.1 Fluoride-mediated syntheses

The diquaternary OSDAs investigated in this work were first screened over a range of aluminum and water contents and the results are reported in Table 7-2. Several different products were produced using these diquats depending on the water and aluminum content. CIT-8P was found as a product in these screening reactions along with ***BEA**, CIT-7, **IWV**, **STF**, and **STW.** This competition demonstrates the weak nature of the structure direction exhibited by these diquats, and is similar to the behavior observed in our recent work reporting CIT-7.[17] Additionally, many of these products have been reported before with other diquaternary OSDAs in fluoride media, such as ***BEA** and **STF**.[18] CIT-8P forms in reactions with relatively high amounts of aluminum (Si/Al=15, 20), and decreasing the aluminum content generally led to the formation of CIT-7, **IWV**, or **STF**. Seeding these higher-silica syntheses with CIT-8P materials was not successful in eliminating the formation of competing phases. Therefore, CIT-8P could only be formed from a limited range of synthesis compositions. Synthesis times to form CIT-8P were around 12 days without seeds added, and around 5 days when they were added (some variation in these times was observed in different synthesis trials). Phase competition was also observed, and once a pure-phase sample of CIT-8P was obtained, seeds were used in all subsequent reactions to help favor the formation of CIT-8P.

The PXRD of CIT-8P is shown in Figure 7-2 along with the product that results from calcination, (identified as a HEU-type material). A framework also formed by topotactic condensation similar to **HEU**, **RRO**, has been previously reported as RUB-39 for the layered precursor and RUB-41 for

the calcined framework (**RRO**).[19,20] RUB-41 is formed from heulandite-type layers and has a similar

PXRD pattern as **HEU**. However, careful analysis of the diffraction patterns for the two materials

shows distinct reflections for each of the materials. For **HEU**, there are strong reflections near 17°

and 22° 2Θ that are not present in **RRO**. The calcined material had a micropore volume of 0.10

cc/g from nitrogen adsoption (Figure 7-4). SEM images of the as-made and calcined material are

shown in Figure 7-9. Both the as-made and calcined materials exhibit a plate-like morphology,

similar to what has been observed in other materials prepared via topotactic condensation.

EDS analysis of the calcined material found a Si/Al ratio of 9.8 +/- 0.7. Since the starting gel

had a Si/Al=20, a large portion of the silica initally present was not incorporated in the final

product. It is evident from 13C CPMAS NMR that the organic is occluded intact in as-made

CIT-8P (Figure 7-5). The state of the aluminium in CIT-8P and CIT-8 was studied using 27Al

NMR and the spectra are shown in Figure 7-3. In CIT-8P, only tetrahedral aluminium was

observed. Calcination caused the formation of some octahedral aluminium (near 0 ppm).

Deconvolution of the spectra shows that the calcined material contains *c.a.* 21% octahedral
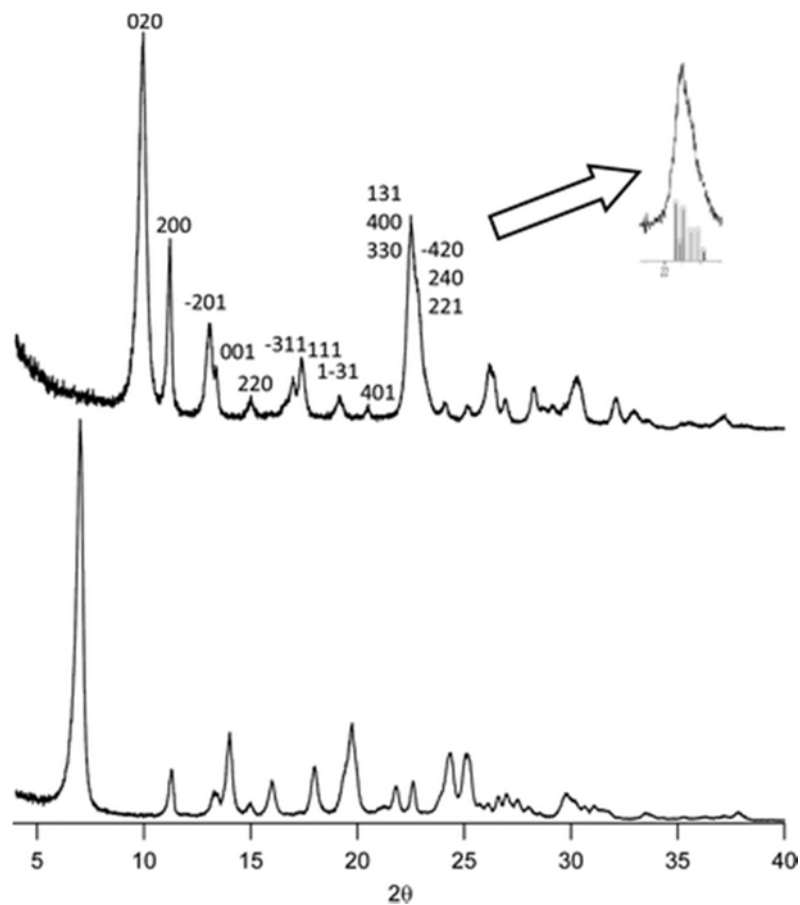
aluminium.

Figure 7-2. PXRD of CIT-8P (lower) and CIT-8 (upper) prepared via topotactic condensation. The upper trace contains the crystallographic directions of some of the main peaks and the arrow points to a deconvolution of the prominent peak located near 22° 2θ.

Table 7-2. Synthesis results in fluoride media

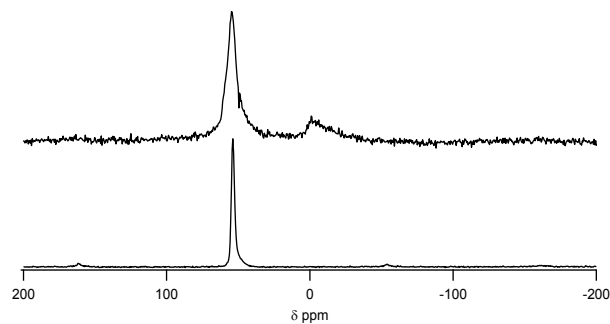| Linker Length	Si/Al=15 H_2O/SiO_2=4	Si/Al=20 H_2O/SiO_2=4	Si/Al=20 H_2O/SiO_2=7	Si/Al=30 H_2O/SiO_2=4	Si/Al=50 H_2O/SiO_2=4	Si/Al=50 H_2O/SiO_2=7
3		PREFER	CIT-8P +PREFER		CIT-7	Dense
4	CIT-8P	CIT-8P, CIT-7	CIT-7	CIT-8P + CIT-7	CIT-7 + CIT-8P	CIT-7
5		CIT-8P	CIT-8P		CIT-7+ CIT-8P	IWV
6		CIT-8P	*BEA		Unknown	STF

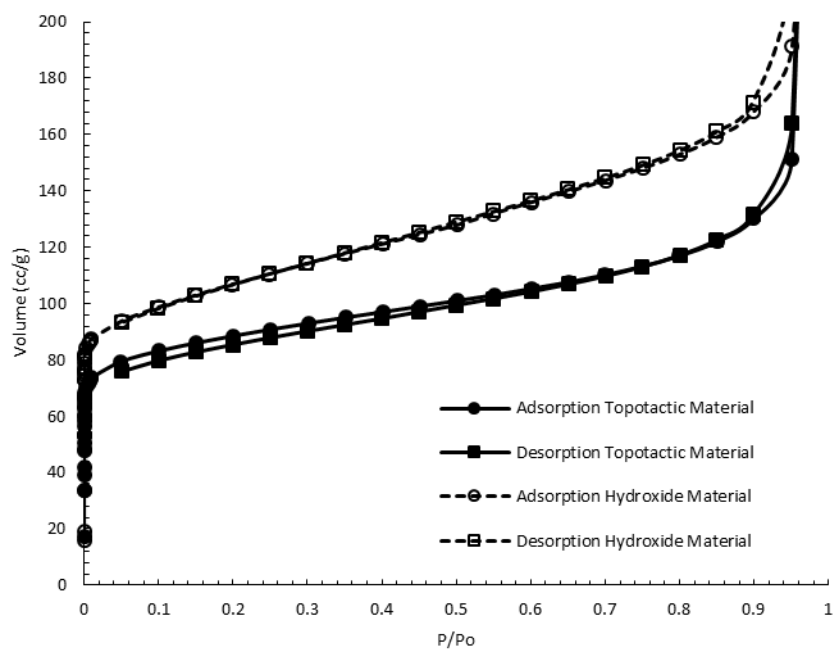Figure 7-3. ^{27}Al MAS NMR of CIT-8P (lower) and CIT-8 prepared by calcination to 580°C (upper)

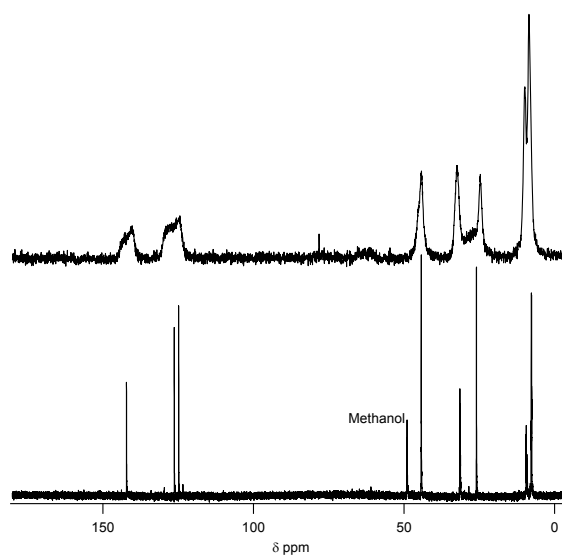Figure 7-4. Nitrogen isotherms for proton form CIT-8 and CIT-8H

Figure 7-5. ^{13}C liquid NMR of the diquat with a 5-carbon chain (lower) compared to the ^{13}C CPMAS NMR of as-made CIT-8P (upper)

7.4.2 Mechanism of topotactic condensation

Topotactic condensations can occur with layered materials that contain terminal silanol groups (coordination of $Si(OSi)_3(OH)$, Q^3 Si). With calcination, these terminal silanol groups condense, releasing water and forming Si-O-Si bonds. In this process, a 2-dimensional material is converted into a 3-dimensional framework material. The presence of silanol groups in CIT-8P was investigated by using ^{29}Si MAS and CPMAS NMR of the as-made and calcined materials. ^{29}Si CPMAS NMR was used on the as-made material in addition to MAS NMR to confirm the resonances (due poor signal to noise ratio with MAS NMR often found prior to calcination). The ^{29}Si NMR spectra are shown in Figure 7-7. In the calcined material, three resonances can be found at -113.8, -108.2, and -102.7 ppm. In accordance with the resonances reported for other heulandite materials, the peak at -113.8 ppm is assigned to $Si(OSi)_4$ coordination environment, and the peaks at -108.2 and -102.7 ppm are assigned to $Si(OAl)(OSi)_3$ coordination environments.[21–24] The amount of

Si(OAl)$_2$(OSi)$_2$ coordination present is very small, and deconvolution determined that the amount

of aluminium in this coordination is insignificant (see Supporting Information). When the ^{29}Si MAS

NMR of the calcined material was deconvoluted, the Si/Al ratio was found to be 9.8, in good

agreement with the ratio found using EDS, further supporting the peak assignments (see

Supporting Information). Both the as-made and calcined materials contain a resonance near -

113.5 ppm that is attributed to Si(OSi)$_4$, Q^4 coordination environment as well as a resonance near -

109 ppm that is attributed to Si(OAl)(OSi)$_3$ coordination environment. The resonance in the as-

made material near -103 ppm that largely disappears upon calcination is attributed to silanol

groups (Si(OSi)$_3$(OH)), or Q^3 Si species that are abundant on the surface of the layered material as

well as Si(OAl)(OSi)$_3$ coordinated Si. [25–27] The resonance at -103 ppm decreases significantly after

calcination as the topotactic condensation (vide infra) causes the materials to lose surface silanols

and form Si-O-Si bonds. Integration of the resonances in the as-made material from the ^{29}Si MAS

NMR shows that *c.a.* 30% of the Si is in a Q^3 environment. For the ideal case of a pure-silica layered

precursor, 22.22% of the Si atoms should be in this environment (see Supporting Information);

however, the presence of aluminum also complicates the spectrum, so finding a result close to the

ideal case supports the assignments. All of the results from ^{29}Si NMR are consistent with a

topotactic condensation process occurring as Q^3 Si disappears upon calcination.

CIT-8P was investigated by variable temperature PXRD (Figure 7-10) in order to elucidate the

structural changes caused by the condensation. Two main events are observed in the variable

temperature PXRD. The first is that the low angle peak starts to shift to a higher angle around

280°C. When the PXRD data are combined with the TGA results (Figure 7-6), it is apparent that the

observed PXRD peak shift coincides with the first mass loss. The second main event observed in

the variable temperature PXRD is a dramatic change between 430 and 480°C, where the low angle

peak either disappears or quickly shifts to become the main peak in HEU. In the same temperature

range, the TGA results show a mass loss as the final HEU framework is formed.
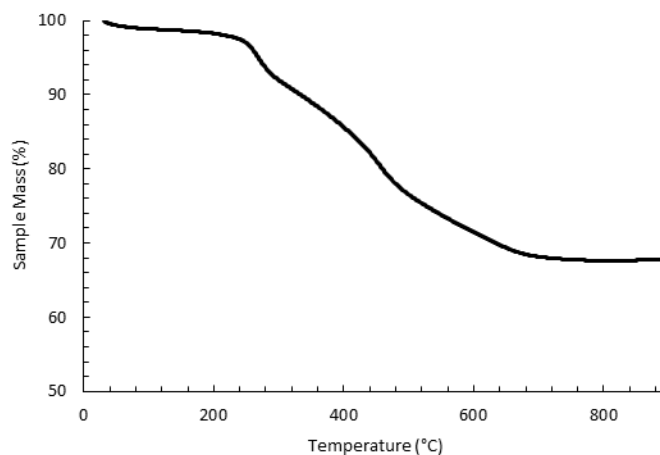

Figure 7-6. TGA of CIT-8P (30.5wt% mass loss due to organic and fluoride)

The structural changes caused by the condensation reaction were elucidated by monitoring

the changes of the PXRD patterns from as-made material transformed via calcination. It is clear

from the variable-temperature PXRD that peak positions for $h0l$ reflections remain during heating,

while the peak positions for the hkl ($k{\neq}0$) reflections are shifted to higher 2θ angles (i.e., lower d-

spacing). This result indicates that the condensation occurs along the b-axis of the **HEU** structure

and that the a and c axes are intact in the layered material. The as-made material was further

studied using the RED technique. Three-dimensional RED tomography data (see Figure 7-11)

shows diffraction streaks between diffraction spots along b-axis clearly, without a significant

indication of diffraction streaks along a- and c-axes. These data indicate that in the as-made

material there is some disorder in the b-direction, but no disorder in the a- and c-directions,

consistent with ordered inorganic layers separated by a disordered organic layer. As the material

condenses along the b-axis, both the 10- and 8 MRs are formed (see graphical depiction shown in

167

Figure 7-8). In the as-made material, the low angle peak corresponds to an interplanar spacing of

~12.8 Å. As the organic begins to degrade in the material (evident by TGA), the spacing is shrunk

by ~3.9 Å until the final **HEU** framework is formed by topotactic condensation.
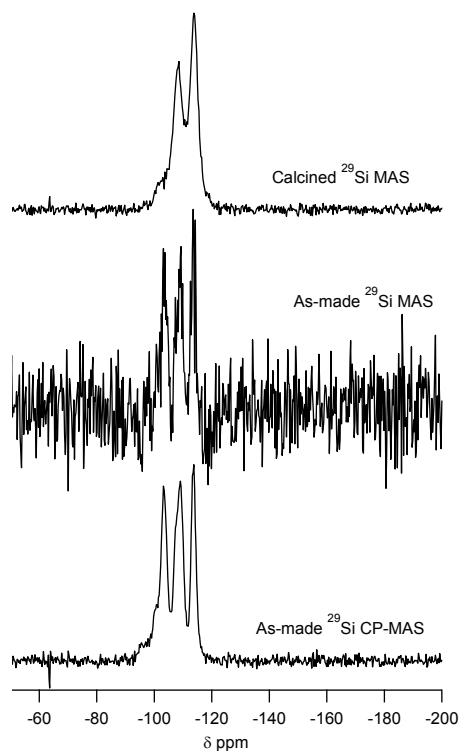

Figure 7-7. ^{29}Si NMRs of CIT-8P by CPMAS (lower), MAS NMR (middle) compared to the calcined
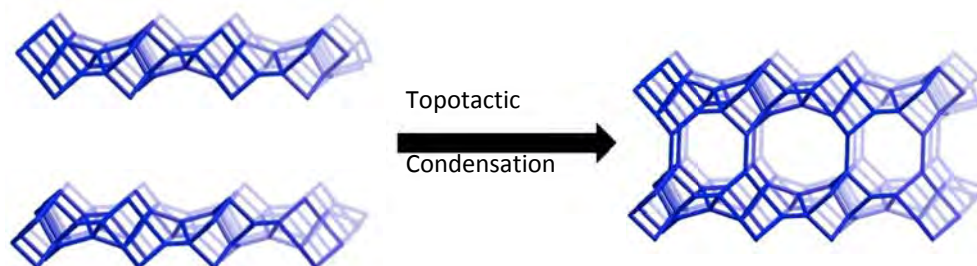
material (upper)

Figure 7-8. Schematic representation of the topotactic condensation process
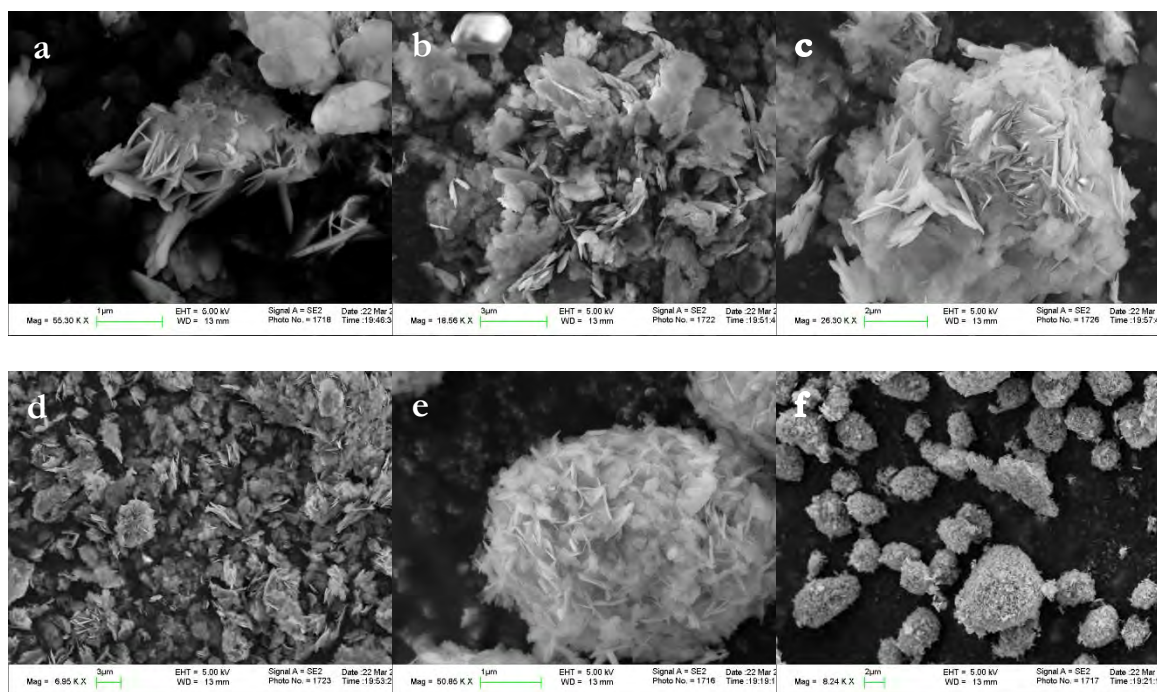
Figure 7-9. SEM images: a,b) CIT-8P, c,d) CIT-8, and e,f) calcined CIT-8H
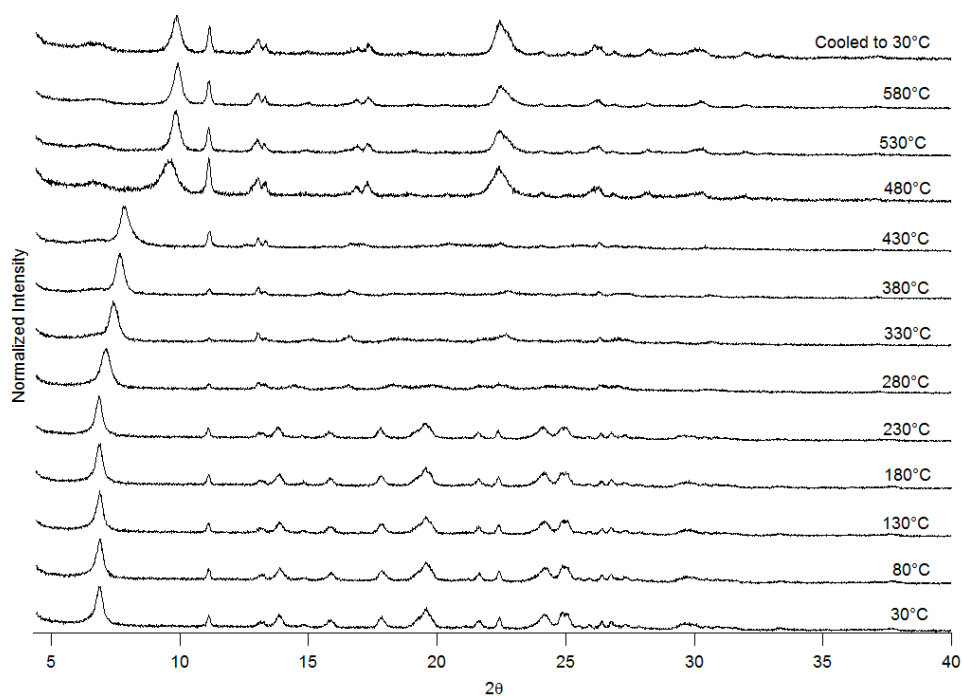
Figure 7-10. Variable temperature PXRD of CIT-8P forming CIT-8. The low angle peak observed in

higher traces is an instrument artifact due to the high temperature chamber.
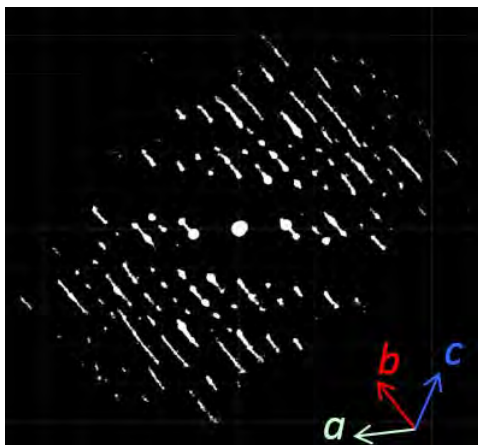
Figure 7-11. RED of as-made CIT-8P

7.4.3 Titanium aluminosilicate HEU

In order to prepare a material with both Brønsted and Lewis acidity, the fluoride preparation

was modified by adding titanium, with the final gel molar ratio:

$1SiO_2:0.05Al:0.02Ti:0.5ROH:0.5HF:4H_2O$. This synthesis composition also produced the layered

material CIT-8P, evident by PXRD, and the **HEU** framework after calcination. After calcination, the

state of the titanium was studied using UV-VIS spectroscopy, and the results are shown in Figure

7-12 compared to the aluminosilicate material. The band observed near 220 nm is consistent with

tetrahedral titanium, indicating framework incorporation, and demonstrating the synthesis of

titanium aluminosilicate **HEU**.
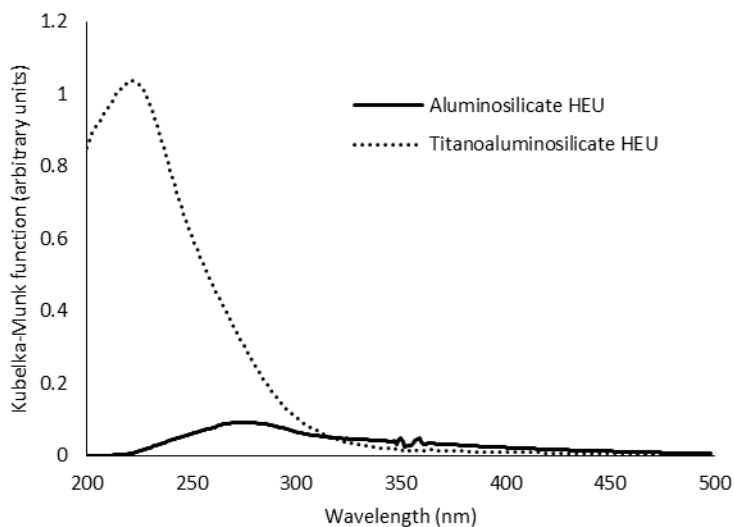
Figure 7-12. UV-VIS of the calcined topotactic HEU with and without titanium.

7.4.4 Hydroxide-mediated reactions

The diquat containing a 4-carbon chain was used in hydroxide-mediated syntheses in an attempt to produce **HEU**-type zeolites. Various Si/Al ratios were tested, both with and without seeds, and the conditions and experimental results are shown in Table 7-3. It was found that **HEU**-type zeolites would not form above a gel ratio of Si/Al=5, even when seeds were present; CIT-7 was found as a product instead. At a gel ratio of both Si/Al=4.15 and 5, CIT-8H was found to form with and without seeds. Adding CIT-8H seeds at a gel Si/Al=5 significantly lowered the synthesis time from greater than 40 days to only 24 days. When seeds of CIT-7 were added at this gel ratio, CIT-7 forms instead. The CIT-8H formed from a gel with Si/Al=5 (product Si/Al ratio of 6.4 +/- 0.3) was found to be stable in proton form and have a micropore volume of 0.10 cc/g (Figure 7-4). From TGA analysis of the as-made material there was 8.4wt% organic occluded that was found to be intact by ^{13}C CPMAS NMR. SEM images of the calcined material are shown in Figure 7-9 and the material exhibits a plate like morphology, similar to that observed for the material prepared via

topotactic condensation. The ^{27}Al MAS NMR of the material in proton form (Figure 7-13) showed that all of the aluminium was in tetrahedral coordination, indicating framework incorporation. The material prepared in hydroxide media exhibits good thermal stability as it was stable to calcination, ammonium exchange, and a subsequent calcination to convert it to proton form.

Table 7-3. Synthesis results in hydroxide media using the 4-carbon diquat

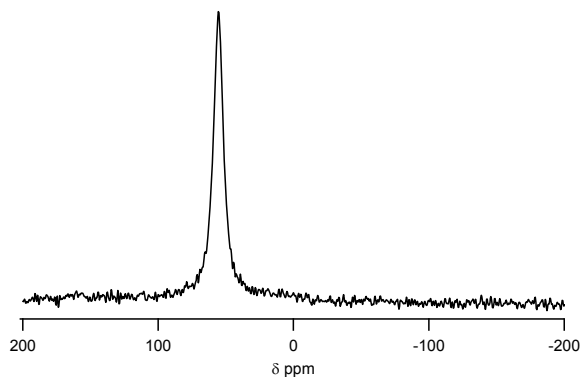| Gel Si/Al	Gel Na/Si	Gel ROH/Si	Gel H_2O/Si	Temp (°C)	Seeds	Time (days)	Product
4.15	0.25	0.16	30	160	None	51	CIT-8H
5	0.25	0.16	30	160	None	43	CIT-8H
5	0.25	0.16	30	160	CIT-7	35	CIT-7
5	0.25	0.16	30	160	CIT-8H	24	CIT-8H
7.5	0.25	0.16	30	160	CIT-8H	20	CIT-7
10	0.25	0.16	30	160	CIT-8H	20	CIT-7

Figure 7-13. ^{27}Al NMR of CIT-8H in proton form

7.5 Conclusions

Diquaternary imidazolium compounds have been found to lead to a wide range of microporous material frameworks depending on the inorganic conditions. The synthesis of high-silica **HEU**-type zeolite (CIT-8) can occur via a topotactic condensation from a layered precursor (CIT-8P) as well as via direct synthesis in hydroxide media (CIT-8H). CIT-8 has a significantly higher Si/Al ratio than previously reported materials with the **HEU** framework. The ability to prepare **HEU**-type zeolites at a higher silica composition and in the absence of trace impurities commonly encountered in natural materials opens up possibilities for use in new applications, such as catalysis. The inclusion of additional heteroatoms in the **HEU** framework, with Ti^{4+} as an example, demonstrates flexibility in the inorganic elements included in the inorganic framework and opens up this framework to additional applications, such as combined Brønsted and Lewis acidity.

7.6 Acknowledgements

7.7 Notes and references

(1)   Colella, C.; Wise, W. S. The IZA Handbook of Natural Zeolites: A Tool of Knowledge on the

Most Important Family of Porous Minerals. *Microporous Mesoporous Mater.* **2014**, *189*, 4–10.

(2) Yilmaz, B.; Müller, U. Catalytic Applications of Zeolites in Chemical Industry. *Top. Catal.* **2009**, *52* (6-7), 888–895.

(3) Gottardi, G.; Galli, E. *Natural Zeolites*; Springer-Verlag, 1985.

(4) Three-Letter Framework Type Codes (boldface Capital Letters) for All Zeolites Mentioned in the Text Are given in Parentheses.

(5) Simancas, R.; Dari, D.; Velamazán, N.; Navarro, M. T.; Cantín, A.; Jordá, J. L.; Sastre, G.; Corma, A.; Rey, F. Modular Organic Structure-Directing Agents for the Synthesis of Zeolites. *Science* **2010**, *330* (6008), 1219–1222.

(6) Baerlocher, C.; Mccusker, L. B. Database of Zeolite Structures, <http://www.iza-structure.org/databases/>. Accessed December 8, 2014.

(7) Zhao, D.; Cleare, K.; Oliver, C.; Ingram, C.; Cook, D.; Szostak, R.; Kevan, L. Characteristics of the Synthetic Heulandite-Clinoptilolite Family of Zeolites. *Microporous Mesoporous Mater.* **1998**, *21* (4-6), 371–379.

(8) Related, F.; Data, A.; Meros, P. E. J. SILICON SUBSTITUTED ZEOLITE COMPOSITIONS AND PROCESS FOR PREPARING SAME. *US Pat. 4,503,023* **1985**.

(9) Chiyoda, O.; Davis, M. E. Hydrothermal Conversion of Y-Zeolite Using Alkaline-Earth Cations. *Microporous Mesoporous Mater.* **1999**, *32* (3), 257–264.

(10) Satokawa, S.; Itabashi, K. Crystallization of Single Phase (K, Na)-Clinoptilolite. *Microporous Mater.* **1997**, *8* (1-2), 49–55.

(11) Williams, C. D. Synthesis of Pure Clinoptilolite without the Use of Seed Crystals. *Chem. Commun.* **1997**, No. 21, 2113–2114.

(12) Zhao, D.; Kevan, L.; Szostak, R. Hydrothermal Synthesis of Alkali Cation Heulandite Aluminosilicate Molecular Sieves. *Zeolites* **1997**, *19* (5-6), 366–369.

(13) Jayaraman, A.; Hernandez-maldonado, A. J.; Yang, R. T.; Chinn, D.; Munson, C. L.; Mohr, D. H. Clinoptilolites for Nitrogen / Methane Separation. *Chem. Eng. Sci.* **2004**, *59* (3), 2407–2417.

(14) Hathaway, P. E.; Davis, M. E. High Resolution, Quasi-Equilibrium Sorption Studies of Molecular Sieves. *Catal. Letters* **1990**, *5* (4-6), 333–347.

(15) Zhang, D.; Oleynikov, P.; Hovmöller, S.; Zou, X. Collecting 3D Electron Diffraction Data by the Rotation Method. *Zeitschrift für Krist.* **2010**, *225* (2-3), 94–102.

(16) Wan, W.; Sun, J.; Su, J.; Hovmöller, S.; Zou, X. Three-Dimensional Rotation Electron Diffraction: Software RED for Automated Data Collection and Data Processing. *J. Appl. Crystallogr.* **2013**, *46* (Pt 6), 1863–1873.

(17) Schmidt, J. E.; Xie, D.; Rea, T.; Davis, M. E. CIT-7, a Crystalline, Molecular Sieve with Pores Bounded by 8 and 10-Membered Rings. *Chem. Sci.* **2015**, *6*, 1728–1734.

(18) Jackowski, A.; Zones, S. I.; Hwang, S.-J.; Burton, A. W. Diquaternary Ammonium Compounds in Zeolite Synthesis: Cyclic and Polycyclic N-Heterocycles Connected by Methylene Chains. *J. Am. Chem. Soc.* **2009**, *131* (3), 1092–1100.

(19) Wang, Y. X.; Gies, H.; Marler, B.; Müller, U. Synthesis and Crystal Structure of Zeolite RUB-41 Obtained as Calcination Product of a Layered Precursor: A Systematic Approach to a New Synthesis Route. *Chem. Mater.* **2005**, *17* (1), 43–49.

(20) Gies, H.; Müller, U.; Yilmaz, B.; Tatsumi, T.; Xie, B.; Xiao, F.; Bao, X.; Zhang, W.; Vos, D. De. Interlayer Expansion of the Layered Zeolite Precursor RUB-39: A Universal Method To Synthesize Functionalized Microporous Silicates. *Chem. Mater.* **2011**, *23* (10), 2545–2554.

(21) Godelitsas, a; Charistos, D.; Tsipis, A.; Tsipis, C.; Filippidis, A.; Triantafyllidis, C.; Manos, G.;

Siapkas, D. Characterisation of Zeolitic Materials with a HEU-Type Structure Modified by Transition Metal Elements: Definition of Acid Sites in Nickel-Loaded Crystals in the Light of Experimental and Quantum-Chemical Results. *Chemistry* **2001**, *7* (17), 3705–3721.

(22) Godelitsas, a.; Charistos, D.; Tsipis, C.; Misaelides, P.; Filippidis, a.; Schindler, M. Heterostructures Patterned on Aluminosilicate Microporous Substrates: Crystallization of cobalt(III) tris(N,N-Diethyldithiocarbamato) on the Surface of a HEU-Type Zeolite. *Microporous Mesoporous Mater.* **2003**, *61* (1-3), 69–77.

(23) Ward, R. L.; McKague, H. L. Clinoptilolite and Heulandite Structural Differences as Revealed by Multinuclear Nuclear Magnetic Resonance Spectroscopy. *J. Phys. Chem.* **1994**, *98* (4), 1232–1237.

(24) Lippmaa, E.; Magi, M.; Samoson, a; Tarmak, M.; Engelbardtlb, G. Investigation of the Structure of Zeolites by Solid-State High-Resolution 29Si NMR Spectroscopy. *J. Am. Chem. Soc.* **1981**, *103* (17), 4992–4996.

(25) Yang, B.; Wu, H.-H.; Wu, P. Synthesis, Characterization and Catalytic Properties of Interlayer Expanded Aluminosilicate IEZ-PLS-3. *J. Phys. Chem. C* **2014**, 140929194213007.

(26) Ruan, J.; Wu, P.; Slater, B.; Zhao, Z.; Wu, L.; Terasaki, O. Structural Characterization of Interlayer Expanded Zeolite Prepared From Ferrierite Lamellar Precursor. *Chem. Mater.* **2009**, *21* (13), 2904–2911.

(27) Wu, P.; Ruan, J.; Wang, L.; Wu, L.; Wang, Y.; Liu, Y.; Fan, W.; He, M.; Terasaki, O.; Tatsumi, T. Methodology for Synthesizing Crystalline Metallosilicates with Expanded Pore Windows through Molecular Alkoxysilylation of Zeolitic Lamellar Precursors. *J. Am. Chem. Soc.* **2008**, *130* (26), 8178–8187.

7.8 Supporting Information for Chapter 7

Deconvolution of CIT-8 ^{29}Si MAS NMR.
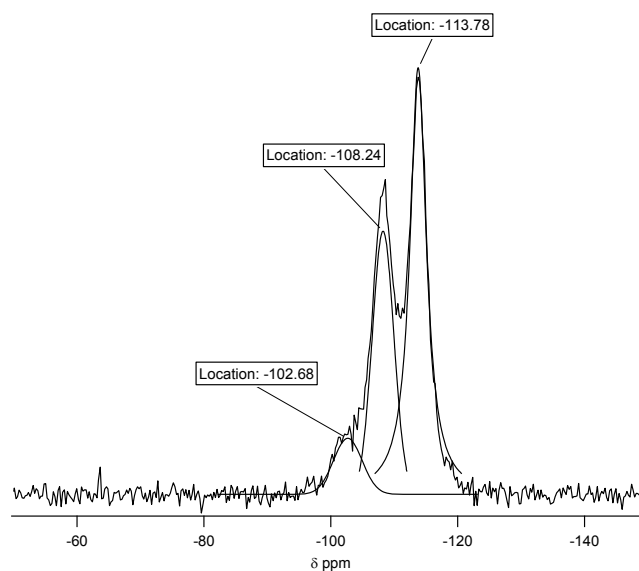
Peak location	Normalized Area	Coordination
-113.78	1.00	$Si(OSi)_4$
-108.24	0.54	$Si(OAl)(OSi)_3$
-102.68	0.15	$Si(OAl)(OSi)_3$

The Si/Al ratio was found to be 9.8.

Deconvolution of the CIT-8 ^{29}Si MAS NMR including a $Si(OAl)_2(OSi)_2$ resonance that was found

to be insignificant
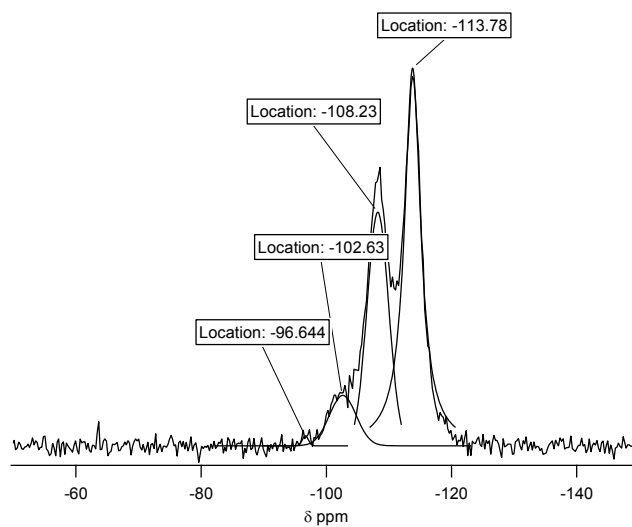
Peak location	Normalized Area	Coordination
-113.78	1.00	$Si(OSi)_4$
-108.23	0.545	$Si(OAl)(OSi)_3$
-102.63	0.147	$Si(OAl)(OSi)_3$
-96.644	0.007	$Si(OAl)_2(OSi)_2$

The Si/Al ratio was found to be 9.8.

Silanol Calculation

There are 5 crystallographic unique T sites in **HEU**. T-2 atoms are the only ones

exposed to the surface of the layer. The multiplicity of the 5 unique T atoms are:

T1 = 8; T2 = 8; T3 = 8; T4 = 8; T5 = 4.

So, ideally, there are T2 / (T1+T2+T3+T4+T5) = 8/36 = 22.22% silicon atoms as silanols.

Chapter 8. The Synthesis of Aluminophosphate and Germanosilicate LTA Using a Triquaternary Structure Directing Agent

8.1 Abstract

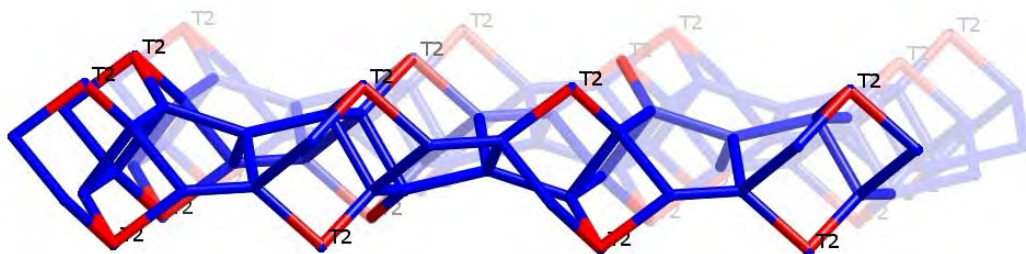The use of triquaternary organic structure directing agents (OSDAs) for the synthesis of microporous materials is relatively unexplored. Here a triquaternary OSDA prepared by reacting 1,2-dimethylimidazole with 1,3,5-tris(bromomethylbenzene) promotes the formation of LTA in the aluminophosphate or germanosilicate reaction chemistries.

8.2 Introduction

Microporous materials are used in a wide variety of applications, and at present, over 200 different frameworks have been identified (each designated by a three-letter code).[1,2] In many applications, only a single structure will give optimal performance. This specificity in the structure-property relationships for crystalline, microporous materials is one of the major driving forces behind much of the research directed at creating new structures.[3] Currently, most discovery of new materials is based on trial and error, though there are numerous guiding principles as well as attempts to computationally predict materials.[4,5]

The use of organic structure directing agents (OSDAs) has been one of the most critical aspects in the discovery of new microporous materials. The use of OSDAs began with the pioneering work of Barrer and Denny to incorporate alkylammonium cations in reactions [6], and since this time,

numerous mono-, di-, and polyquaternary OSDAs have been examined in microporous materials

syntheses.[7–17] The use of these OSDAs has not only led to the discovery of new frameworks, but

has also expanded the composition range for many materials and allowed for enhanced material

properties, e.g., catalytic activity and stability.

In recent years, there has been interest in creating materials with large pores and cages that

could be used for shape-selective transformations with large reactants that are inaccessible with

known materials.[5,16] One strategy to produce these materials is through the use of large, rigid

OSDAs that require large, open volumes to be occluded in microporous materials. The size of these

molecules is limited by their carbon to quaternized nitrogen ratio (C/N^+), as it has been shown that

there is an optimal range to create organics of moderate solubility which perform best in

microporous materials syntheses (commonly recognized to be C/N^+=11-15).[9,18,19] As many of these

large organics are prepared through Diels-Alder or Michael Addition reactions and involve several

reaction steps and purifications, they are difficult and costly to access.[7,20] A final shortcoming of

many of the largest OSDAs, that are normally diquaternary, is that they tend to be linear in nature,

and in many cases this leads to known, large pore materials, that lack large cages.[16]

To overcome these limitations, we have been exploring triquaternary OSDAs in the synthesis

of microporous materials. The first work to report the use of triquaternary OSDAs involved the

synthesis of ZSM-18.[21,22] Here, we prepare triquaternary OSDAs using simple quaternization

chemistry (shown in the general scheme in Figure 8-1), that is based on the methods provided in

reference [23] and gives products in high yields. Similar OSDAs have been previously reported in

microporous materials syntheses where NR_3 was triethylamine or quinuclidine, and in an

magnesioaluminophosphate reaction system, these OSDAs led to the formation of the SAO or BPH

framework topologies, respectively.[24] One inherent limitation of these systems is the torsional

degrees of freedom around the bridging carbon groups; we sought to minimize this feature by limiting NR_3 to rigid groups. The specific triquat used in this work is shown in Figure 8-2, and was found to form LTA as well as ITQ-24.
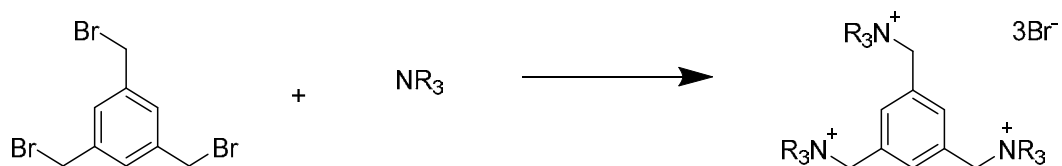
Figure 8-1. General reaction scheme used to produce triquaternary OSDAs, NR_3=tertiary amine
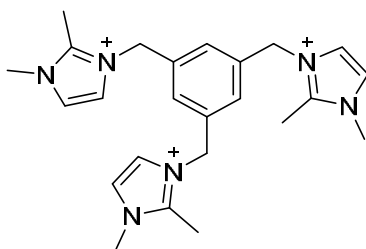
Figure 8-2. Triquat explored in this work (T1)

8.3 Experimental

8.3.1 OSDA Synthesis

Unless otherwise noted, all reagents were purchased from Sigma-Aldrich and were used as received. Hydroxide ion exchanges were performed using strongly basic hydroxide exchange resin. Titrations were performed using a Mettler-Toledo DL22 autotitrator using 0.01 M HCl as the titrant. All liquid NMR spectra were recorded with a 400 MHz Varian Spectrometer.

The triquat used in this work was synthesized by the general scheme shown in Figure 8-1, and is denoted **T1** (Figure 8-2). A typical synthesis is as follows: 300 mmol of 1,2-dimethylimidazole

was dissolved in absolute ethanol in a 500 mL round bottom flask. Then 84 mmol (30 g) of 1,3,5-

tris(bromomethyl)benzene was added to the solution, and it was refluxed overnight. After this

time the mixture was cooled in the freezer and the product precipitated. One additional

recrystallization was performed in absolute ethanol to ensure product purity and the solid was

then dried under vacuum. The product was verified using both ^{1}H and ^{13}C liquid NMR. The product

in its bromide form was then hydroxide exchanged, concentrated using rotary evaporation,

titrated, and stored in a refrigerator. ^{1}H-NMR (500 MHz, D$_2$O): δ 2.56 (s, 9H), 3.81 (s, 9H), 5.37 (s,

3H), 7.18 (s, 3H)., 7.33 (d, 3H), 7.40 (d, 3H). ^{13}C-NMR (125 MHz, D$_2$O): δ 9.86, 35.47, 51.38,

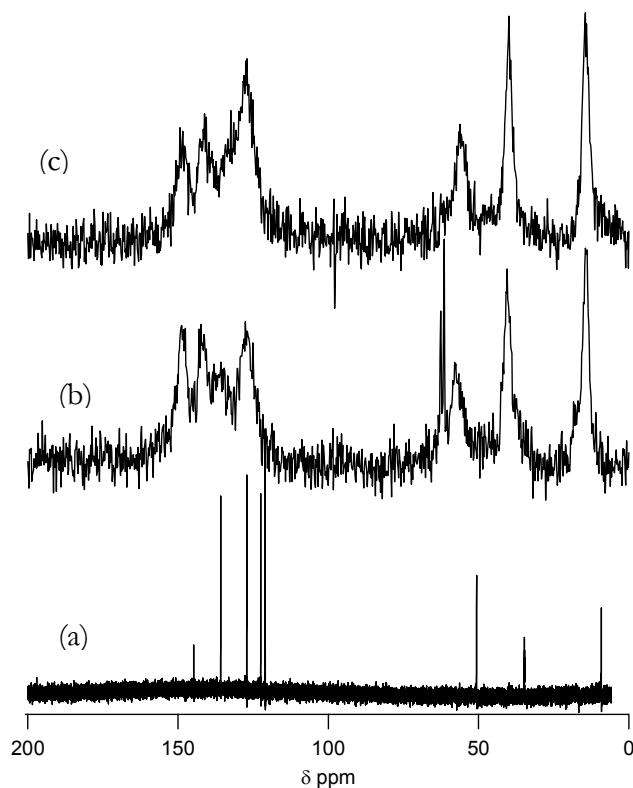121.67, 123.19, 127.83, 136.54, 145.52 (^{13}C NMR shown in Figure 8-3a).

Figure 8-3. ^{13}C NMR spectra: (a) ^{13}C liquid NMR of triquat, (b) ^{13}C CPMAS NMR of AST/LTA mixture

showing presence of TMAOH, and (c) ^{13}C CP-MAS NMR of pure-phase LTA

8.3.2 Microporous Materials Synthesis

8.3.2.1 Characterization

A general synthesis procedure for the microporous materials can be found below. In all situations where a rotating oven was used, the samples were spun at 43 rpm. All powder X-ray diffraction (XRD) characterizations were conducted on a Rigaku MiniFlex II with Cu K$_\alpha$ radiation. All TGA/DSC measurements were performed on Netzsch STA 449C Jupiter. Unless otherwise noted, samples were heated in air to 600°C at a rate of 1 K/min, and then held at 600°C for two hours to ensure complete combustion of the organic. ^{13}C CP-MAS solid-state NMR spectra were recorded on a Bruker CXP-200 spectrometer (4.7 T) with a Bruker 7 mm MAS probe at a spectral frequency of 50.29 MHz with a rotation rate of 4000 Hz and were referenced relative to adamantane as an external standard (2 ms contact time, 2 s delay). SEM images were acquired on a ZEISS 1550 VP FESEM, equipped with in-lens SE. EDS spectra were acquired with an Oxford X-Max SDD X-ray Energy Dispersive Spectrometer system. Nitrogen adsorption isotherms were acquired using a Quantachrome Autosorb iQ.

8.3.2.2 Pure-Silica and Germanosilicates

Tetraethylorthosilicate (TEOS) and germanium ethoxide (if necessary) were added to **T1** in its hydroxide form. The container was closed and stirred overnight to allow for complete hydrolysis. The lid was then removed, and the ethanol and appropriate amount of water were allowed to evaporate under a stream of air. Once the appropriate mass was reached, the material was transferred to a Teflon Parr Reactor and aqueous HF was added. The mixture was stirred by hand until a homogenous gel was obtained. The autoclave was sealed and placed in a rotating oven at temperatures ranging from 140 to 175°C. Aliquots of the material were taken periodically by first

quenching the reactor in water and then removing enough material for XRD.

8.3.2.3 Aluminophosphates

Gel molar ratios used to prepare aluminophosphates were:

$$1P_2O_5:1Al_2O_3:1.6HF:1.6(Triquat)_{1/3}OH:300H_2O$$

$$1P_2O_5:1Al_2O_3:1.6(Triquat)_{1/3}OH:300H_2O$$
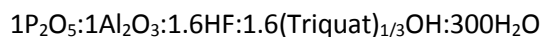
The following procedure was used for the syntheses, it was found to be sensitive to mixing times. The OSDA in hydroxide form was mixed with aluminum isopropoxide and stirred fo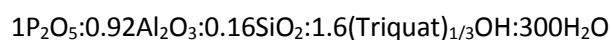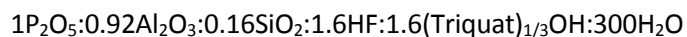r 1 hour in a covered vessel. Phosphoric acid was then added to the gel, and it was stirred while covered for 15 minutes. Finally, the gel was transferred to a Teflon Parr Reactor, and the HF was added directly to the reactor (if necessary). The reactor was sealed and manually shaken to ensure good mixing of the reagents. The reactor was placed in either a static or rotating oven at 160 to 180°C (no differences in the product were found in this operating range). In situations where silicon was used, it was added as TEOS, and the molar ratios were normally adjusted to:

$$1P_2O_5:0.92Al_2O_3:0.16SiO_2:1.6HF:1.6(Triquat)_{1/3}OH:300H_2O$$

$$1P_2O_5:0.92Al_2O_3:0.16SiO_2:1.6(Triquat)_{1/3}OH:300H_2O$$

8.3.3 Molecular Modelling

The location and the van der Waals (vdW) interaction energy of the OSDA within the LTA framework were studied by molecular mechanics simulations using the Materials Studio 6 software.[25] The CVFF forcefield [26] was selected for the calculation, and the most stable locations for the OSDA molecules were obtained by simulated annealing. The unit cell was fixed during the calculation, and in this case, there is no need to generate a supercell. Initially, one OSDA was docked per unit cell, and then the number was increased. The results indicated that the most stable situation was when the large cavity was occupied by one OSDA molecule, with their three

imidazolium groups folded to form a spherical-like shape.

8.4 Results and Discussions

8.4.1 Aluminophosphate

When the OSDA was used in aluminophosphate reactions with or without fluoride, the only product obtained was aluminophosphate LTA ($AlPO_4$-42); an XRD pattern of a representative sample is shown in Figure 8-4a. $AlPO_4$-42 has been reported before, and can be made using a variety of organic and inorganic cations and anions.[27–32] With the addition of fluoride, **T1** was able to produce LTA in as little as four hours, and the material produced was stable under reaction conditions for at least 150 hours. **T1** was also able to produce $AlPO_4$ LTA without the addition of fluoride; however, the synthesis time was on the order of days rather than hours.
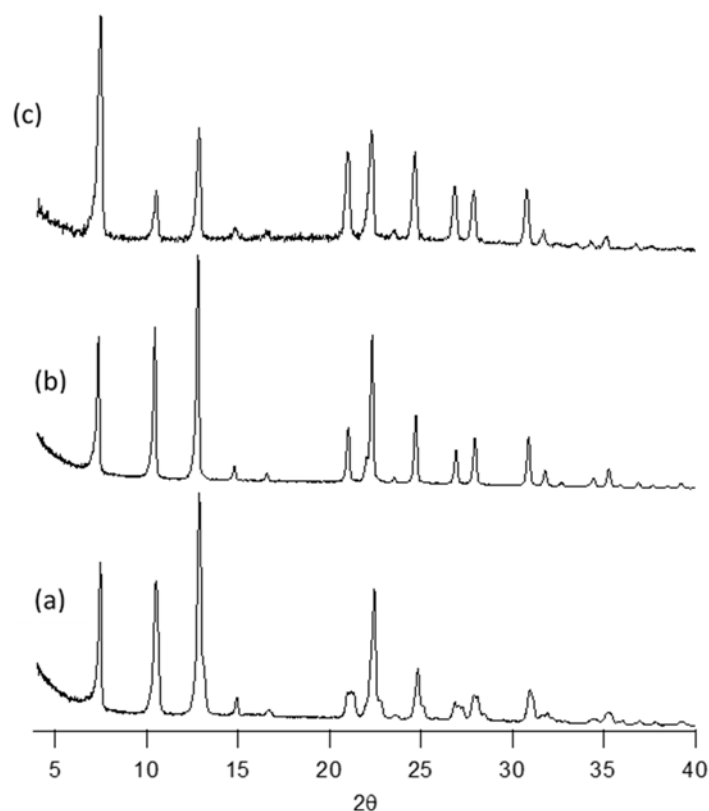
Figure 8-4. XRD of as-made: (a) AlPO$_4$ LTA with fluoride, (b) SAPO LTA with fluoride, and (c) SAPO LTA without fluoride

Silicon can be incorporated in the framework by adding TEOS to the syntheses, and no impurities were present in the final product (determined from XRD, Figure 8-4a). The SAPO material can also be made without fluoride (Figure 8-4c). Additionally, a variety of transition metals can be incorporated into the LTA structure when using **T1**. Transition metals that were tested include cobalt, copper, iron, magnesium, manganese, nickel, and zinc. A SEM image showing the morphology of the SAPO material made with fluoride is shown in Figure 8-5a. In the fluoride syntheses, the morphology is more consistent with previously reported rhombohedral LTA, rather than the typical cubic morphology that is normally reported; however, the XRD pattern

does not show any evidence of peak splitting, which would be encountered in this symmetry.[33]

The organic was removed from the SAPO material using calcination in air at 600°C and an XRD

pattern is shown in Figure 8-6. It has been previously reported that aluminophosphate LTA

shows structure collapse upon calcination [33], so the integrity of the material was evaluated using

nitrogen adsorption, and the isotherm is shown in Figure 8-7. The micropore volume was found

to be only 0.11 cm^3/g (t-plot method), much less than the reported value of 0.23 cm^3/g for

aluminophosphate LTA synthesized using an ionothermal method [31], demonstrating framework

collapse. Ozone was used to remove the occluded organic at 200°C in an attempt to prevent

framework damage, but the resulting material had a nitrogen micropore volume of only 0.12

cm^3/g (t-plot method, Figure 8-7), showing that even a milder treatment resulted in significant

damage to the material. The material was not evaluated further, as the organic could not be

removed without causing significant damage to the framework.
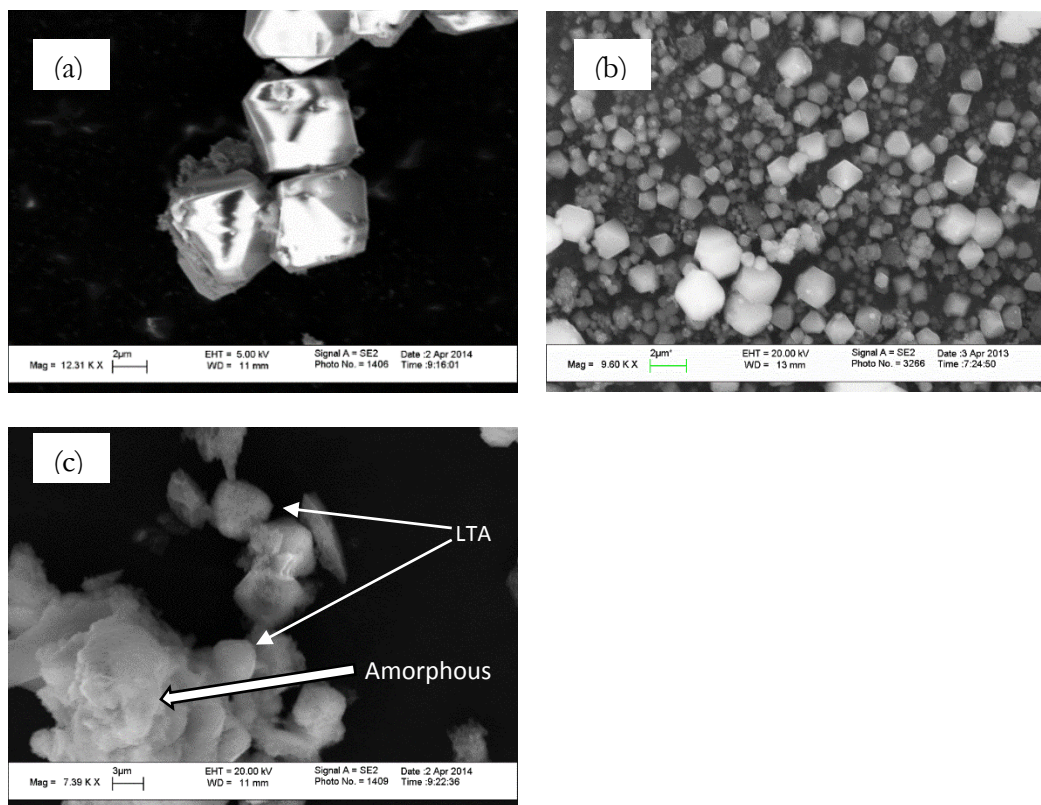
Figure 8-5. SEM images of: (a) SAPO LTA, (b) germanosilicate LTA with gel Si/Ge=2, and (c) germanosilicate LTA with high gel Si/Ge
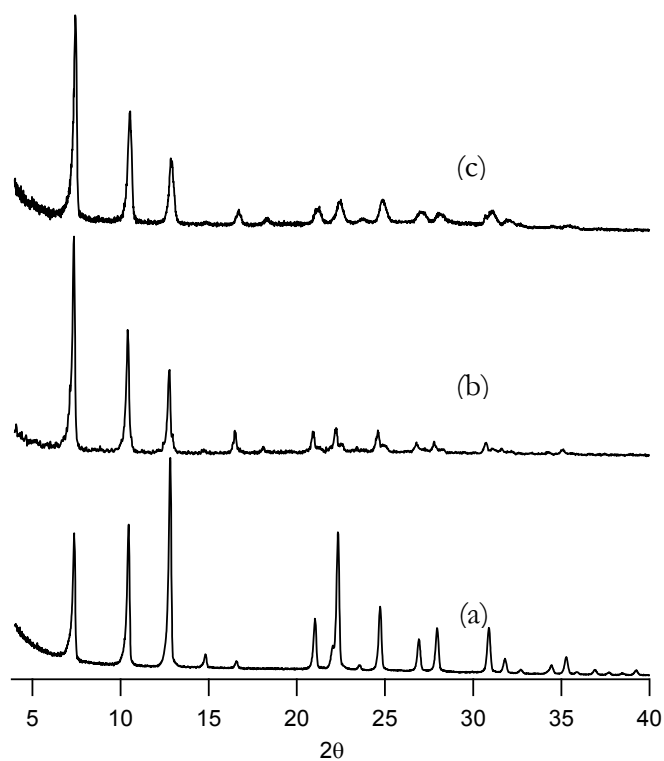
Figure 8-6. XRD of: (a) as-made SAPO LTA, (b) SAPO LTA calcined in air to 600°C and (c) SAPO LTA

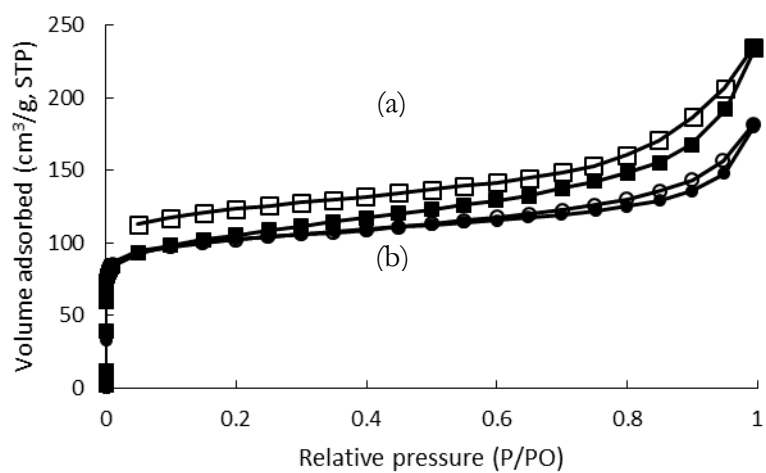with organic removed with ozone at 200°C

Figure 8-7. Nitrogen isotherms of (a) SAPO LTA calcined in air to 600°C and (b) SAPO LTA with

organic removed with ozone at 200°C. Closed symbols are adsorption and open symbols are

desorption.

8.4.2 Germanosilicate and Pure-Silica Materials

There are two known methods to make germanosilicate LTA, and only a single reported

method to produce pure-silica LTA (ITQ-29). Germanosilicate LTA has been prepared using the

cyclic crown ether Kryptofix 222 (Figure 8-8a), which is also known to produce aluminophosphate

LTA.[28,29,33,34] It was reasoned that this OSDA led to aluminophosphate LTA because its large, space-

filling nature is able to fill the α-cage of LTA. Methylated julolidine (Figure 8-8b) is able to produce

germanosilicate LTA as well as pure-silica LTA.[35] This OSDA was the first reported to form pure-

silica LTA in combination with tetramethylammonium hydroxide (TMAOH). It was determined that

the julolidine led to ITQ-29 by forming a supramolecular assembly of two molecules per α-cage.

TMAOH was necessary in these syntheses as it promotes the formation of sodalite cages and

compensates charge from the fluoride anions. Fluoride is known to reside in double four rings

(D4Rs, LTA has 6 independent D4Rs per unit cell), so four additional TMAOH molecules per unit

cell are necessary if all D4RS are occupied with fluoride (the julolidine will compensate for two

charges). ITQ-29 will only form at very low amounts of water (H_2O/SiO_2=2), and often AST will form

instead as a competing phase. Germanosilicate LTA crystallizes more readily than pure-silica LTA,

and TMAOH is not necessary in its synthesis. It is likely that germanium promotes the formation of

LTA, as it is known to favor the formation of D4Rs, and all T-atoms in LTA are in D4Rs [36,37]
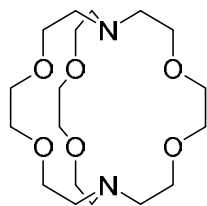
(a)
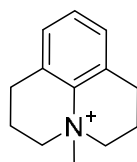
(b)

Figure 8-8. OSDAs known to produce LTA: (a) Kryptofix 222 and (b) methylated julolidine

8.4.3 Germanosilicate Syntheses

Syntheses were conducted with **T1** to attempt to make LTA based on the methods used to make ITQ-29. The first LTA trials used the conditions in Table 8-1, entry 1. Several of these syntheses were carried out, but over all time periods, it was found that the product formed was a mixture of LTA and AST (a representative XRD is shown in Figure 8-9a). In general, the relative amount of AST present increased over time. When the samples were studied using ^{13}C CP-MAS NMR, a strong resonance for TMAOH was present (shown in Figure 8-3b), indicating that it was present in the final product (and likely led to the formation of the AST). In the cases where the syntheses were allowed to proceed for extended times and showed nearly complete conversion to AST, ^{13}C CP-MAS NMR showed that nearly all of the organic present was TMAOH. The results of these syntheses established that it was possible produce germanosilicate LTA using **T1**; however,

the AST impurity needed to be eliminated.

Table 8-1. Results in germanosilicate and pure-silica systems

Molar Ratios

Entry	Si	Ge	Al	$R_{1/3}OH$	TMAOH	HF	H_2O	Temp.	Seeds	Product	Gel Si/Ge	Product Si/Ge
1	0.67	0.33		0.25	0.25	0.50	2-7	140°C		AST+LTA	2	
2	0.67	0.33		0.50	0.01	0.51	2-7	140°C		LTA	2	
3	0.67	0.33		0.50		0.51	2-7	140°C	Yes	LTA	2	2.1
4	0.9	0.1		0.50		0.50	7	140°C	Yes	Small LTA	9	Crystals 4.7
5	0.95	0.05		0.50		0.50	7	140°C	Yes	Small LTA	19	Crystals 4.4
6	1			0.50	0.01-0.25	0.50	2-14	140°C	Yes	AST	∞	
7	1			0.50		0.50	2-14	140-160°C	Yes	Amph.	∞	
8	1			0.50		0.50	7	175°C	Yes	ITQ-24	∞	
9	0.67	0.33		0.50		0.50	2-14	175°C		ITQ-24	2	
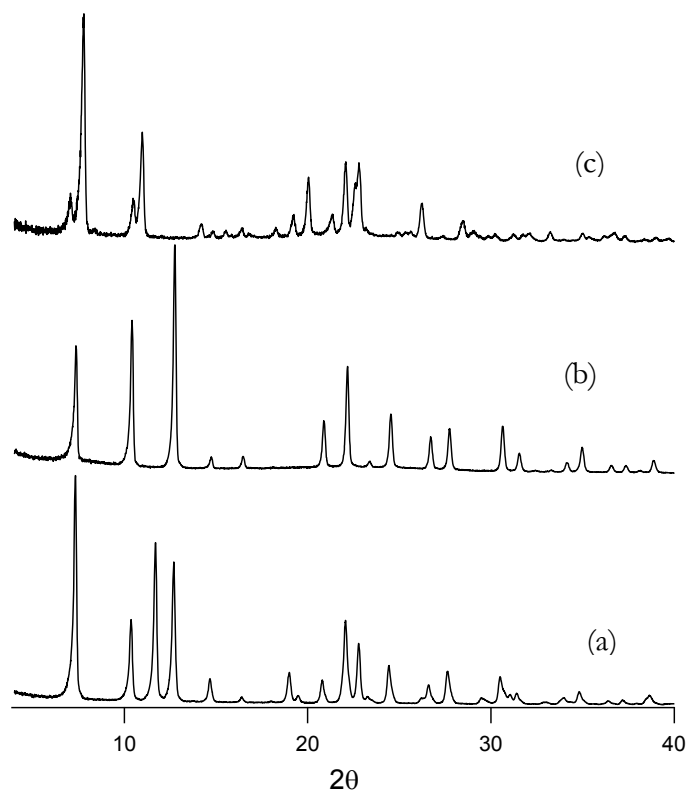
Figure 8-9. XRD of as-made: (a) AST/LTA phase mixture, (b) pure-phase LTA and (c) ITQ-24 (IWR)

Reducing the TMAOH to a very small amount (Table 8-1, entry 2) led to pure phase

germanosilicate LTA (shown in Figure 8-9b). However, over long time periods, AST would always

begin to form if any TMAOH was present. The use of seeds was found to be the most robust

method to produce pure-phase germanosilicate LTA (Table 8-1, entry 3). The organic was found to

be fully intact in this material using ^{13}C CP-MAS NMR (Figure 8-3c), with no evidence of TMAOH

present. The morphology of the sample is shown in Figure 8-5b, and is consistent with

rhombohedral LTA, even though there is no evidence for this symmetry by XRD.

8.4.4 Germanosilicate Composition and Characterization

The germanosilicate LTA was normally produced with a gel composition of Si/Ge=2 in

accordance with the previously reported work [35]. Using this gel composition, the product had a composition of Si/Ge=2.1 (EDS), similar to ITQ-29 that reports Si/Ge=2.16 and calculated Si/Ge=2.2 from a Rietveld refinement [35]. The gel composition was varied in order to reduce the amount of germanium in the product by increasing the Si/Ge ratios. Table 8-1, entries 4 and 5 show that when the Si/Ge ratio in the gel was increased, the product Si/Ge ratio also increased. However, it was evident that there were large amorphous regions in the products of these syntheses, with small amounts of crystalline products. The reported Si/Ge ratios are of the crystalline product. The composition of the regions that appeared amorphous were also measured using EDS, and showed much higher Si/Ge ratios. A representative SEM image of a sample containing crystals of germanosilicate LTA as well as high-silica amorphous regions is provided in Figure 8-5c.

The fluoride environment in the germanosilicate LTA was measured using ^{19}F NMR, and is shown in Figure 8-10. The spectrum is consistent with the expected position of fluoride occluded in double four rings with different amounts of silicon and germanium present (leading to different environments) [38,39]. The germanosilicate LTA was further characterized by ^{29}Si CP-MAS NMR, and the deconvolution of the spectrum is in Figure 8-11. The main peak is located at -108 ppm, which is consistent with $Si(OSi)_4$ coordination. Additionally, there is another resonance at -102 ppm that can be attributed to silicon coordinated to germanium atoms via bridging oxygen atoms [40].
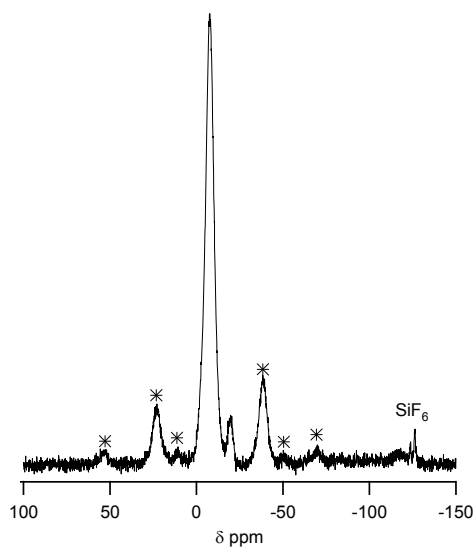
Figure 8-10. ^{19}F NMR of germanosilicate LTA, * denotes spinning side bands
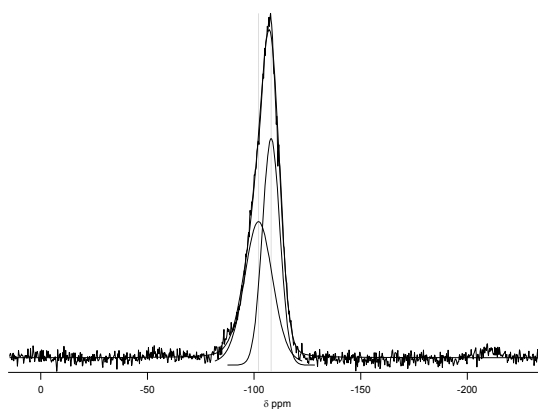
Figure 8-11. Deconvolution of ^{29}Si CPMAS NMR of germanosilicate LTA showing peaks at -102 and -108 ppm

Thermogravimetric analysis of the material showed that the amount of occluded organic and fluoride was 19.1wt%. If the final material had 1 molecule of **T1** occluded per unit cell and three corresponding fluoride anions to balance the charge, the mass loss should be 20.6wt% (one organic and 6 fluoride anions to fill all D4Rs would give 22.6wt%). The observed mass loss agrees well with one organic molecule per unit cell, with only half of the D4Rs occupied with fluoride.

After calcination, the material slowly degraded due to ambient humidity, shown by monitoring the

material using XRD (Figure 8-12). This behavior is commonly observed for germanosilicate

materials, as the germanium is known to change its coordination from tetrahedral to octahedral in

the presence of atmospheric water, and the degradation is especially pronounced after calcination

[41]. The organic can also be removed using ozone at 150°C, which led to a less severe degradation

of the framework, as is illustrated by XRD in Figure 8-13. This material still shows degradation over

time due to coordination of germanium with water. Due to the time dependent degradation

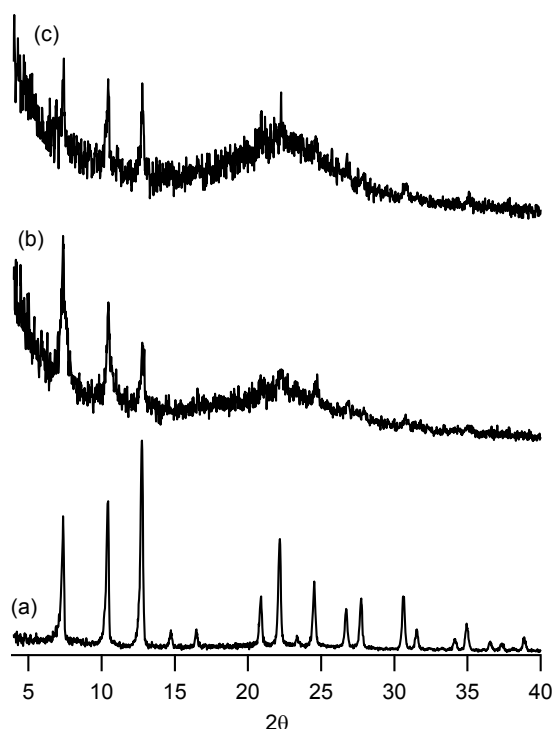observed in these materials, they were not characterized any further.

Figure 8-12. Germanosilicate LTA: (a) as-made, (b) immediately after calcination to 600°C, and (c)

after 5 days at ambient conditions
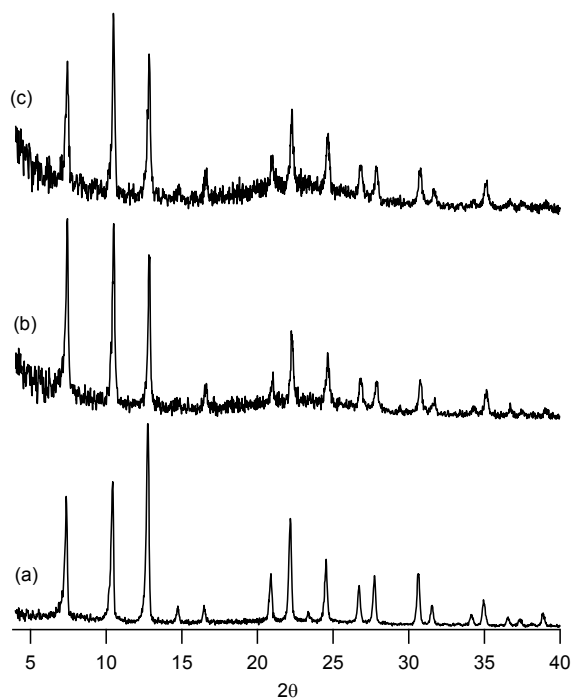
Figure 8-13. Germanosilicate LTA: (a) as-made, (b) organic removed using ozone at 150°C, and (c) after 4 days at ambient conditions

8.4.5 ITQ-24 Synthesis

In exploring the phase space under which germanosilicate LTA would form, reactions were run at 175°C (Table 8-1, entry 9). At this temperature, it was found that OSDA led to the formation of ITQ-24 (IWR) across a wide range of H_2O/TO_2=2-14, and a representative XRD pattern is shown in Figure 8-9c. Additional details of this phase will be published elsewhere[42].

8.4.6 Pure-silica

The germanosilicate results showed that the Si/Ge ratio can be increased by increasing the gel Si/Ge ratio, however, they appear to reach a maximum of Si/Ge < 5. This limitation made it impossible to synthesize a high-silica germanosilicate (in order to increase the material's stability or remove the germanium after the synthesis and heal the defects using methods reported with

other germanosilicate systems) [43,44]. The first trials to produce pure-silica LTA incorporated

TMAOH into the reaction mixture, as was done with ITQ-29, to promote the formation of sodalite

cages and compensate charge from the fluoride. These syntheses were conducted with

H_2O/SiO_2=2-14 and at a variety of temperatures, in all cases, AST was the only product formed

(Table 8-1, entry 6). When the TMAOH was eliminated from the reaction, no product was

observed, despite adding germanosilicate LTA seeds and running the reactions for over 2 months

in some cases (Table 8-1, entry 7). A large range of compositions and temperatures were explored,

but the only crystalline product produced was ITQ-24 in one instance (Table 8-1, entry 8).

8.4.7 Molecular Modelling

In the two reported cases of germanosilicate LTA, large, space-filling OSDAs were used. With

Kryptofix 222, individual molecules served as the OSDA, while for the case with methylated

julolidine, the OSDA formed a supramolecular assembly. In order to more completely understand

why **T1** led to germanosilicate LTA, molecular modelling was used to find the most favorable

conformation of **T1** in the LTA structure. It was known from thermogravimetric analysis that one

molecule of **T1** was occluded per unit cell. The molecular modelling calculations showed that it

was occluded in the α-cage of LTA in a space-filling conformation, and that each molecule was fully

contained in the α-cage. Views of the organic conformation and the organic in the α-cage are

shown in Figure 8-14. The spherical, space-filling conformation of the organic is in agreement with

the other reported OSDAs for LTA, showing that a large organic is needed to fill the α-cage to

promote the formation of LTA.
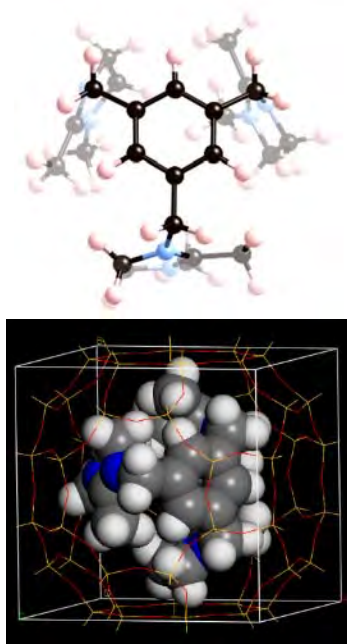
Figure 8-14. Calculated conformation of the triquat in LTA

8.5 Conclusions

This work reports the third known method to synthesize germanosilicate LTA. The inorganic

product undergoes degradation due to ambient humidity once the organic is removed, as

reported with many other germanosilicate microporous materials. In agreement with previously

reported results, a large, space-filling organic is necessary to form this difficult to access

framework. The triquaternary OSDA used in the synthesis was able to make a microporous

material with a large cage, supporting the hypothesis behind using this type of OSDA. In the

future, we plan to explore adding different groups using the general scheme in Figure 8-1.

8.6 Acknowledgements

The authors would like to thank Chevron Energy and Technology Company for providing

8.7 References

(1)   Davis, M. E. Ordered Porous Materials for Emerging Applications. *Nature* **2002**, *417* (6891), 813–821.

(2)   Baerlocher, C.; Mccusker, L. B. Database of Zeolite Structures, <http://www.iza-structure.org/databases/>. Accessed December 8, 2014.

(3)   Pophale, R.; Daeyaert, F.; Deem, M. W. Computational Prediction of Chemically Synthesizable Organic Structure Directing Agents for Zeolites. *J. Mater. Chem. A* **2013**, *1* (23), 6750–6760.

(4)   Verheyen, E.; Joos, L.; Van Havenbergh, K.; Breynaert, E.; Kasian, N.; Gobechiya, E.; Houthoofd, K.; Martineau, C.; Hinterstein, M.; Taulelle, F.; Van Speybroeck, V.; Waroquier, M.; Bals, S.; Van Tendeloo, G.; Kirschhock, C. E. A.; Martens, J. A. Design of Zeolite by Inverse Sigma Transformation. *Nat. Mater.* **2012**, *11* (12), 1059–1064.

(5)   Moliner, M.; Rey, F.; Corma, A. Towards the Rational Design of Efficient Organic Structure-Directing Agents for Zeolite Synthesis. *Angew. Chem. Int. Ed. Engl.* **2013**, *52* (52), 13880–13889.

(6)   Barrer, R. M.; Denny, P. J. 201. Hydrothermal Chemistry of the Silicates. Part IX. Nitrogenous Aluminosilicates. *J. Chem. Soc.* **1961**, 971–9825.

(7)   Burton, A.; Zones, S. Organic Molecules in Zeolite Synthesis: Their Preparation and Structure-Directing Effects. *Stud. Surf. Sci. Catal.* **2007**, *168*, 137–179.

(8)   Zones, S. I.; Burton, A. W.; Lee, G. S.; Olmstead, M. M. A Study of Piperidinium Structure-

Directing Agents in the Synthesis of Silica Molecular Sieves under Fluoride-Based Conditions. *J. Am. Chem. Soc.* **2007**, *129* (29), 9066–9079.

(9)   Jones, W.; Rao, C. Towards the Rational Design of Zeolite Frameworks. In *Supramolecular organization and materials design*; Cambridge University Press: Cambridge, UK, 2002; pp 83–102.

(10)   Zones, S. I.; Hwang, S. A Novel Approach to Borosilicate Zeolite Synthesis in the Presence of Fluoride. *Microporous Mesoporous Mater.* **2011**, *146* (1-3), 48–56.

(11)   Moini, A.; Schmitt, K.; Valyocsik, E.; Polomski, R. The Role of Diquaternary Cations as Directing Agents in Zeolite Synthesis. *Zeolites* **1994**, *14* (7), 504–511.

(12)   Ren, L.; Wu, Q.; Yang, C.; Zhu, L.; Li, C.; Zhang, P.; Zhang, H.; Meng, X.; Xiao, F.-S. Solvent-Free Synthesis of Zeolites from Solid Raw Materials. *J. Am. Chem. Soc.* **2012**, *134* (37), 15173–15176.

(13)   Camblor, M.; Villaescusa, L.; Diaz-Cabanas, M. Synthesis of All-Silica and High-Silica Molecular Sieves in Fluoride Media. *Top. Catal.* **1999**, *9*, 59–76.

(14)   Zones, S. I.; Hwang, S.-J.; Elomari, S.; Ogino, I.; Davis, M. E.; Burton, A. W. The Fluoride-Based Route to All-Silica Molecular Sieves; a Strategy for Synthesis of New Materials Based upon Close-Packing of Guest–host Products. *Comptes Rendus Chim.* **2005**, *8* (3-4), 267–282.

(15)   Camblor, M. A.; Barrett, P. A.; Díaz-Cabañas, M.-J.; Villaescusa, L. A.; Puche, M.; Boix, T.; Pérez, E.; Koller, H. High Silica Zeolites with Three-Dimensional Systems of Large Pore Channels. *Microporous Mesoporous Mater.* **2001**, *48* (1-3), 11–22.

(16)   Jiang, J.; Yu, J.; Corma, A. Extra-Large-Pore Zeolites: Bridging the Gap between Micro and Mesoporous Structures. *Angew. Chem. Int. Ed. Engl.* **2010**, *49* (18), 3120–3145.

(17)   Takewaki, T.; Beck, L. W.; Davis, M. E. Zeolite Synthesis Using 1,4-diazabicyclo[2,2,2]octane

(DABCO) Derivatives as Structure-Directing Agents. *Microporous Mesoporous Mater.* **1999**, *33* (1-3), 197–207.

(18) Cejka, J.; Corma, A.; Zones, S. *Zeolites and Catalysis*; Čejka, J., Corma, A., Zones, S., Eds.; Wiley-VCH Verlag GmbH & Co. KGaA: Weinheim, Germany, 2010.

(19) Kubota, Y.; Helmkamp, M. M.; Zones, S. I.; Davis, M. E. Properties of Organic Cations That Lead to the Structure-Direction of High-Silica Molecular Sieves. *Microporous Mater.* **1996**, *6* (4), 213–229.

(20) Zones, S. I. Translating New Materials Discoveries in Zeolite Research to Commercial Manufacture. *Microporous Mesoporous Mater.* **2011**, *144* (1-3), 1–8.

(21) Lawton, S. L.; Rohrbaugh, W. J. The Framework Topology of ZSM-18, a Novel Zeolite Containing Rings of Three (Si,Al)-O Species. *Science* **1990**, *247* (4948), 1319–1322.

(22) Schmitt, K. D.; Kennedy, G. J. Toward the Rational Design of Zeolite Synthesis: The Synthesis of Zeolite ZSM-18. *Zeolites* **1994**, *14* (8), 635–642.

(23) Howarth, J.; Al-Hashimy, N. a. A Homochiral Tripodal Receptor with Selectivity for Sodium (R)-2-Aminopropionate over Sodium (S)-2-Aminopropionate. *Tetrahedron Lett.* **2001**, *42* (33), 5777–5779.

(24) Patinec, V.; Wright, P. A.; Aitken, R. A.; Lightfoot, P.; Purdie, S. D. J.; Cox, P. A.; Kvick, Å.; Vaughan, G. The Use of Triquaternary Alkylammonium Ions in the Synthesis of STA-5, a Magnesioaluminophosphate with the BPH Framework Topology. *Chem. Mater.* **1999**, *11* (9), 2456–2462.

(25) Materials Studio 6.0, Accelrys, Inc.: San Diego, CA, 2012.

(26) Dauber-Osguthorpe, P.; Roberts, V. A.; Osguthorpe, D. J.; Wolff, J.; Genest, M.; Hagler, A. T. Structure and Energetics of Ligand Binding to Proteins: Escherichia Coli Dihydrofolate

Reductase-Trimethoprim, a Drug-Receptor System. *Proteins* **1988**, *4* (1), 31–47.

(27) Cannan, T. R.; Flanigen, E. M.; Gajek, R. T.; Lok, B. M.; Messina, C. A.; Patton, R. L. Crystalline Silicoaluminophosphates. US Pat. 4440871, 1984.

(28) Harbuzaru, B.; Paillaud, J.-L.; Patarin, J.; Bats, N.; Simon, L.; Laroche, C. IM-11 Crystalline Solid with Structure Type LTA, and a Process for Its Preparation. *US Pat. 7,056,490* **2006**.

(29) Schreyeck, L.; D'agosto, F.; Stumbe, J.; Caullet, P.; Mougenel, J. C. Synthesis of the LTA-Type AlPO4 in the Presence of the Diazapolyoxa Macrocycle "Kryptofix 222." *Chem. Commun.* **1997**, No. 13, 1241–1242.

(30) Burton, A.; Shayib, R. Method for Preparing LTA-Type Zeolites Using a Novel Structure Directing Agent. *US Pat. 8,337,808* **2013**.

(31) Fayad, E. J.; Bats, N.; Kirschhock, C. E. a; Rebours, B.; Quoineaud, A.-A.; Martens, J. a. A Rational Approach to the Ionothermal Synthesis of an AlPO4 Molecular Sieve with an LTA-Type Framework. *Angew. Chem. Int. Ed. Engl.* **2010**, *49* (27), 4585–4588.

(32) Sierra, L.; Deroche, C.; Gies, H.; Guth, J. L. Synthesis of New Microporous AlPO4 and Substituted Derivatives with the LTA Structure. *Microporous Mater.* **1994**, *3* (1-2), 29–38.

(33) Schreyeck, L.; Stumbe, J.; Caullet, P.; Mougenel, J.-C.; Marler, B. The Diaza-Polyoxa-Macrocycle `Kryptofix222' as a New Template for the Synthesis of LTA-Type AlPO4. *Microporous Mesoporous Mater.* **1998**, *22* (1-3), 87–106.

(34) Huang, A.; Caro, J. Steam-Stable Hydrophobic ITQ-29 Molecular Sieve Membrane with H2 Selectivity Prepared by Secondary Growth Using Kryptofix 222 as SDA. *Chem. Commun. (Camb).* **2010**, *46* (41), 7748–7750.

(35) Corma, A.; Rey, F.; Rius, J.; Sabater, M. J.; Valencia, S. Supramolecular Self-Assembled Molecules as Organic Directing Agent for Synthesis of Zeolites. *Nature* **2004**, *431* (7006), 287–

290.

(36) Paillaud, J.; Lorgouilloux, Y. Structure Orienting Role of Germanium in Zeolite Synthesis. *Stud. Surf. Sci. Catal.* **2007**, *170*, 389–396.

(37) Zwijnenburg, M. A.; Bromley, S. T.; Jansen, J. C.; Maschmeyer, T. Computational Insights into the Role of Ge in Stabilising Double-Four Ring Containing Zeolites. *Microporous Mesoporous Mater.* **2004**, *73* (3), 171–174.

(38) Pulido, A.; Corma, A.; Sastre, G. Computational Study of Location and Role of Fluoride in Zeolite Structures. *J. Phys. Chem. B* **2006**, *110* (47), 23951–23961.

(39) Sastre, G.; Pulido, A.; Corma, A. Pentacoordinated Germanium in AST Zeolite Synthesised in Fluoride Media. A 19F NMR Validated Computational Study. *Chem. Commun. (Camb).* **2005**, *1* (18), 2357–2359.

(40) Blasco, T.; Corma, A.; Díaz-Cabañas, M. J.; Rey, F.; Vidal-Moya, J. A.; Zicovich-Wilson, C. M. Preferential Location of Ge in the Double Four-Membered Ring Units of ITQ-7 Zeolite. *J. Phys. Chem. B* **2002**, *106* (10), 2634–2642.

(41) Moliner, M.; Díaz-Cabañas, M.; Fornés, V.; Martínez, C.; Corma, A. Synthesis Methodology, Stability, Acidity, and Catalytic Behavior of the 18×1018×10 Member Ring Pores ITQ-33 Zeolite. *J. Catal.* **2008**, *254* (1), 101–109.

(42) Personal Communication, Dr Ana Pinar and Prof Lynne McCusker, ETH Zurich, 2014.

(43) Burel, L.; Kasian, N.; Tuel, A. Quasi All-Silica Zeolite Obtained by Isomorphous Degermanation of an As-Made Germanium-Containing Precursor. *Angew. Chem. Int. Ed. Engl.* **2013**.

(44) Liu, X.; Kasian, N.; Tuel, A. New Insights into the Degermanation Process of ITQ-17 Zeolites. *Microporous Mesoporous Mater.* **2014**, *190*, 171–180.

Chapter 9. Conclusions and Future Recommendations

The central theme of the work presented here has been the exploration of imidazolium-based OSDAs across a wide range of microporous material synthesis conditions. Much of this work was motivated by experimental predictions for forming pure-silica STW using pentamethylimidazolium. From this basis a wide range of mono, di, and triquaternary OSDAs were explored across a comprehensive set of screening reactions. Some of the frameworks encountered in these studies include CSV, STW, RTH, LTA, HEU, AEI, IWV, *BEA, MTW, STF, and ITW as a non-comprehensive list. The variety of frameworks and material compositions encountered in this work reinforce the utility of imidazolium based OSDAs. They are simple and robust, and should be relatively easy to manufacture at scale, opening opportunities for commercial applications.

Continuation of the exploration of imidazolium OSDAs has limitless possibilities as there are many organic and inorganic variables to pursue. A few specific areas to concentrate on are the topotactic materials formed via low-water syntheses in fluoride-mediate reactions. This class of synthesis has led to the synthesis of high-silica HEU as well as a method to produce pure-silica RTH (reference given in the Appendix). The layered precursor to RTH can also be pillared to obtain a novel microporous material framework.

One final area to continue to explore is that of a method to produce bulk, enantiopure samples of microporous materials. The STW framework explored in chapter 2 presents what may be the most promising framework to date for this type of sample. In order to make bulk, enantiopure samples, enantiopure OSDAs must be used which are large enough to stabilize a single enantiomer of the final framework with a favorable interaction energy while not being able to fit in the other enantiomer. Efforts are currently underway to this end that combine computational predictions with experimental efforts. If successful, this result will demonstrate

proof of concept for one of the long-stand grand challenges in microporous material synthesis.

Appendix

The following is a list of other publications that I worked on during my PhD work but did not fit the general theme of my thesis.

1. Pinar, A. B.; McCusker, L.; Bärlocher, C.; Hwang, S.; Schmidt, J.; Davis, M. E.; Zones, S. Location of Ge and Extra-Framework Species in the Zeolite ITQ-24. Dalt. Trans. 2015, 6288–6295. doi: 10.1039/C4DT03831B

2. Dusselier, M.; Schmidt, J. E.; Moulton, R.; Haymore, B.; Hellums, M.; Davis, M. E. Influence of Organic Structure Directing Agent Isomer Distribution on the Synthesis of SSZ-39. *Chem. Mater.* **2015**, *27* (7), 2695–2702.doi: 10.1021/acs.chemmater.5b00651

3. Deimund, M. a.; Schmidt, J. E.; Davis, M. E. Effect of Pore and Cage Size on the Formation of Aromatic Intermediates During the Methanol-to-Olefins Reaction. *Top. Catal.* **2015**, *58* (7-9), 416–423. doi: 10.1007/s11244-015-0384-y

4. Schmidt, J. E.; Deem, M. W.; Lew, C.; Davis, T. M. Computationally-Guided Synthesis of the 8-Ring Zeolite AEI. *Top. Catal.* **2015**, *58* (7-9), 410–415. doi: 10.1007/s11244-015-0381-1